ÅBO AKADEMI

INSTITUTIONEN FÖR
KEMITEKNIK

DEPARTMENT OF CHEMICAL
ENGINEERING

Processkemiska centret

Process Chemistry Centre

REPORT 13-03

Modeling of Fireside Deposit Formation in Two Industrial Furnaces

Bingzhi Li

Doctoral Thesis

Laboratory of Inorganic Chemistry

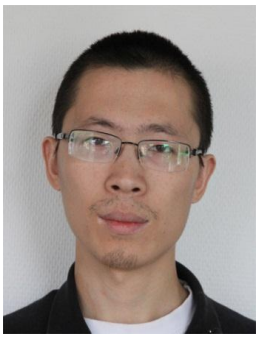

Bingzhi Li

Born in 1983, Weifang, Shandong Province, P. R. China

B. Sc. Chemical Engineering in Light Industry, 2004
Shandong Institute of Light Industry, P. R. China

M. Sc. Chemical Engineering, 2006
Åbo Akademi University, Finland

PhD defence, 2013
Åbo Akademi University, Finland

Modeling of Fireside Deposit Formation in Two Industrial Furnaces

Bingzhi Li

Academic Dissertation

Inorganic Chemistry
Process Chemistry Centre
Department of Chemical Engineering
Åbo Akademi University

Turku/Åbo, Finland, 2013

Supervisors
Docent Anders Brink
Åbo Akademi University
Department of Chemical Engineering
Turku, Finland

Professor Mikko Hupa
Åbo Akademi University
Department of Chemical Engineering
Turku, Finland

Reviewer
Professor Antti Oksanen
Tampere University of Technology
Chemistry and Bioengineering'
Tampere, Finland

Reviewer and Opponent
Professor Roman Weber
Clausthal University of Technology
Institute for Energy Process Engineering and Fuel Technology
Clausthal-Zellerfeld, Germany

ISSN 1459-8205
ISBN 978-952-12-2953-4 (paper version)
ISBN 978-952-12-2964-0 (pdf version)
Painosalama
Turku/Åbo, Finland, 2013

PREFACE

The work presented in this thesis was carried out at the Laboratory of Inorganic Chemistry, Department of Chemical Engineering, Åbo Akademi University during 2007-2013. This work has been a part of the activities of the Åbo Akademi Process Chemistry Centre, funded by the Academy of Finland in their Centers of Excellence Program 2006-2011. This work was carried out within the framework of research projects Multi-Phase Chemistry in Process Simulation, INTER, ERA-NET, FUSEC and FA Symbiosis. Financial support from National Technology Agency of Finland, Academy of Finland, and industrial partners Outotec Oyj, Andritz Oy, Metso Power Oy, Oy Metsä-Botnia Ab, Foster Wheeler Energia Oy, UPM-Kymmene Oyj, Top Analytica Oy Ab, Clyde Bergemann GmbH, and International Paper Inc. via the research projects is gratefully acknowledged. I would also like to acknowledge the Rector of Åbo Akademi University, Professor Jorma Mattinen for the three-month scholarship during the last stage of the work.

I would like to thank my supervisors Docent Anders Brink and Professor Mikko Hupa. Without their guidance and supervision, I would not be able to come to this stage finishing my doctoral study. During my study, I have had many discussions with Anders regarding research ideas, preparation of publications and even coding. He is always willing to give advices and helping hands. I have been given the freedom to try my own ideas and to work at my own pace. However, when I lost in some unnecessary details, Anders came with a timely little push and the help I actually needed. Thank you, Anders, for your patience and guidance. Professor Hupa has been there to define and steer this work. Thank you also for your concise and effective advice on the structure of the publications and on this thesis.

This doctoral thesis is a milestone in my study and in my life, especially in my life here in Finland. I have stayed in Finland for nine years by now, and it has been an inspiring, fruitful and joyful period of time. I would like to express my gratitude to the persons who made it possible. Professor Menghua Qin, the initiator to encourage students from the former Shandong Institute of Light Industry (SILI) to apply for Master Programme at Åbo Akademi University, thank you for paving a new road for me and the fellow SILI students here. I had the naive thought that CFD is all about computer and coding when I started to work in the Laboratory of Inorganic Chemistry in 2005 as a summer worker. I was lucky to have Docent Christian Mueller as my supervisor when I started to learn to use CFD as a modeling tool to study combustion related problems. I would like to thank Chiristian for trusting me and giving me the opportunity to work with CFD.

I am grateful to all present and former colleagues at the Laboratory of Inorganic Chemistry for a pleasant work atmosphere. My roommates Markus and Oskar, thank you for always being helpful and cheerful, and always sharing the refreshing videos with me. Special thanks to Doctor Daniel Lindberg for co-authoring one publication and helping me set up the thermodynamic calculations.

I am also grateful to all my friends sharing the time with me, being it gardening, biking, fishing, playing games and so on. You all make my life here intriguing and colorful. Special thanks to Leo Harju for leading me to the practice of permaculture. Brothers and sisters of the SILI-Åbo family, I am proud to be one member of this ever-expanding family. I will appreciate this special tie among us during my whole life.

Finally, my dear mother and father, thank you for your love, support and encouragement all the way. Dear Shaoxia, you are the one making my life joyful and meaningful during these years. Thank you for your love to me and your devotion to our family. And Yicheng, my dear son, your smile means the world to me!

Bingzhi Li

Åbo, September 2013

ABSTRACT

Fireside deposits can be found in many types of utility and industrial furnaces. The deposits in furnaces are problematic because they can reduce heat transfer, block gas paths and cause corrosion. To tackle these problems, it is vital to estimate the influence of deposits on heat transfer, to minimize deposit formation and to optimize deposit removal. It is beneficial to have a good understanding of the mechanisms of fireside deposit formation. Numerical modeling is a powerful tool for investigating the heat transfer in furnaces, and it can provide valuable information for understanding the mechanisms of deposit formation. In addition, a sub-model of deposit formation is generally an essential part of a comprehensive furnace model. This work investigates two specific processes of fireside deposit formation in two industrial furnaces.

The first process is the slagging wall found in furnaces with molten deposits running on the wall. A slagging wall model is developed to take into account the two-layer structure of the deposits. With the slagging wall model, the thickness and the surface temperature of the molten deposit layer can be calculated. The slagging wall model is used to predict the surface temperature and the heat transfer to a specific section of a super-heater tube panel with the boundary condition obtained from a Kraft recovery furnace model. The slagging wall model is also incorporated into the computational fluid dynamics (CFD)-based Kraft recovery furnace model and applied on the lower furnace walls. The implementation of the slagging wall model includes a grid simplification scheme. The wall surface temperature calculated with the slagging wall model is used as the heat transfer boundary condition. Simulation of a Kraft recovery furnace is performed, and it is compared with two other cases and measurements. In the two other cases, a uniform wall surface temperature and a wall surface temperature calculated with a char bed burning model are used as the heat transfer boundary conditions. In this particular furnace, the wall surface temperatures from the three cases are similar and are in the correct range of the measurements. Nevertheless, the wall surface temperature profiles with the slagging wall model and the char bed burning model are different because the deposits are represented differently in the two models. In addition, the slagging wall model is proven to be computationally efficient.

The second process is deposit formation due to thermophoresis of fine particles to the heat transfer surface. This process is considered in the simulation of a heat recovery boiler of the flash smelting process. In order to determine if the small dust particles stay on the wall, a criterion based on the analysis of forces acting on the particle is applied. Time-dependent simulation of deposit formation in the heat recovery boiler is carried out and the influence of deposits on heat transfer is investigated. The locations prone to deposit formation are also identified in the heat recovery boiler.

Modeling of the two processes in the two industrial furnaces enhances the overall understanding of the processes. The sub-models developed in this work can be applied in other similar deposit formation processes with carefully-defined boundary conditions.

SVENSK SAMMANFATTNING

I förbränningsanläggningar är beläggningar i eldstaden och värmeväxlarområdet ett stort problem. Beläggningarna minskar värmeöverföringen, hindrar rökgasflödet och kan ge upphov till korrosion. För att tackla och förstå dessa problem är det av stor vikt att beräkna hur beläggningar påverkar värmeöverföringen, att minimera uppkomsten av beläggningar och att optimera borttagandet av beläggningar. Ett verktyg som används för att få en bättre förståelse för hur beläggningar bildas är numerisk modellering. Numeriska modeller för bildandet av beläggningar utgör även en viktig del då hela förbränningsanläggningar simuleras. I detta arbete har modeller för bildandet av beläggningar i två olika pannor utvecklats.

Den första i avhandlingen studerade processen är en s.k. slaggande pannvägg. Med detta menas att yttemperaturen på beläggningen överstiger askans smältpunkt, med påföljden att ytskiktet blir flytande och på så sätt begränsar beläggningstjockleken. I avhandlingen utvecklades en modell som tar detta fenomen i beaktande. Modellen kan beräkna tjockleken och yttemperaturen av den flytande askbeläggningen. Modellen har används i en detaljstudie av yttemperaturen och av värmeöverföringen i en av överhettarna i en sodapanna. I avhandlingen har den utvecklade modellen även använts vid simulering av en hel sodapanna med simuleringsverktyget CFD (Eng: computational fluid dynami cs, Sve: numerisk strömningsdynamik). Resultatet har jämförts med resultat baserade på mer etablerade modeller för yttemperaturen. Resultaten visar att väggtemperaturen är liknande i de olika fallen och att de faller inom det intervallet som observerats vid mätningar. Den i avhandlingen utvecklade modellen har visat sig vara fördelaktig eftersom den kräver avsevärt kortare numerisk beräkningstid.

Den andra i avhandlingen studerade processen är formation av beläggningar driven av termofores. Termofores är en diffusionsprocess som transporterar partiklar från varmt mot kallt. För att avgöra om små dammpartiklar belägger sig på väggen har ett kriterium baserat på analysen av krafter som påverkar partiklarna applicerats. Tidsberoende simulering av beläggningarna i värmeåtervinningspanna har utförts och inverkan av beläggningarna på värmeöverföringen har undersökts. Områdena speciellts utsatta för beläggningar har också kunnat identifierats.

Modelleringen av beläggningsprocesserna i de två industriella pannorna har förbättrat förståelsen för de icke-önskvärda beläggningarna. Modellerna utvecklade i detta arbete kan användas i andra motsvarande processer med beläggningsproblem med väldefinierade randvillkor.

LIST OF PUBLICATIONS

The thesis is based on the following papers, given as appendices. The papers are referred to in the text by their numbers.

I. Bingzhi Li, Markus Engblom, Daniel Lindberg, Anders Brink, Mikko Hupa, Ralf Koschask, and Christian Mueller, *Numerical investigation of Kraft recovery furnace wall temperature*, Journal of Science & Technology for Forest Products and Processes, 2 (5), pp. 41-48, 2012

II. Bingzhi Li, Anders Brink, and Mikko Hupa, *CFD investigation of slagging on a super-heater tube in a Kraft recovery boiler*, Fuel Processing Technology, 105, pp. 149-153, 2013

III. Bingzhi Li, Anders Brink, and Mikko Hupa, *A simplified model for determining local heat flux boundary conditions for slagging wall*, Energy & Fuels, 23(7), pp. 3418-3422, 2009

IV. Bingzhi Li, Anders Brink, and Mikko Hupa, *CFD investigation of deposition in a heat recovery boiler: Part II – deposit growth modeling*, Progress in Computational Fluid Dynamics, 9(8), 453-459, 2009

V. Anders Brink, Bingzhi Li, and Mikko Hupa, *CFD investigation of deposition in a heat recovery boiler: Part I – a dual layer particle conversion model*, Progress in Computational Fluid Dynamics, 9(8), 447-452, 2009

Contributions of the Author

Paper I. The author implemented the slagging wall model into the Åbo Akademi Furnace model and analyzed the simulations results and the IR videos from a measurement campaign. The author wrote the manuscript.

Paper II. The author carried out the simulation, and wrote the manuscript.

Paper III. The author worked on the development and the implementation of the analytical approach of the model, and wrote the manuscript.

Paper IV. The author worked on the development and the implementation of the model, and wrote the manuscript.

Paper V. The author worked on the implementation of the particle conversion model into CFD and wrote that part of the manuscript.

Supporting Publications

1. Bingzhi Li, Anders Brink, and Mikko Hupa, *CFD investigation of slagging on a super-heater tube in a Kraft recovery boiler*, Proceedings of Impacts of Fuel Quality on Power Production and the Environment, Saarisärkä, 2010
2. Bingzhi Li, Anders Brink, and Mikko Hupa, *CFD analysis of an uptake shaft with slagging walls – the slag model*, Proceedings of Finnish-Swedish Flame Days, 2009

3. Bingzhi Li, Anders Brink, and Mikko Hupa, *A model for calculating heat transfer through a slagging wall*, Proceedings of Impacts of Fuel Quality on Power Production and the Environment, Banff, 2008
4. Anders Brink, Bingzhi Li, and Mikko Hupa, *A particle model for investigation of deposits in a heat recovery boiler*, Proceedings of AFRC-JFRC Joint International Symposium, Hawaii, 2007
5. Bingzhi Li, Anders Brink et al, *Spray models for CFD of black liquor recovery furnace*, Proceedings of the 15th International Flame Research Foundation Members' Conference, Pisa, 2007

TABLE OF CONTENTS

NOMENCLATURE

Acronyms

CCSEM	Computer Controlled Scanning Electron Microscopy
CFD	Computational Fluid Dynamics
CHP	Combined Heat and Power
DPM	Discrete Phase Model
DTA	Differential Thermal Analysis
IR	Infrared
Prenflo	Pressurized entrained-flow
SEM	Scanning Electron Microscopy
TGA	Thermal Gravimetric Analysis

Latin Letters

c	Gas species concentration	[mol/m^3]
c_p	Specific heat	[J/kg-K]
c_v	Specific heat of gas at constant volume	[J/mol-K]
d	Diameter	[m]
h	Heat transfer coefficient	[W/m^2-K]
k_B	Boltzmann's constant	[J/K]
k	Thermal conductivity	[W/m-K]
$\dot{m}$	Mass flow rate	[kg/s]
q''	Heat flux	[W/m^2]
u	Velocity	[m/s]
A	Area	[m^2]
C	Mass concentration	[kg/m^3]
C_c	Cunningham slip correction	
C_m, C_s, C_t	Function constant for thermophoretic coefficient	
D	Mass diffusivity, diffusion coefficient	[m^2/s]
F	Force	[N]
	Fraction	
$\dot{H}$	Enthalpy flow rate	[W]
K_n	Knudsen number	[J/K]
M	Molecular mass	[kg/mol]
Q	Heating value	[GJ/kg]
$\dot{Q}$	Heat transfer rate	[W]
R	Thermal resistance	[m^{2}K/W]
	Universal gas constant	8.314 [J/K-mol]
$R_{b/a}$	Fouling index based on base-to-acid ratio	
S	Particle to gas density ratio	

Sc	Schmidt number	
Sn	Normal momentum accommodation coefficient	
St	Stokes number	
	Tangential momentum accommodation coefficient	
T	Temperature	[K]
$\left\|\vec{U}\right\|$	Absolute value of particle velocity	[m/s]
Y	Mass fraction	

Greek Letters

α	Function parameter	
β	Mass transfer coefficient	[m/s]
γ	Specific heat ratio of gas	
σ	Stefan Boltzmann's constant	5.67×10^{-8} [W/m^2-K^4]
ε	Emissivity	
λ	Gas mean free path	[m]
ϕ	Function parameter	
π	Pi	3.14159265…
ν	Kinematic viscosity	[m^2/s]
π_1	Function parameter	
τ	Shear stress	[Pa]
	Particle relaxation time	
μ	Dynamic viscosity	[Pa·s]
ρ	Density	[kg/m^3]
δ	Thickness	[m]
ψ	Correction factor	
∇	Gradient	

Subscripts

ash	Ash property
c	Cylindrical tube
	Critical value
cond	Condensation
conv	Convective heat flux
d	Deposit property
	Deposition
Diff	Diffusion
flow	Fluid flow of molten deposits
g	Gas properties
i	Ash forming vapor species
m	Molecular property
metal	Tube metal

n	Normal component
p	Particle
s	Solid
th	Thermophoresis
w, wall	Wall property
∞	Bulk property

Superscripts

″	Flux
+	Dimensionless variable
*	Symbol for friction velocity
˙	Rate per second

1. INTRODUCTION

Fireside deposit formation has long been a problem in steam-raising boilers. In boilers for heat and power generation, deposits are found on the furnace walls, on the superheaters and on the heat exchangers. Figure 1.1 shows examples of deposits in different parts of boilers. Slagging and fouling on the heat transfer surfaces hinder the heat transfer. Massive deposits built up in the superheater region can block the gas paths. The deposits can cause severe corrosion of boiler tubes. One or more of these problems can also occur in other industrial boilers, e.g., the heat recovery boiler of the flash smelting process (Yang, 1996).

Great efforts have gone into understanding fireside deposit formation and into the pursuit of solutions to deposit-related problems. In 1996, Bryers presented a comprehensive overview of fireside slagging, fouling and high-temperature corrosion of heat-transfer surfaces due to impurities in steam-raising fuels (Bryers, 1996). He stated that the empirical art of ash deposition from impurities in combustion gases was being transformed into the science of mineral transformation and ash deposition. A large pool of knowledge on deposit formation with coal combustion has been established based on extensive research dating back over a century. Combustion of alternative fuels or fuel mixtures has also raised new challenges in dealing with fireside ash problems (Baxter, 1993). Notably, numerical modeling has increasingly been used to investigate deposit formation and its influence on the performance of the combustion facility. The development of numerical modeling, especially computational fluid dynamics (CFD) simulation, of deposit formation can be found in the reviews from Wang and Harb (1997) and Weber et al. (2013a).

(a)

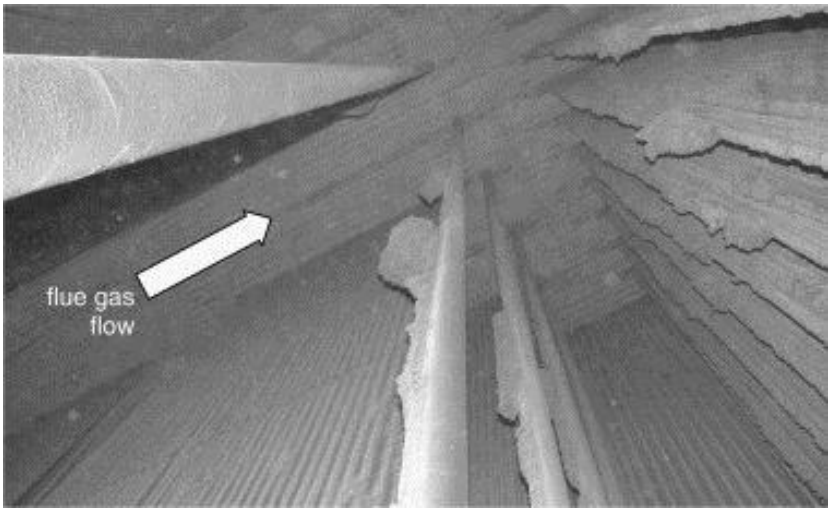

(b)

Figure 1.1: (a) Slag formation on boiler tubes (Rosemount Analytical, 2012); (b) View of superheater deposits (Tomeczek & Waclawiak, 2009).

1.1 OBJECTIVE

The objective of this work was to enhance the understanding of fireside deposit formation by means of modeling two specific deposition processes in two industrial furnaces. One process is the slagging wall found in Kraft recovery furnaces with molten deposits running on the wall or on the superheater tubes. The other process is deposit formation due to thermophoresis of fine particles to the heat transfer surfaces in the heat recovery boiler of the flash smelting process.

The contributions of this work are:

- Development and implementation of a sub-model for slagging walls in furnaces for CFD. In the slagging wall sub-model, the two-layer (solid and fluid) structure of the deposits is considered, and the fluidity of the molten deposit is taken into account in the calculation of the thickness of the molten deposit layer. The thickness, together with the surface temperature of the molten deposit layer, is calculated with an iterative algorithm. To the author's knowledge, models with a similar concept appear in two earlier works. One is on modeling of slag flow in an entrained-flow gasifier (Seggiani, 1998), and the other is on modeling of a coal-fired slagging combustor (Wang et al., 2007). This work is the first attempt at modeling slagging walls in Kraft recovery furnaces with such a dedicated sub-model.
- Development and implementation of a sub-model for thermophoresis-induced deposit formation for CFD. A particle conversion model and the deposition model are used in the simulation of deposit formation in a heat recovery boiler of the flash smelting process. To the author's knowledge, this work is the first attempt on the topic.
- Better understanding of deposit formation and the behavior of the deposits in the two types of industrial furnaces.

1.2 THESIS STRUCTURE

This thesis consists of an introductory section and five attached publications. The introductory section includes the background (Chapter 2); the modeling of the slagging wall in a Kraft recovery furnace (Chapter 3); the modeling of deposit formation due to thermophoresis (Chapter 4); and the conclusions (Chapter 5). The background briefly covers the mechanisms of fireside deposit formation and the relevant modeling works from the literature, and it presents the basis of this work: the Åbo Akademi Furnace Model. The modeling of the two processes follows a similar structure: a brief introduction of the process; the development of the model; the model parameters; the test case; and the results and discussion. The conclusion chapter summarizes the main findings of this work and provides an overview of the potential areas for future work.

2. BACKGROUND

Fireside deposit formation (i.e., slagging and fouling) is a complex process. Benson et al. (1993a) have listed a few factors governing the fireside deposit formation process. Fireside deposit formation depends on the transformation of the inorganic components found in the fuels (i.e., minerals and organically-associated inorganic elements) during and after the fuel conversion process. The transformation includes physical changes and chemical reactions under varied conditions in a furnace. The transformation is influenced by the interactions among the ash-forming elements, and between the ash-forming elements and the carbonaceous species. Those interactions are affected by conditions such as the position of the ash-forming elements in the matrix of the fuel and the chemical reactions with different kinetics. Build-up and removal of the deposits on heat transfer surfaces is another crucial stage of the process. Bryers (1996) added that the inorganic components in fuel, and the fly ash generated, are heterogeneous with regard to size and composition, and that individual species behave differently during and after combustion. He further indicated the factors that can determine the degree of deposit formation throughout a steam-raising boiler, e.g., the local gas temperatures; the tube temperatures; the gas velocities; and the tube orientation.

Fireside deposit formation must be considered already in the design stage of steam-raising boilers. In order to tackle the deposit-related problems, it is important to estimate the influence of deposits on heat transfer, to minimize deposit formation and to optimize deposit removal. Therefore, a good understanding of the mechanisms of fireside deposit formation is essential. Numerical modeling is a powerful tool for investigating the heat transfer in furnaces, and it can provide valuable information for understanding the mechanisms of deposit formation. Baukal et al. (2001) pointed out that sub-model of deposit formation is generally a fundamental part of a comprehensive furnace model.

2.1 MECHANISMS OF FIRESIDE DEPOSIT FORMAITON

For steam-raising boilers, the incombustible, inorganic materials in the fuel are the source of the fireside deposit problem. During combustion, the ash-forming matters are released from the fuel. The fly ash particles and the ash in vapor form are transported by the gas flow to the heat transfer surfaces. The transport mechanisms vary, primarily depending on the size of the ash particle and the gas flow condition in the boiler (Baxter, 1993&1998). The form and location of the deposits are associated with the transport mechanisms of the ash particles. The behavior of deposits on the heat transfer surfaces, i.e., growth, depletion, sintering or melting, is then influenced by the form and location of the deposits.

2.1.1 Ash Formation

Ash formation is closely allied with the combustion process, especially with char burning, and it has strong interaction with the operating conditions in the boiler. From fuel to ash, the mineral matters undergo a series of physical and chemical transformations. With new experiences, Weber et al. (2013a) modified the diagram from Sarofim and Helble (1994) showing the fate of mineral matters during coal combustion. The modified diagram is adapted here, as shown below (Figure 2.1). Weber et al. (2013a)

summarized the thermal processes in the transformation of minerals according to Bryers (1996):

a) Decomposition of minerals into simple compounds;
b) Vaporization of minerals and formation of aerosols;
c) Formation of new materials in the combustion zone; and
d) Fusion and liquefaction of incombustible matter.

Ash is generated in the forms of gas, liquid and solid as the product of mineral transformation. The properties and behaviors of ash depend on the association of the inorganic components in the fuel particle; the chemical characteristics of the inorganic components; the characteristics of the fuel particles; and on the combustion conditions (Weber et al., 2013a).

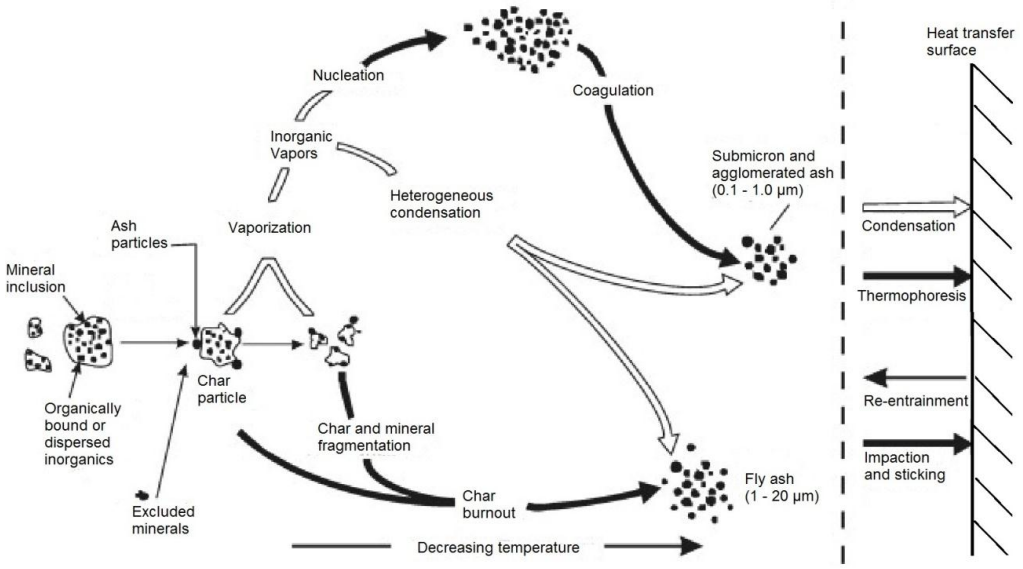

Figure 2.1: Schematic diagram of the fate of mineral matters during coal combustion (Weber et al., 2013a).

The development of analytical techniques based on Scanning Electron Microscopy (SEM) helps in understanding the interactions among the mineral matters during combustion. For example, the Computer Controlled-SEM (CCSEM) can be used to quantify the particle size, shape and composition of mineral matters of a coal or ash sample on a two-dimensional basis. It can also reveal the amount and nature of the excluded minerals in the coal. The SEM-based analyses indicate that dozens of reactions are involved in the mineral matter transformations in different parts of an ash particle (Frandsen, 2009). Thermodynamic equilibrium calculations can be used to assess the compositions and amounts of gas phase, liquid phase, and solid phase in complex combustion processes, including the ash compounds (Carling et al., 1983).

2.1.2 Ash Particle Transport Mechanisms

Mueller et al. (2005a) have summarized the transport mechanisms for particles of different sizes: Inertial impaction is important for particles larger than 10 μm; turbulent eddy impaction is the relevant transport mechanism for particles between 1 and 10 μm; eddy diffusion and thermophoresis are the key transport mechanisms for particles smaller than around 1 μm. Theis (2006) made a similar summary based on literatures: Particles larger than 10-15 μm are transported to the surface by inertial impaction; particles smaller than 1-10 μm are transported to the surface by thermophoresis and eddy diffusion; still smaller particles are mainly transported to the surface by diffusion, Brownian motion, etc. The mechanism by which the particles are transported to the heat transfer surfaces is also determined by the location and the orientation of the surfaces. Thus, the relative importance of the mechanisms in a boiler depends on the fuel composition, the boiler design and the boiler operating conditions. Brief descriptions of the ash transport mechanisms are provided in the following sections, including inertial impaction; thermophoresis; turbulent eddy impaction and diffusion; and condensation.

Inertial Impaction

Larger particles traveling with the gas flow have too much inertia to adapt to the changing streamlines around an obstacle. In furnaces, the larger ash particles are more likely to impact on the windward side of the heat transfer surfaces. For a cylindrical tube in a cross flow, the angle of impaction is 0° at the windward centerline, 90° at the side of the tube; and 180° at the leeward centerline. Baxter (1993) stated that, under conditions typical of combustion operation, the rate of inertial impaction drops essentially to zero when the impaction angle is larger than about 50°. Weber et al. (2013a) also mentioned that deposits are formed within a 50-60° sector on the windward side of the tube. As a result, mountain- shaped deposits are often observed on the windward side of the superheater tubes, as shown in Figure 1.1(b).

Figure 2.2 shows an example of large particles impacting on a cylindrical tube in a particle-laden flow. Inertial impaction occurs if the distance a particle travels before it fully adapts to the changing streamline is larger than the length scale of the obstacle. The ratio of these two lengths is defined as the particle Stokes number. In the case of a cylinder in a cross flow, the Stokes number is given as (Wessel & Righi, 1988)

$$St = \frac{\rho_p d_p^2 U_0}{18 \mu_g R} \qquad (2\text{-}1.),$$

where ρ_p and d_p are the particle density and particle diameter, respectively. U_O is the free-stream gas velocity, and μ_g is the gas dynamic viscosity. R represents the radius of the cylinder.

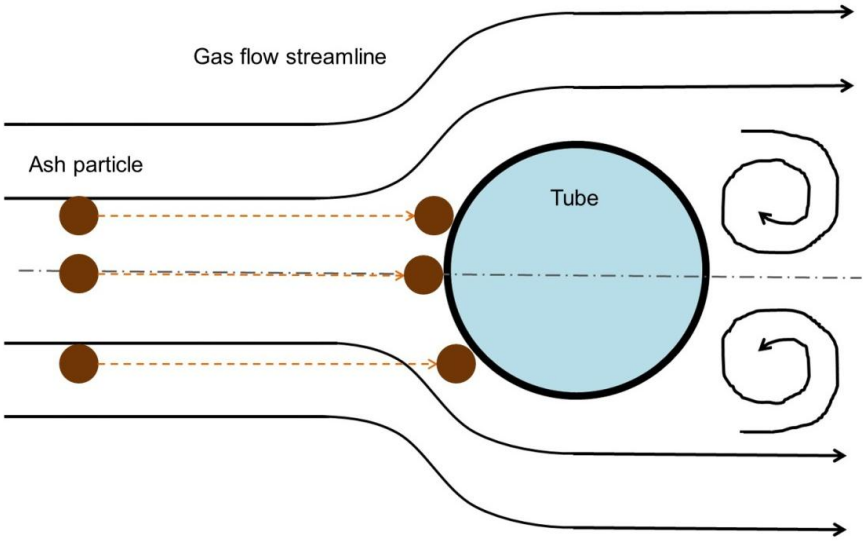

Figure 2.2: Inertial impaction of large ash particles on a cylindrical tube in a particle-laden flow.

Zbogar et al. (2009) summarized that the rate of inertial impaction depends on the geometry of the obstacle; the particle size and density; the angle of impaction; and the gas flow properties. The ratio of the number of particles impacting on a surface to the number of particles originally traveling toward the surface is defined as the impaction efficiency. Israel and Rosner developed a correlation between the impaction efficiency and the particle Stokes number for potential flow around a circular cylinder, shown below (Israel & Rosner, 1983):

$$\text{Impaction efficiency} = \frac{1}{1 + 1.25(St - 0.125)^{-1} - 0.014(St - 0.125)^{-2} + 0.508 \cdot 10^{-4}(St - 0.125)^{-3}}$$ (2-2.).

The Stokes number is calculated for each particle traveling toward a cylindrical tube, and the corresponding impaction efficiency can be determined. The correlation has been used in several CFD-based mathematical models, e.g., by Kær et al. (2006) and by Zhou et al. (2007).

The capture efficiency is defined as the propensity of impacting ash particles to stick on the surface of the obstacles, i.e., the heat transfer surfaces in furnaces. In addition to the rate of inertial impaction and the impaction efficiency, the particle capture efficiency also strongly affects the deposit growth. The particle capture efficiency is influenced by the composition and phase (solid or liquid) of the particle and by the composition, phase and morphology of the deposits on the heat transfer surfaces.

Thermophoresis

Thermophoresis is a particle transport mechanism caused by a local temperature gradient. Molecules with higher temperatures have higher kinetic energy. If there is a temperature gradient in the fluid surrounding a particle, the molecules at the hot side of the particle collide with the particle more intensely than the molecules at the cold side. This imbalance gives rise to a net force on the particle in the opposite direction of the temperature gradient, driving the movement of the particle. The temperature gradient can inherently be in the fluid, or it can be induced by the particle itself if the surface temperature of the particle is not uniform (Baxter, 1993). In furnaces, a steep temperature gradient exists at the boundary layer of the heat transfer surfaces, especially when the surfaces are clean. Small ash particles arriving at the boundary layer can be transported to the heat transfer surfaces due to the thermophoretic force, as shown in Figure 2.3. The temperature of the heat transfer surfaces increases due to deposit formation; this leads to a smaller temperature gradient and weakens thermophoresis. However, as discussed by Kær (2001), diminishing thermophoresis does not necessarily reduce the overall deposition rate of the sub-micron particles. He speculated that the increased surface roughness would enhance deposition by turbulent eddy impaction and diffusion, which would balance the weakened thermophoresis.

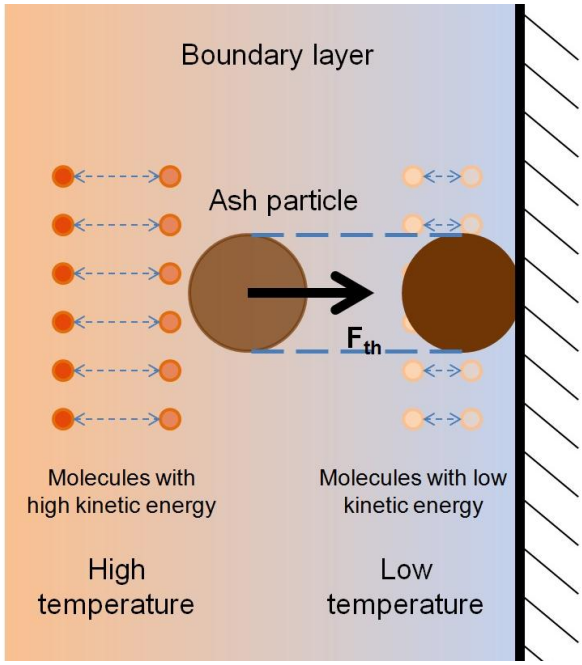

Figure 2.3: A simple illustration of the principle of thermophoretic force on an ash particle – the direction of the net force given by the surrounding molecules is opposite to the temperature gradient.

Kær (2001) indicated that condensation of inorganic vapors plays an important, or even dominant, role in the deposit formation process in straw-fired boilers. This process is more significant in the initial stages of deposit formation when thermophoresis is strong

because of the lower temperature at the heat transfer surfaces. In Kær's work, three different equations for calculating the thermophoretic force were reviewed; the equation from He and Ahmadi (1998) was used because it provides better predictions compared to experimental data. The equation from He and Ahmadi (1998) is likewise applied in this work. The equation expresses the thermophoretic force as a function of Knudsen number:

$$F_{th} = \frac{1.15K_n\left[1-\exp(-\frac{\alpha}{K_n})\right]\sqrt{\frac{4}{3\pi}\phi\pi_1 K_n}\frac{k_B}{d_m^2}\nabla T d_p^2}{4\sqrt{2}\alpha(1+\frac{\pi_1}{2}K_n)} \qquad (2\text{-}3.),$$

where

$$\phi = 0.25(9\gamma - 5)\frac{c_v}{R} \qquad (2\text{-}4.),$$

$$\alpha = 0.22\left(\frac{\frac{\pi}{6}\phi}{1+\frac{\pi_1}{2}K_n}\right)^{1/2} \qquad (2\text{-}5.),$$

$$\pi_1 = 0.18\frac{\frac{36}{\pi}}{(2-S_n+S_t)\frac{4}{\pi}+S_n} \qquad (2\text{-}6.),$$

and the molecular diameter

$$d_m = \left(\frac{5}{16\mu}\right)^{1/2}\left(\frac{MK_BT_g}{\pi}\right)^{1/4} \qquad (2\text{-}7.),$$

and the temperature gradient is evaluated in the viscous boundary sub-layer

$$\nabla T = \frac{q_{conv}}{Ak_g} \qquad (2\text{-}8.).$$

Here, the Knudsen number is $K_n = 2\lambda/d_p$, in which λ is the gas mean free path. The gas mean free path can be approximated as $\lambda = \nu(\pi M/2RT)^{1/2}$. k_B is the Boltzmann's constant; γ is the specific heat ratio of gas; c_v is the specific heat of gas at constant volume; and R is the universal gas constant. S_n and S_t are the normal and tangential momentum accommodation coefficients, respectively. μ is the molecular viscosity; M is the molecular mass; and T_g is the gas temperature. q_{conv} is the convective heat flux; A is the area; and k_g is thermal conductivity of gas phase.

For spherical particles in an ideal gas, an expression of the thermophoretic force from Talbot et al. (1980) is reformulated in the work of Weber et al. (2013a), as:

$$F_{th} = -D_{T,p}\frac{1}{m_p T}\frac{\partial T}{\partial x} \qquad (2\text{-}9.).$$

$D_{T,p}$ stands for the thermophoretic coefficient:

$$D_{T,p} = -\frac{6\pi d_p \mu_g^2 C_s (K + C_t K_n)}{\rho (1+3C_m K_n)(1+2K+2C_t K_n)} \qquad (2\text{-}10.).$$

K is the ratio of the gas thermal conductivity based on translational energy to the particle thermal conductivity: $K = k_g/k_p$, $k_g = 15/4\mu_g R$. The coefficients in Equation (2-4.) take the following values: $C_s = 1.17$, $C_t = 2.18$, $C_m = 1.14$.

Turbulent Eddy Impaction and Diffusion

Transport of smaller ash particles to the heat transfer surfaces by turbulent eddy impaction and different diffusion processes is part of the boundary layer controlled deposition (Kær, 2001). The diffusion processes include Fick's diffusion, describing the movement of molecules caused by a local concentration gradient; Brownian diffusion (the random movement of small particles); and eddy diffusion, representing diffusion in turbulent systems (Zbogar et al., 2009).

Kær (2001) discussed the contributions of turbulent eddy impaction and diffusion to deposit formation with the concept of deposition velocity. Deposition velocity u_d describes how fast ash particles in the vicinity of a heat transfer surface are moving toward the surface. The deposition rate $\dot{m}_d''$ can be expressed as

$$\dot{m}_d'' = u_d C_{particle} \qquad (2\text{-}11.),$$

where $C_{particle}$ is the ash particle mass concentration. Writing the deposition velocity in a dimensionless form yields

$$u_d^+ = \frac{u_d}{u^*} \qquad (2\text{-}12.),$$

where u^* is the friction velocity (m/s) expressed as $u^* = \left(\tau_w/\rho_g\right)^{1/2}$. τ_w is the wall shear stress, and ρ_g is the gas density. In addition, the dimensionless particle relaxation time can be written as

$$\tau_p^+ = \frac{1}{18} C_c S d_p^{+2} \qquad (2\text{-}13.),$$

with the dimensionless particle diameter $d_p^+ = d_p u^*/\nu$ where ν is the kinematic viscosity; S is the particle to gas density ratio; and C_c is the Cunningham slip correction, which represents the change in drag due to rarefied flow effects. This can be expressed as

$$C_c = 1 + \frac{2\lambda}{d_p}\left[1.257 + 0.4exp\left(-\frac{1.1 d_p}{2\lambda}\right)\right] \qquad (2\text{-}14.),$$

As shown in Figure 2.4, the dimensionless deposition velocity is plotted as a function of the dimensionless particle relaxation time. The figure is adapted from the work of Young and Leeming (1997), and it is based on a number of experiments concerning deposition onto a cylindrical pipe. The grey zone indicates the area covered by the experimental data points in the original figure, and a trend line has been added.

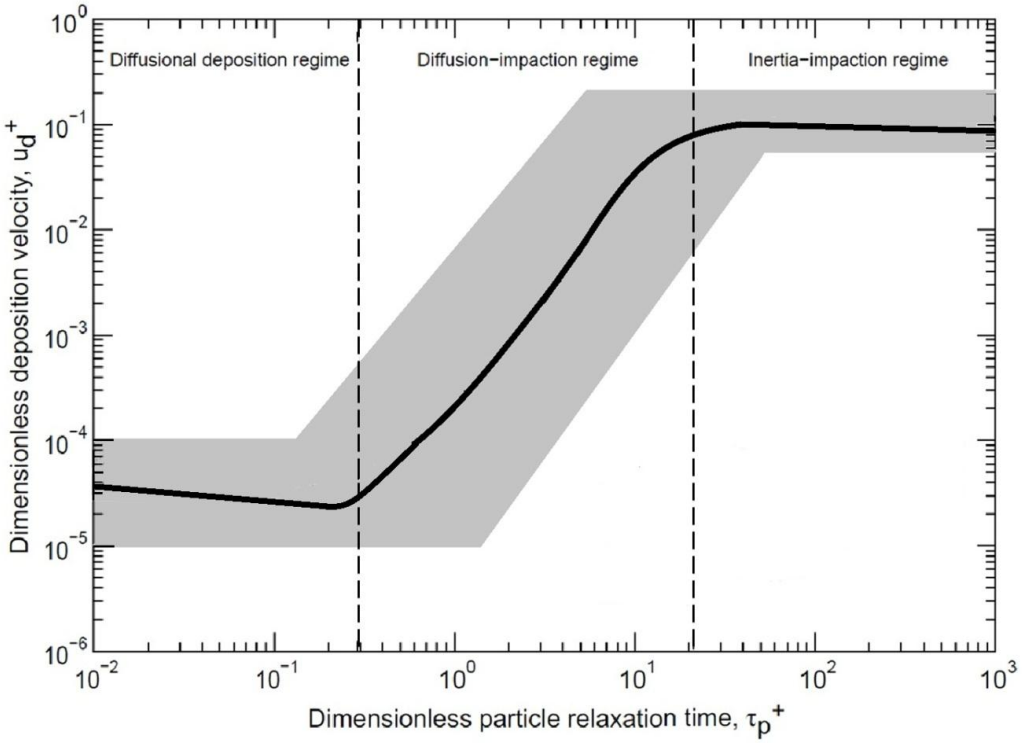

Figure 2.4: Characteristic regimes of dimensionless deposition velocity as a function of dimensionless particle relaxation time, adapted from Young and Leeming (1997).

Figure 2.4 shows three regimes of different transport mechanisms for particles with different dimensionless deposition velocities and relaxation times. In the "inertia-impaction regime," the dimensionless relaxation time of a particle is above 20 and can be much higher, while the dimensionless deposition velocity shows a slightly declining trend. This implies that inertia plays a dominant role in the motion of the particles, and that the response of the particles to turbulent flow is hindered by inertia. In contrast, the dimensionless deposition velocity of particles in the "diffusion-impaction regime" is very sensitive to their relaxation time. In the "diffusion-impaction regime," the particles have dimensionless relaxation times ranging from around 0.25 to around 20, whereas they have a four orders of magnitude change in the dimensionless deposition velocity. According to Kær (2001), the significant change in the dimensionless deposition velocity corresponding to the dimensionless relaxation time is attributed to a complex interaction between the particles and the turbulent structures near the wall. Kær (2001) presented the free-flight concept from Friedlander and Johnstone (1957) and the coherent structures or turbulent bursts concept from Owen (1969). Both theories are used to explain the processes controlling particle deposition velocities in the "Inertial-impaction regime" and in the "Diffusion-impaction regime." The free-flight concept theorizes that particles are transported by turbulent diffusion to within one "stop-distance" from the wall, and from there they acquire sufficient momentum to penetrate the viscous sub-layer. The coherent

structures or turbulent bursts concept does not ignore the unsteady flow structures near a solid wall; this concept suggests that particles are carried to the wall by fluid eddies generated from so-called turbulent bursts. In the absence of inertial impaction and thermophoresis, turbulent eddy impaction is the dominant mechanism of ash particle deposition.

For very small particles with diameters less than 0.1 μm, Brownian and eddy diffusion are the principal deposition mechanisms in the absence of thermophoresis. The "Diffusional deposition regime" in Figure 2.4 shows that the dimensionless deposition velocity is slightly decreasing as a function of the dimensionless relaxation time. Kær (2001) presented a correlation between the dimensionless diffusional deposition velocity and the particle Schmidt number, derived by Wood (1981):

$$u_{d,Diff}^{+} = \frac{u_{d,Diff}}{u^{*}} = 0.057 Sc_p^{-2/3} \qquad (2\text{-}15.)$$

The particle Schmidt number $Sc_p = \nu / D_p$. D_p is the particle diffusivity, which can be derived from the Stokes-Einstein relation:

$$D_p = \frac{k_B T C_c}{3\pi\mu d_p} \qquad (2\text{-}16.)$$

Condensation

Here, condensation depicts the process of ash-forming elements in gas phase entering the thermal boundary layer around an obstacle, condensing and being deposited. As shown in Figure 2.5, it includes the following components: (a) vapor passes the boundary layer around an obstacle and condenses heterogeneously; (b) vapor nucleates homogeneously in the boundary layer and deposits by thermophoresis; (c) vapor condenses heterogeneously on the particles in the boundary layer of an obstacle and deposits by thermophoresis (Baxter, 1993).

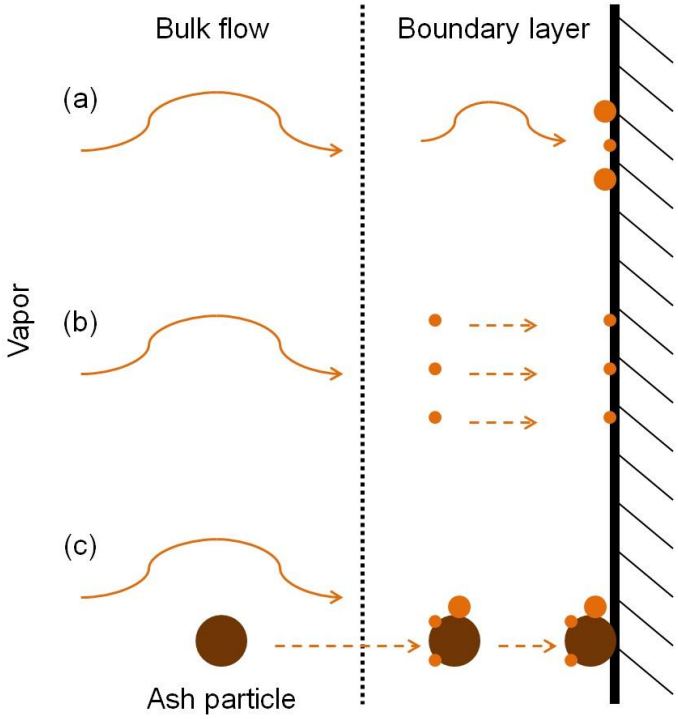

Figure 2.5: Schematic illustration of three forms of condensation of ash-forming elements on the surface of an obstacle: (a) vapor passes the boundary layer and condenses heterogeneously; (b) vapor nucleates homogeneously in the boundary layer and deposits by thermophoresis; (c) vapor condenses heterogeneously on the particles in the boundary layer and deposits by thermophoresis.

Condensation of ash-forming vapors plays an important role in fouling on the convective heat transfer surfaces in a boiler. Fouling can be initialized by the formation of a layer of alkali condensates on the heat transfer surfaces with lower temperatures. Fly ash particles are more likely to stick on such a layer; therefore, deposit formation will proceed at a significantly higher rate. Weber et al. (2013a) stated that condensation-induced deposit formation is more significant in boilers firing lignite, biomass, or co-firing coal with biomass, than in those firing hard coal. Alkali compounds are common among the ash-forming vapor species: KCl, NaCl, $PbCl_2$, $ZnCl_2$, etc. The condensation rate of an ash-forming vapor species near a cold wall with a temperature lower than or equal to the condensation temperature can be given as:

$$\dot{m}_{i,cond} = M_i \beta (c_\infty - c_{wall}) \quad (2\text{-}17.),$$

where M_i is the molecular mass of vapor species, and where c_∞ and c_{wall} are the species concentrations in the bulk flow and the saturation concentration at the wall, respectively. β is the mass transfer coefficient, which can be calculated using correlations for the Sherwood number. For a vapor species with a faster formation rate than the turbulent transport rate in the gas phase, thermodynamic equilibrium calculation can be used to

calculate its concentration. For the sulfates whose formation rate may be kinetically controlled, kinetic data is needed to obtain their concentrations.

2.1.3 Form and Location of Fireside Deposits

Fireside problems in steam-raising boilers include slagging, fouling and corrosion. Slagging and fouling represent two forms of deposit problems, and they are found in different parts of a boiler. Slagging stands for the deposition of fly ash on heat transfer surfaces in the furnace primarily subject to radiant heat transfer. Bryers (1996) stated that, although the name "slag" suggests a molten or semi-molten ash, the term "slagging" may also applied to sintered deposits and dry ash formed in liberally-sized, low-pressure steam generator furnaces, or in furnaces fired with coals containing high moisture and alkaline earth ash. Due to their high temperatures, slagging deposits can be partially or completely molten, and they are chemically active. The original chemical and physical structures of ash particles undergo substantial changes during slagging. Slagging deposits are often hard, and thus are difficult to clean by soot blowing. Fouling consists of deposit formation in the heat recovery section of a boiler subject to convective heat transfer. At this location, the fly ash is quenched to a temperature below its melting range and the ash vapors are condensed. The deposits created by fouling may vary from light sintering to complete fusion. Typically, the original chemical and physical structures of ash particles are retained in the impacted particles. Figure 2.6 shows a schematic of the locations where slagging and fouling occur in a typical steam-raising boiler.

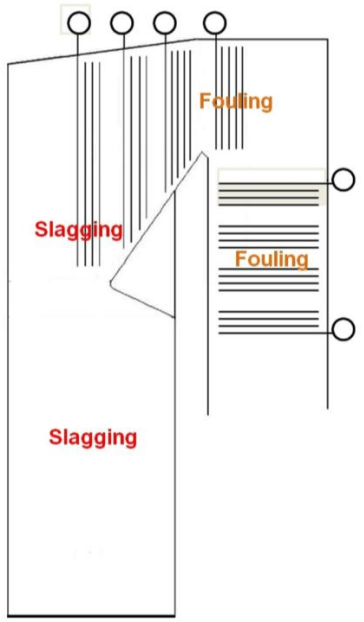

Figure 2.6: Schematic distribution of slagging and fouling in a typical steam-raising boiler: slagging on the furnace wall and the superheater tubes subject to radiant heat transfer and fouling on convective heat transfer tube banks.

The relative importance of various ash particle transport mechanisms also differs across distinct parts of a boiler. In the furnace of a boiler, the furnace wall and the first few rows of superheater tubes exposed to the furnace gas are more prone to slagging. In this location, inertial impaction plays a dominant role in the deposit growth and leads to the formation of a coarse-grained deposit. On the other hand, thermophoresis, condensation, and different diffusion processes may give rise to fouling problems on the heat exchange tubes in the convective pass. The deposits here are fine-grained and more evenly distributed around the tubes (Zbogar et al., 2009). For a superheater tube directly exposed to the furnace gas, all the ash particle transport mechanisms can contribute to the deposit formation. As shown in Figure 2.7, on the windward side of the tube, mountain-shaped, coarse-grained deposits form mainly due to inertial impaction. On the lee side of the tube, more evenly distributed, fine-grained deposits form due to thermophoresis and diffusion of smaller ash particles.

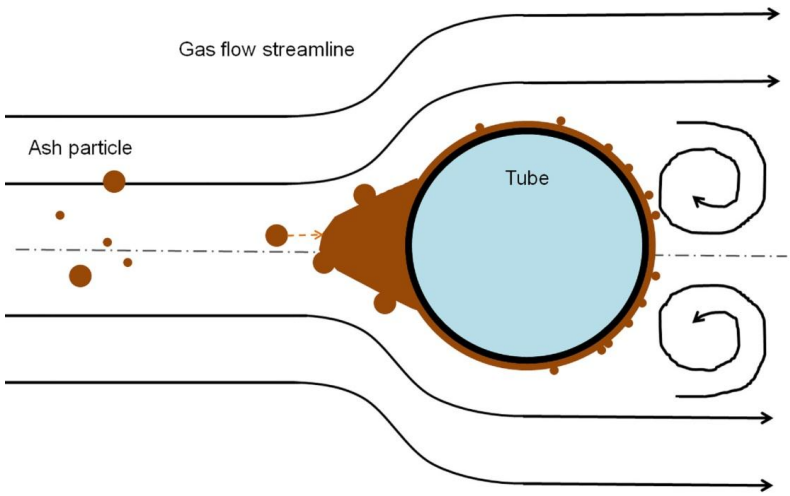

Figure 2.7: Example of deposit formation on a superheater.

Different types of deposits are built up during various stages of deposit formation on a clean surface (e.g., the furnace walls and tubes in a new boiler, or the superheater tubes after a soot-blowing session). Generally, thermophoresis, condensation and diffusion processes are important at the earlier stage of deposit formation. For example, thermophoresis is more significant at the early stage because the temperature gradient in the thermal boundary layer of a clean heat transfer surface is steep. The temperature gradient then decreases, since the deposits lead to a higher surface temperature. Condensation is also important at the early stage. The condensate can increase the contacting area, not only among the deposit particles but also between the deposit particles and the heat transfer surface, by several orders of magnitude (Baxter, 1993). Inertial impaction normally becomes significant for deposit formation after a layer of fine-grained deposits has formed on the heat transfer surface, because particles impacting on a clean surface are less likely to stick. However, inertial impaction can also be important on a clean heat transfer surface in cases where the impacting ash particles are

molten and very sticky. This is the case in Kraft recovery boilers where the alkali-rich, low-melting-temperature ash particles are fully molten and sticky at the entrance to the superheaters.

2.1.4 Evolvement of Fireside Deposits

Fireside deposits consist of characteristics such as the morphology, the thickness, the binding strength, the thermal properties (e.g., emissivity and conductivity), and the corrosivity. These characteristics are affected by the composition of the deposits; the pattern and velocity of the gas flow; the temperature in the furnace; and the temperature of the heat transfer surface. Fireside deposit formation is a dynamic process; evolvement of the fireside deposits, which is often accompanied by phase change, includes growth, sintering, and shedding.

Growth

The growth of deposits is mainly caused by the capture of ash particles transported by the above-mentioned mechanisms. Not all ash particles arriving at a heat transfer surface, either clean or covered with a layer of deposits, will remain there. Some particles will rebound; others can cause erosion of the deposit layer. In addition to the above-mentioned physical transport mechanisms, chemical reactions between furnace gases and the deposits also contribute to the deposit growth.

In some circumstances, the continuous growth of deposits leads to blockage of the gas path in the superheater region and in the convective pass. In other circumstances, the surface temperature of the deposits increases as the deposits grow; this leads to melting of the deposits, which then run down along the heat transfer surface (referred to as the slagging wall in this work). Although the molten deposits are sticky, the deposit layer may stop growing as later-arriving ash particles become molten and flow away. At this point, the thickness of the deposit layer comes to a stable state. Certain furnaces, e.g., the slag-trap furnace and the entrained flow gasifier, are designed to have ash removed by slagging.

Sintering

Sintering describes the particle-to-particle attachment in the deposits at high temperatures. Zbogar et al. (2009) reviewed several types of sintering that differ in their mechanisms of mass transfer. In the evaporation-condensation sintering process, material transfer occurs due to the differences in vapor pressure at different parts of the system. The differences in vapor pressure exist because of the varying surface curvatures at the particle surface and the particle neck area. At the particle surface, the radius of curvature is positive, which gives rise to a higher vapor pressure. At the particle neck area that connects the particles, the radius of curvature is negative, leading to a lower vapor pressure. Liquid state sintering depends on the amount and on the properties of the melt forming in the system. Chemical reaction sintering occurs when the reaction products form the neck between the particles. The chemical reactions occur among the particles or between the particles and the gas phase. Solid state sintering is generally a slower process than sintering processes that involve melt. Material transfer in the solid state sintering process includes vapor transport; surface diffusion from the particle surface; lattice

diffusion from the particle bulk; and grain boundary diffusion. Sintering increases the contact among the ash particles in a deposit.

Shedding
The process of deposit removal from the heat transfer surfaces can be defined as deposit shedding. Zbogar et al. (2009) presented a comprehensive review on shedding of ash deposits and on their relevant characteristics. Shedding of ash deposits can occur spontaneously due to erosion by non-sticky ash particles, gravity force and thermal stresses. Shedding of deposits can also be induced artificially, e.g., by soot-blowing or load change. The mechanisms involved in either spontaneous or artificial shedding include erosion; gravity shedding; melting; thermal shock; brittle break-up; and debonding. The characteristics of the deposits determine the dominant shedding mechanisms in different parts of a boiler. The strength of the deposits, e.g., compressive, bending and tensile strength, affects erosion, gravity-shedding and brittle break-up mechanisms. The viscosity and the melting behavior of the deposits govern the gravity-shedding mechanisms. The thermal expansion coefficients of the deposits and the tube materials influence the shedding of deposits due to thermal shock. The debonding mechanism for hard deposits is influenced by the adhesion strength between the deposit and the tube surface.

2.2 MODELING OF FIRESIDE DEPOSIT FORMATION

2.2.1 Sticking Criteria

Identifying the criteria for determining whether an ash particle will deposit, i.e., the sticking propensity of the particle, is an important aspect of the deposit formation problem, and is an essential component in a model of deposit formation. Weber et al. (2013a) reviewed three approaches for estimating the sticking propensity of an ash particle on a heat transfer surface.

The first approach is the critical velocity approach, which compares the kinetic energy of a particle and the energy dissipated at the impaction (Thornton & Yin, 1991) (Thornton & Ning, 1998). If the energy dissipated at the impaction is larger than the kinetic energy of the particle, the particle is judged to stick. Otherwise, if the particle has more kinetic energy than the energy dissipated by the collision, the particle is judged to rebound. A critical particle velocity $\left|\overrightarrow{U_c}\right|$ is determined for the situation at which the kinetic energy of a particle equals the energy dissipated at the impaction. Then the absolute value of the particle velocity $\left|\vec{U}\right|$ or its normal component $\left|\overrightarrow{U_n}\right|$ can be compared with the critical velocity. The particle will stay on the surface when

$$\left|\vec{U}\right| \leq \left|\overrightarrow{U_c}\right| \text{ or } \left|\overrightarrow{U_n}\right| \leq \left|\overrightarrow{U_c}\right| \qquad (2\text{-}18.).$$

This approach, however, is more frequently used in particle technology to estimate the bouncing probability of solid particles impacting on a clean surface.

The second approach is the viscosity-based method. This method has been used to determine the sticking propensity of molten coal ash particles. Coal ash particles mainly

consist of silicates, which form a viscous liquid. The viscosity-based method has two forms. In one form, the viscosity of fly ash μ_{ash} is calculated as a function of the temperature and the composition of the ash particle (Urbain et al., 1981). Then a critical viscosity μ_c is used as a criterion to determine the sticking propensity of an ash particle. Walsh et al. (1990) developed a commonly-used model:

$$Sticking\ probability = \min(\frac{\mu_c}{\mu_{ash}}, 1) \quad (2\text{-}19.)$$

Here, the sticking probability of an ash particle is inversely proportional to its effective viscosity if the effective viscosity is larger than the critical viscosity. If the effective viscosity is smaller than the critical viscosity, the sticking probability equals one. Weber et al (2013a) offers several examples of critical viscosity; these clearly show that the critical viscosity is coal-dependent. The other form of the viscosity-based method uses the temperature of critical viscosity as the criterion. The temperature of critical viscosity is the temperature at which an abrupt change occurs in the viscosity-temperature relationship; it depends on the composition of the ash. Here, the ash particle will stick to the heat transfer surface if its temperature is higher than the temperature of critical viscosity.

The third approach addresses the melting behavior of the ash. The ash fusion test has been historically the most frequently-used method for assessing the slagging propensity of coal. Bryers (1996) summarized the standard ash fusion test methods from different countries and organizations. Usually, the softening temperature of the sample from the ash fusion test is used as the criterion to determine the sticking propensity of ash particle, for example in the work of Epple et al. (2005). If the particle temperature is higher than the softening temperature, then the particle is judged to be able to stick. The use of the melt fraction as the sticking criterion started with the study on deposition problems in Kraft recovery boilers (Isaak et al., 1986) (Backman et al., 1987). Isaak et al. (1986) reported that a strong adhesion occurred when the melt fraction of fly ash particles exceeded 18-20%. Generally, melting curves of deposits are produced by using differential thermal analysis (DTA) or by performing thermodynamic calculations. From the melting curve, the temperatures corresponding to certain melt fractions can be obtained: e.g., T_0 the first melting temperature, T_{15} the sticky temperature, T_{75} the flowing temperature and T_{100} the complete melting temperature (Backman et al., 1987). If the temperature of the impacting fly ash particle is higher than the sticky temperature but lower than the flowing temperature, the particle will be judged to stick. In another work, T_{10}, i.e., the temperature corresponding to 10% melt fraction in the deposit, is used as the sticky temperature (Zhou et al., 2007). This method of utilizing the melting curve of deposits has lately been more frequently applied in the prediction of deposit formation in biomass combustion (Mueller, 2005a) (Kær et al., 2006) (Zhou et al., 2007) (Akbar et al., 2010). For the second and the third approaches, the stickiness of both the ash particle and of the heat transfer surface with a deposit layer should be taken into account.

2.2.2 Deposit Formation Models

As mentioned earlier, fireside deposit formation in steam-raising boilers is a complex phenomenon. Wang and Harb (1997) summarized the issues to be addressed in a fundamentally-based deposition model: (1) ash formation; (2) fluid dynamics and ash particle transport; (3) particle impaction and sticking; (4) deposit growth as a function of location in the combustion chamber; (5) deposit properties and strength development; (6) heat transfer through the deposit; (7) the effect of deposition on operating conditions; e.g., temperatures and heat fluxes, in the combustor; and (8) deposit structure and its effect on flow patterns in the combustion facility.

Over the years, deposit formation models with varying emphases and complexities have been developed to aid in the design and operation of boilers. Zhou et al. (2007) catalogued the models into three levels: empirical indices models; mechanistic models; and computational fluid dynamics (CFD) models. Traditionally, empirical indices are calculated to predict the severity of coal ash deposition. In the mechanistic models, the calculations of the combustion processes and of the fluid dynamics are simplified. The mechanistic models have been used for assessing ash deposition tendencies and for predicting ash deposit behavior. CFD models include detailed information on the combustion processes and the fluid dynamics, aside from sub-models describing fundamental mechanisms of ash particle transportation and deposition. This section presents examples from the literature of different deposit formation models, including a more detailed description of three slagging wall models.

Empirical Indices Models

For coal, empirical indices based on ash fusion, viscosity and ash chemistry have been widely used in industry for boiler design and coal selection (Wang & Harb, 1997). In his comprehensive review of the fireside ash problems, Bryers (1996) presented the historical evolvement of the empirical approach, including the indices to characterize the slagging and fouling potentials of impurities in fuels. A commonly-used fouling index is the base-to-acid ratio (Jenkins et al., 1998):

$$R_{b/a} = \frac{Fe_2O_3+CaO+MgO+K_2O+Na_2O}{SiO_2+TiO_2+Al_2O_3} \quad \text{(2-20.)},$$

where M_xO_y represents the corresponding weight concentration of the compound in the ash. The melting temperature of ash tends to be a parabolic function with respect to $R_{b/a}$, and for coal, it often reaches a minimum when $R_{b/a}$ is 0.75 (Jenkins et al., 1998). The empirical indices are derived from average chemical properties of the coal and ash, and they do not adequately account for the complex heterogeneous chemistry that actually exists. In addition, they do not consider the effects of operating conditions on the deposits. Therefore, although the empirical indices are widely used, they are usually restricted to one type of coal and to certain operating conditions in a boiler.

The indices developed for coal are of limited value for biomass fuels. A recent review of indices for biomass fuels can be found in the work of Sommersacher et al. (2012). Jenkins et al. (1998) suggested the alkali index as a threshold indicator for fouling and

slagging. The alkali index describes the ratio between the amount of alkali oxide in the fuel and the heating value of the fuel (Jenkins et al., 1998),

$$Y_f^a\left(Y_{K_2O}^a + Y_{N_2O}^a\right)/Q \quad \text{(2-21.)},$$

where Y_f^a is the mass fraction of ash in the fuel; $Y_{K_2O}^a$ and $Y_{N_2O}^a$are the mass fractions of K_2O and Na_2O in the ash; and Q is the heating value of the fuel, for which the higher heating value is commonly used. Miles et al. (1995) suggested that fouling is probable when the alkali index is above 0.17 kg/GJ, and that it is virtually certain to occur when the index is above 0.34 kg/GJ. The threshold levels of the alkali index are principally empirical. The alkali index is useful as a general guide, although it is not a complete descriptor of fouling behavior (Jenkins et al., 1998). Another index is the stoichiometric ratio of Cl and S to the alkali K and Na in the fuel (Robinson et al., 2002),

$$(Cl + 2S)/(Na + K) \text{ (2-22.)},$$

which can indicate the potential formation of low-melting alkali sulfates and chlorides. However, this ratio neglects the actual availability and reactivity of the reactants. Theis (2006) pointed out that the alkali can also be bound as silicates, or that the reactants may not all meet. As is the case for the indices for coal, the indices for biomass fuels are also sensitive to the composition of the fuel and ash, and they depend on the combustion conditions.

Mechanistic Models

Based upon deeper knowledge of the characteristics of the fuel and ash, and of the physical and chemical processes involved in deposit formation, mechanistic models have been developed to assess deposit formation tendencies and to predict deposit formation behavior. A mechanistic model may address different aspects of deposit formation, e.g., the composition and occurrence of ash-forming matter; the transformation of ash-forming matter; and the deposition processes. The mechanistic models can also be applied more generally than is the case with the empirical indices.

Mechanistic models of deposit formation were first applied to coal-fired boilers. The pioneering modeling works of coal ash formation and deposition have been reviewed by Bryers (1996) and Wang and Harb (1997). Beér et al. (1992) presented a model for prediction of the fouling tendency of coal. Their model used fuel characterization by computer-controlled scanning electron microscopy (CCSEM) as input. The size and composition distributions of fly ash were predicted using a partial coalescence model. Beér et al. (1992) calculated the impaction probability of fly ash particles with the effective Stokes number, and used a critical viscosity as the sticking criterion. Their model was used to determine the relative fouling tendencies of different types of coal; the results compared favorably with experimental data collected in a 1-2 MW flame tunnel (Barta et al., 1994). However, their model does not take into account the boiler design aspects or any deposit removal processes. Benson et al. (1993b) used a mechanistic model for ash formation and deposition as a measure to help minimize ash deposition. Their model utilized a microscopic analysis and a step-leaching chemical fractionation

analysis of the coal mineral matter as inputs, and included eight indices: Na content; Ca content; total mineral content; content of organically-bound minerals; content of small quartz particles; ratio of included vs. excluded minerals; calcite content; and clay content. Baxter and DeSollar (1993) presented a deposit formation model that addressed the different ash transport mechanisms and the composition of deposits. Their model was tested in a 600 MW pulverized coal combustor. More examples of mechanistic models for coal ash deposition can be found in the works of Huang et al. (1996), Hecken et al. (1999), and other authors.

Baxter (1993) also addressed the mechanistic approach for ash deposition during biomass combustion. He noted that most of the mechanistic approaches developed for coal combustion also hold for biomass fuel boilers. However, the relative importance of the mechanisms differs substantially due to different compositions and behaviors of the fuel and ash. For biomass fuels, the content of the molten phase is more frequently-used as the sticking criterion for fly ash particles, whereas a critical viscosity is normally used for coal ash. Zhou et al. (2007) presented a dynamic mechanistic model of superheater deposit growth and shedding in a biomass-fired grate boiler. The model was developed and validated based on a horizontal cooled probe in the boiler. Measured flue gas temperature, ash particle size distribution and chemical composition of the fly ash were used as input parameters. The model includes sub-models of ash drop formation and detachment based on Bond number; deposition due to inertial impaction; thermophoresis; Brownian and eddy diffusion and condensation; deposition on the downstream side of the tube due to large-scale eddies; a correlation of the ash melt fraction as a function of the temperature and chemical composition; and deposit shedding by melting.

CFD Models

More detailed sub-models for the individual deposit formation steps have been incorporated into the mechanistic models; however, the calculations of the combustion processes and the fluid dynamics are normally simplified. The combustion processes in the boiler and the fluid dynamics of the flow have significant influences on deposit formation by altering particle residence time; particle motion; mixing processes; temperature distribution; and heat transfer rate. Therefore, combining deposit formation models with CFD models presented a logical next step. Wang and Harb (1997) and Lee and Lockwood (1999) have reported examples of earlier work on CFD simulation of ash deposition in coal fired facilities. Weber et al. (2013a) provided a review of the relevant work carried out in the past decade; they created a table summarizing those works on CFD-based predictions of deposit formation in industrial boilers. Table 2.1 presents an adaptation of their table with inclusion of the two earlier works.

Weber et al. (2013a) also discussed the details of the sub-models used for CFD prediction of ash behavior. The sub-models cover most of the eight issues summarized by Wang and Harb (1997) outlined at the beginning of Section 2.2.2. Some of the sub-models can be found in the earlier-mentioned mechanistic models, while some are based on CFD models. Figure 2.8 below is based on their discussion and summarizes the various sub-models for deposit formation. The sub-models focus on three subjects of the problem: the

gas phase; the ash; and the deposits. In the case of combustion furnaces, these three subjects are closely aligned with one another.

Table 2.1: CFD-Based Predictions of Deposit Formation in Industrial Boilers, adapted from Weber et al. (2013a).

Work	Boiler/fuel	Mathematical model
Kær (2001) Kær et al. (2006)	Grate-fired boiler, CHP (Combined Heat and Power) Plant, Masnedø, Denmark Fuel: straw Deposit regions considered: free-board; platen superheaters; and tube banks	Fluent CFD code Ash formation model for grate combustion of straw; ash transport through inertial impaction and thermophoresis; ash sticking propensity determined using melting curves for potassium salts and silica-rich particles
Forstner et al. (2006)	Grate-fired 440 kW_t boiler Fuel: waste wood Deposit regions considered: combustion chamber walls; fire tube walls	Fluent CFD code Ash release model for grate combustion of wood; ash release model for ash-forming vapors; ash transport through inertial impaction and condensation of vapors; ash sticking propensity determined using Urbain (1981) viscosity model
Epple et al. (2005)	330 MW_e boiler of Meliti Achlada Florina, Greece Fuel: brown coal Deposit regions considered: furnace walls	FLOREAN code of TU Braunschweig Fly ash properties predicted using a coal combustion model; ash transport through inertial impaction; ash sticking propensity based on ash fusion temperature
Mueller et al. (2003)	105 MW fluidized bed boiler, CHP plant, Idbäcken, Nyköping, Sweden Fuel: wood Deposit regions considered: Free-board; secondary combustion chamber; boiler walls	Fluent CFD code Ash formation model includes fly ash and bottom ash fractions, which are determined using chemical fractionation analysis; ash transport through inertial impaction; ash sticking propensity determined using melting curves for the fly ash; sticking temperature corresponds to 15 wt.% of molten phase in the fly ash
Fan et al. (2001)	300 MW_e tangentially-fired boiler Fuel: hard coal Deposit regions considered: boiler walls	In-house CFD code Fly ash properties predicted using a coal combustion model; ash transport by inertial impaction; ash sticking propensity using a critical viscosity model
Eddings et al. (2001)	900 MW_e tangentially-fired boiler Fuel: bituminous coal	GLACIER code of Reaction Engineering International Fly ash properties predicted using a coal char combustion model;

	Deposit regions considered: boiler walls	separate treatment of extraneous and included pyrite; ash transport by inertial impaction, turbulent eddy transport and thermophoresis; ash sticking propensity based on the critical particle temperature T_{250} of the fly ash
Schnell et al. (2001)	450 MW_e German boiler Fuel: brown coal Deposit regions considered: boiler walls	AIOLOS code of IVD of Stuttgart Fly ash amount and size distribution are model inputs; ash transport through inertial impaction, turbulent eddy transport and thermophoresis; ash sticking propensity determined using linear dependence of the sticking probability with temperature; effects of the deposit on heat transfer rates are determined
Bernstein et al. (1999)	800 MW_e boiler, Schwarze Pumpe, Germany Fuel: brown coal Deposit regions considered: boiler walls	Fluent CFD code Fly ash properties predicted using a coal char combustion model; ash transport by inertial impaction; ash sticking propensity expressed as a product of three terms: melting temperature function, particle concentration function and oxygen concentration function
Lee and Lockwood (1999)	Pilot scale single burner ash deposition test facility Fuel: UK coals, Bentinck, Daw Mill and Silverdale	CINAR code CCSEM fly ash data used as input; arrival rate of fly ash particles characterized by a "critical velocity" and a predefined displacement thickness; ash sticking propensity determined using Urbain (1981) viscosity model; effect of deposition on furnace performance considered
Wang and Harb (1997)	85 MW_e tangentially-fired, forced recirculation pulverized coal unit, Goudey station power plant, U.S. Fuel: bituminous coal Deposit regions considered: boiler walls	PCGC-3 code Fly ash impaction rate determined with a statistically-based particle cloud model; ash sticking propensity determined from viscosity of the particles and the deposit surface; a description of deposit growth as a function of operating conditions included; effect of deposition on operating conditions in the boiler considered

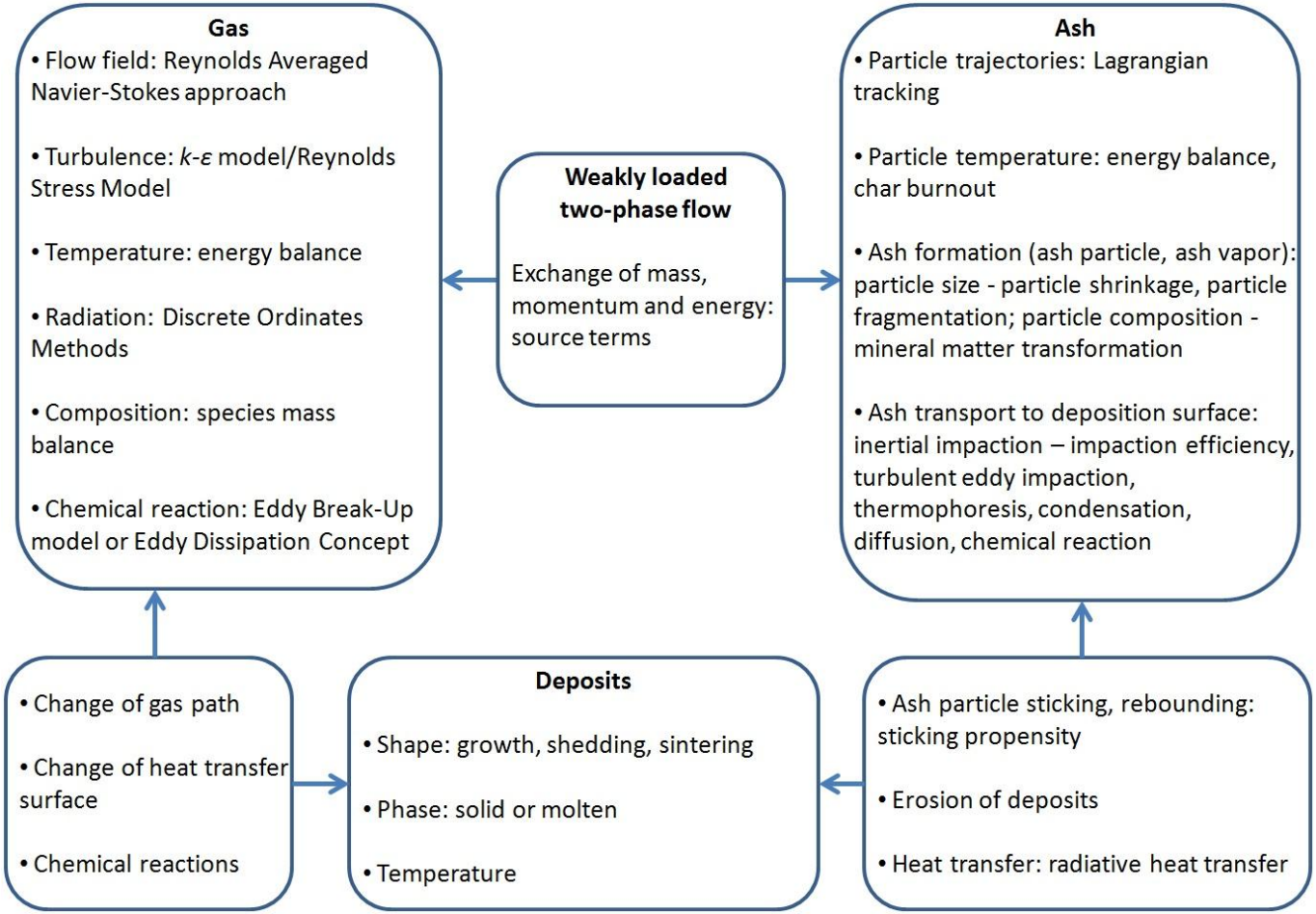

Figure 2.8: Sub-Models for gas, ash and deposits and their interactions in the deposit formation problem.

Weber et al. (2013a) also pointed out the shortcomings in the practice of applying some of the sub-models, as listed below.

a) A certain degree of accuracy is needed in calculating the time-temperature/chemistry history of fuel/ash particles, with information about high-temperature devolatilization and char burning obtained by fuel characterization experiments. The rate of char oxidation for the last 20% of burnout is of particular importance.
b) Fragmentation of fuel particles remains unsolved.
c) An accurate prediction of impaction efficiency for inertial impaction of ash particles is needed. Weber et al. (2013a) stated that this is obtainable with CFD codes only when the flow field in the neighborhood of the deposition surface is accurately resolved. In another work of Weber et al. (2013b), the requirements for accurate predictions of particle impaction on tubes using RANS-based computational fluid dynamics are discussed in more details.
d) Development and validation of mineral transformation models based on fuel characterization, e.g., SEM for particle size, shape and composition of mineral matters, and thermal gravimetric analysis (TGA) for reaction rate.
e) Procedures to determine the ash particle sticking propensity by using melting curves or thermodynamic calculations should be validated.
f) Development of deposits, e.g., reactions, sintering, and shedding, should be studied further.

Weber et al. (2013a) concluded that the current CFD predictions of slagging and fouling in industry boilers are suggestive at best. However, the problems can be tackled by combining CFD predictions with application-dependent advanced fuel characterization.

2.2.3 Slagging Wall Model

As mentioned earlier, deposit growth results in a higher heat transfer resistance between the furnace cavity and the cooling medium (water/steam), thus leading to a higher temperature at the heat transfer surfaces, or more precisely, at the deposits on the heat transfer surfaces. The increase in temperature can lead to melting of the deposits. At some point, the molten deposits start to flow, and a running fluid layer forms on top of the solid deposit layer. The fluidity of the molten deposits depends on the composition of the deposits and on the temperature. The deposits may start to flow when they are not yet fully molten, and may behave as non-Newtonian fluids (Zbogar et al., 2009). If the mass flow of the molten deposits flowing away is in balance with the mass flow of the arriving materials, deposit formation reaches a steady state. In this case, a slagging wall is used to describe a heat transfer surface with flowing molten deposits, as illustrated in Figure 2.9. A slagging wall model may take into account the thicknesses of the solid and the molten deposit layers; the temperatures at the interfaces; and the heat transfer through the slagging wall.

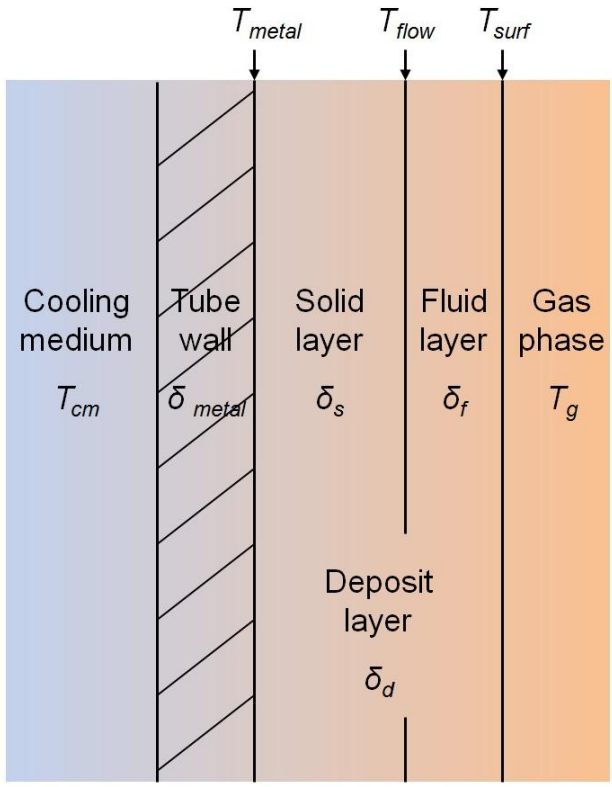

Figure 2.9: A schematic illustration of the slagging wall with a two-layer structure of the ash deposits.

The slagging wall is considered in the modeling of coal-fired cyclone combustors by Boysan et al. (1986). In cyclone combustors, the ash builds up on the walls until an equilibrium thickness is reached. At the equilibrium thickness, the temperature at the deposit surface is sufficiently high that a molten layer is formed and is subsequently removed by gravity or by aerodynamic drag. The coal particles injected into the combustion chamber are centrifuged by a swirling flow onto the molten ash layer, and they are mostly retained and burned on the layer. The work of Boysan et al. (1986) assumed that at steady state conditions, the molten slag-coal mixture on the combustion chamber walls descends toward the bottom of the chamber at a rate dictated by continuity. The flowing temperature T_{flow} was estimated in the range of 1360-1470 °C for coal ash with a silica ratio in the range of 64-88. Accordingly, a slag surface temperature T_{surf} of 1700 K was used as the wall boundary condition, except where the nearby gas temperature was lower, at which locations the wall was assumed to be adiabatic. An emissivity of 0.6, typical of glassy deposits, was used for the slag.

Richards et al. (1993) presented a model for time-dependent simulation of deposit growth under slagging conditions in a pulverized coal-fired pilot scale reactor. The properties of the deposit, i.e., porosity, thermal conductivity, and emissivity, were first calculated for

each time-step in the simulation. The porosity of the deposit φ was obtained using the following equation:

$$\varphi = 1 - \left[(1 - \varphi_0) + \frac{V_l}{Vs}(1 - \varphi_0)\right] \quad (2\text{-}23.).$$

φ_0 is the initial porosity of the deposit, assumed to be 0.6; V_l is the volume of the liquid; and V_s is the volume of the solid. The depositing ash particles were assumed to approach their equilibrium composition if their viscosity at the local deposit temperature was below a critical value (10^4 Pa s). The phase composition of the deposit was then determined based on the phase composition of the particles at equilibrium. Richards et al. (1993) used a correlation from Sugawara and Yoshizawa (1961) to calculate the thermal conductivity of the porous deposit,

$$k = \left(1 - F_g\right)k_s + F_g k_g \quad (2\text{-}24.),$$
$$F_g = \frac{2^n}{2^n - 1}\left(1 - \frac{1}{(1+\varphi)^n}\right) \quad (2\text{-}25.),$$

where k_s is the thermal conductivity of the solid, assumed to be constant at 4 W/m-K; k_g is the thermal conductivity of the gas phase, approximated as that of nitrogen at the local deposit temperature; F_g describes the fraction of the conductivity attributable to the gas phase; and *n* is an empirical parameter, which is 6.5. Following the calculations of the properties of the deposit, the mass and thickness increments of the deposit layer were calculated based on the deposition rate and on the time step size. The thermal resistance of the deposit *R* was then calculated as the accumulative value of the individual deposit layers formed in each time step:

$$R = \sum_{i=1}^{N} \frac{\delta_i}{k_i} \quad (2\text{-}26.).$$

Finally, the surface temperature of the deposit T_{surf} and the heat flux from the gas phase to the deposit q_{tot} were calculated with an iterative procedure based on the following equations:

$$q_{tot} = h\left(T_g - T_{surf}\right) + \epsilon(q_{inc} - \sigma T_{surf}^4) \quad (2\text{-}27.),$$
$$T_{surf} = q_{tot}R + T_{metal} \quad (2\text{-}28.),$$

where q_{inc} is the incident heat flux and T_{metal} is the temperature at the metal tube wall surface, as shown in Figure 2.9. The work of Richards et al. (1993) did not consider the effects of erosion and periodic shedding of deposits, and the formation of a running slag layer presumably did not occur in the pilot scale reactor.

In the work of Seggiani (1998), the modeling is focused on the slag flow on the internal wall of a Prenflo entrained-flow gasifier. The gasifier is designed so that most of the ash leaves as molten slag, either downward along the wall or directly through the tap hole. The molten coal ash particles are transported to the wall of the gasification chamber by

the intensive centrifugal gas flow. The slag building model from Seggiani (1998) can determine the thicknesses of the solid and liquid layers of the slag deposit; the temperature across the deposit; and the heat flux to the metal wall. The model was developed on the basis of the following assumptions:

a) The transition temperature between the solid and liquid slag layers is the temperature of critical viscosity for the coal ash, $T_{flow} = T_{cv}$.
b) The flow of liquid slag is Newtonian, and the flow at the temperature below T_{cv} is negligible.
c) The shear stress between the gas and the slag layer is negligible.
d) The temperature profile across the slag layer is linear.
e) The heat transfer occurs normal to the surface.
f) The model is written in linear coordinates, owing to the large difference between the slag deposit thickness and the gasifier radius.
g) The density, specific heat and thermal conductivity of the slag are independent of temperature.

Seggiani (1998) applied the slag-building model in simulations of the gasifier. The gasification chamber was divided into 15 cells in the axial direction, and the mass, energy and momentum conservation equations were written for each cell. From the momentum conservation equation, Seggiani (1998) derived an analytical expression for the mass flow rate of the liquid slag leaving one cell. The momentum conservation equation for an element at the horizontal position x in the liquid slag layer is given as the force balance between the shear stress and the gravitational force (Bird et al., 2007),

$$\frac{d}{dx}(\mu(x)\frac{dv}{dx}) = -\rho g\cos\theta \qquad \text{(2-29.)},$$

where $\mu(x)$ is the viscosity; dv/dx is the velocity gradient; g is the gravity acceleration; and θ is the slope of the wall. At the surface of the liquid slag layer, a zero-gradient boundary condition is used for the velocity. At the interface of the liquid layer and the solid layer, a non-slip boundary condition is used. Assuming a linear temperature profile across the liquid slag layer, the relationship between the viscosity and the position can be written as (Bird et al., 2007)

$$\mu(x) = \mu(\delta_f)\exp(-\frac{\alpha x}{\delta_f}) \qquad \text{(2-30.)},$$

with $\alpha = -\ln(\mu(0)/\mu(\delta_f))$ and δ_f is the thickness of liquid slag layer. Equations (2-29.) and (2-30.) give

$$v(x) = \frac{\rho g\cos(\beta)\delta_f^{\,2}}{\mu(\delta_f)}\left[\exp(\alpha)(\frac{1}{\alpha}-\frac{1}{\alpha^2}) - \exp(\frac{\alpha x}{\delta_f})(\frac{x}{\alpha\delta_f}-\frac{1}{\alpha^2})\right] \qquad \text{(2-31.)}.$$

By integrating Equation (2-31.) through the liquid slag thickness, the mass flow rate of the liquid slag leaving the cell is obtained as

$$\dot{m} = \frac{L\rho^2 g \cos(\beta)\delta_f{}^3}{\mu(\delta_f)} \left[\exp(\alpha)\left(\frac{1}{\alpha} - \frac{2}{\alpha^2} + \frac{2}{\alpha^3}\right) - \frac{2}{\alpha_3} \right] \qquad (2\text{-}32.),$$

where L is the perimeter of the cell. Other details of the slag-building model from Seggiani (1998) are available in the original literature.

Wang et al. (2007) presented a slag sub-model for modeling of a coal-fired slagging combustor. In the slagging combustor, a molten slag layer covers the wall and captures the depositing particles. In their slag model, the thickness and the average flow velocity of a running slag element are calculated based on the force balance and the mass balance. The force balance considers the shear stress and the gravitational force, with the same expression as Equation (2-29.). However, the shear stress in their model includes both the viscous stress in the running slag and the shear stress on the surface of the running slag induced by the swirling gas and the depositing particles.

2.3 ÅBO AKADEMI FURNACE MODEL

The Åbo Akademi Furnace Model is a compilation of application-specific sub-models and pre- and post-processing software around a generally-applicable flow solver. It is based on a commercial multi-purpose CFD code, FLUENT™ (2013), that has been customized by several specific sub-models for simulation of combustion and gasification processes (Mueller et al., 2005b).

Standard models found in the CFD code and used in the furnace model include the turbulence model; the radiation model; and the discrete phase model (DPM). A standard k-ε turbulence model is used for prediction of the turbulent fluid flow and related turbulent quantities. Radiative heat transfer is calculated with the Discrete Ordinate Radiation Model. In the discrete phase model, particle trajectories are predicted by integrating the force balance around the particle. The force balance is written in a Lagrangian reference frame and accounts for drag and gravitational forces. The influence of turbulent flow on the particle is determined by a stochastic tracking approach using instantaneous fluid velocity; it requires calculations for a sufficient number of particles. More details of the standard models are available in the user's manual of the CFD code (FLUENT, 2013).

The customized process-specific sub-models include droplet and particle conversion models; furnace bed models; particle deposition models; and sub-models for predicting gas-phase combustions, including emission chemistry. For black liquor recovery furnaces, a black liquor droplet model describes the different burning stages of a droplet in-flight, and it takes into account the exchange of mass and energy with the gas phase using the source terms (Mueller et al., 2002) (Järvinen et al., 2007). For chemical conversion of the volatiles released from the black liquor droplet, the methane conversion mechanism of Jones and Lindstedt (1988) is applied. The standard finite rate/eddy

dissipation model from the CFD code is used for the interaction of turbulent flow and chemical reactions. The emission chemistry is also included (Brink et al., 2001). A char bed model describes the burning process (Bergroth et al., 2004&2010) and the shape change (Engblom et al., 2008&2010a) of the black liquor recovery furnace char bed.

3. FURNACE ONE: KRAFT RECOVERY FURNACE

The black liquor recovery boiler is a crucial device in the Kraft chemical pulping line. Black liquor, from the fiber washing stage, contains almost all of the inorganic cooking chemicals, the organic matter separated from the fiber source materials, and water. Concentrated black liquor is burned in the recovery boiler furnace to recover the cooking chemicals and to make use of the energy in the organic matter (Adams, 1997). In this work, a sub-model for slagging wall in Kraft recovery furnace was developed and implemented into CFD. With the slagging wall model, the wall surface temperature and the heat transfer to the furnace wall were investigated.

3.1 SLAGGING WALL IN KRAFT RECOVERY FURNACE

On a dry basis, the content of the inorganic matters in black liquor, i.e., the ash content, is 40% to 50% (Tran H. , 1997). It includes almost all the inorganic cooking chemicals and the inorganic matter from the fiber source materials. Deposit formation is common in Kraft recovery furnaces; deposits can be found on the furnace walls and on the superheater tubes (Reeve et al., 1981) (Tran et al., 1983). Ideally, the deposits, which can become molten at certain locations, should fall off or flow down to the char bed in a controlled manner so that the cooking chemicals can merge back into the main chemical recovery stream.

The recovery furnace deposits consist of alkali compounds that have low melting temperatures. When the proportion of the deposits in the molten phase is less than 15%, build-up of the deposit layer is minimal because the ash particles rebound. When the proportion of the deposits in the molten phase reaches 15%, the ash particles have a higher propensity to stick to the wall. Hence, the temperature at which the proportion of the deposits in the molten phase reaches 15% is referred to as the "sticky temperature" T_{15} (Backman et al., 1987). If the temperature of the deposits is above T_{15}, the deposit layer continues to build up. When the temperature of the deposits rises and the deposits reach 70% molten phase, the deposits start to flow. The temperature of the deposits at this point is referred to as T_{70}, the "radical deformation temperature" or the flowing temperature (Backman et al., 1987). A two-layer structure is formed at locations where the deposits are flowing, as shown in Figure 2.9. The T_{flow} in the figure is equal to T_{70} here. The thicknesses of the two layers depend on the heat fluxes to the deposits, the steam temperature in the tubes and the physical properties of the deposits. The work of Tran (1997) includes a more detailed description of the mechanisms of ash deposition in Kraft recovery furnaces. Deposits can cause substantial additional thermal resistance and hinder the heat transfer to the metal tubes and to the steam. In the lower furnace, black liquor droplets undergoing different combustion stages can reach the furnace walls (Frederick, 1997). After landing on the wall, the droplets continue their combustion processes; the combustion reactions lead to temperature variations on the wall.

3.2 SLAGGING WALL MODEL

The development and application of the slagging wall model have been reported in Papers I, II, and III (see "LIST OF PUBLICATIONS"). In the slagging wall model, the thicknesses of the solid and fluid deposit layers, along with the surface temperature of the fluid running layer exposed to the inner furnace, can be calculated. The slagging wall

model is based on a force balance and a heat balance around an element of the molten deposit flow.

3.2.1 Force Balance

For the force balance, the gravitational force and the shear stress of a molten deposit element are considered, with application of the approach from Seggiani (1998) presented in Section 2.2.3. More specifically, the analytical expression of the mass flow rate of the molten deposits leaving the element (Equation 2-32.) is used to calculate the thickness of the fluid deposit layer. Here, the mass flow of the molten deposits $\dot{m}$ is an input. With the assumption that all the landing deposits are fully molten, the mass flow is the sum of the deposits landing on the element and the deposits flowing down from the element above. Another input to the force balance is the viscosity-temperature correlation of the deposits. The viscosity-temperature correlation is discussed in the test case descriptions in the following sections.

3.2.2 Heat Balance

Figure 3.1 illustrates the heat balance around one element of the running molten deposits at steady state. Here, the convective heat transfer from the gas phase to the deposit surface is neglected. $\dot{H}_{flowin}$ and $\dot{H}_{flowout}$ are enthalpy flow rates of the molten deposits flowing in and out of the element; $\dot{H}_{deposition}$ is the enthalpy flow rate of the impacting ash particles adding to the element; $\dot{Q}_{radiation}$ is the heat transfer rate from gas phase by radiation; and $\dot{Q}_{conduction}$ is the conductive heat transfer rate to the tube wall.

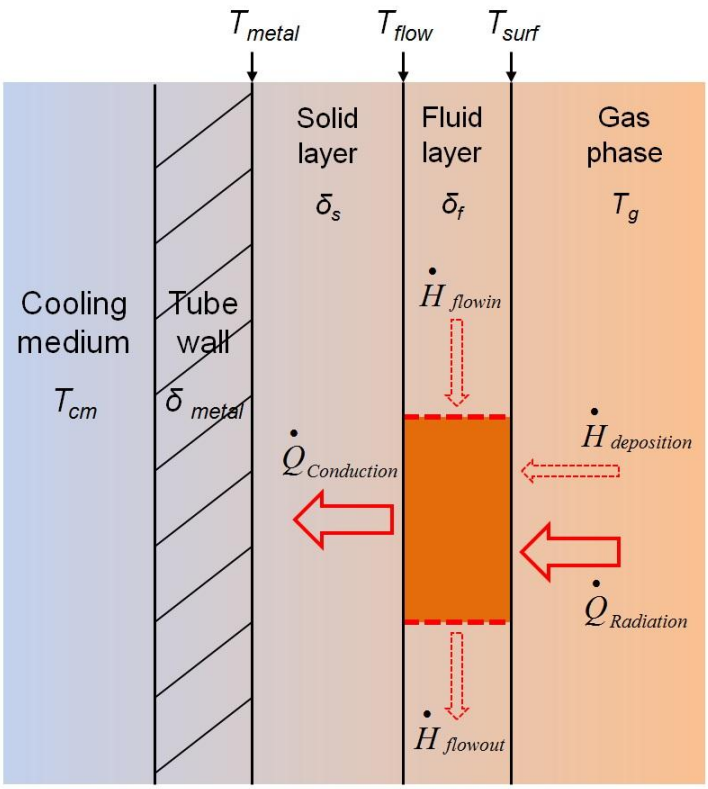

Figure 3.1: Components of the heat balance around a molten deposits element.

The heat balance is described with the following equation:

$$\dot{H}_{flowin} + \dot{Q}_{radiation} + \dot{H}_{deposition} = \dot{Q}_{conduction} + \dot{H}_{flowout} \quad (3\text{-}1.),$$

and

$$\dot{H}_{flowin} = \dot{m}_{flowin} c_p (T_{flowin} - T_{ref}) \quad (3\text{-}2.),$$

$$\dot{H}_{flowout} = \dot{m}_{flowout} c_p (T_{flowout} - T_{ref}) \quad (3\text{-}3.),$$

$$\dot{H}_{deposition} = \dot{m}_{deposition} c_p (T_g - T_{ref}) \quad (3\text{-}4.),$$

$$\dot{Q}_{radiation} = \alpha\varepsilon(T_g^4 - T_{surf}^4) \quad (3\text{-}5.),$$

$$\dot{Q}_{conduction} = \frac{T_{surf} - T_{flow}}{\delta_f / k_f} A \quad (3\text{-}6.),$$

$$\dot{m}_{flowin} + \dot{m}_{deposition} = \dot{m}_{flowout} \quad (3\text{-}7.),$$

where c_p is the specific heat of the molten deposit, assumed to be constant. k_f is the thermal conductivity of the molten deposit; T_{ref} is the reference temperature; T_g is the gas phase temperature; T_{surf} is the temperature at the deposit surface; and T_{flow} is the temperature at the interface of the solid and liquid deposit layers.

After the thickness of the running molten deposit layer is calculated, the heat flux through the running layer can be determined according to Equation (3-6.). The temperature at the interface of the solid deposit and the tube, i.e., the metal surface temperature T_{metal}, can be calculated according to the following equation:

$$T_{metal} = \frac{\dot{Q}_{conduction}}{k_{metal}A}\delta_{metal} + T_{cm} \qquad (3\text{-}8.),$$

where k_{metal} and δ_{metal} are the thermal conductivity and the thickness of the metal tube wall, respectively. The temperature of the cooling medium T_{cm} is assumed to be constant. The thickness of the solid layer δ_s can then be calculated:

$$\delta_s = \frac{T_{flow} - T_{metal}}{\dot{Q}_{conduction}/k_s}A \quad (3\text{-}9.).$$

where k_s is the thermal conductivity of solid deposit layer.

Simplification of the Heat Balance

In Equation (3-1.), if the mass flow rate of the impacting ash particles $\dot{m}_{deposition}$, i.e., the deposition rate, is small compared with the molten deposit flow on the wall $\dot{m}_{flowin}$ or $\dot{m}_{flowout}$, the term $\dot{H}_{deposition}$ can be neglected. In addition, if the temperature of the molten deposits is only slightly changed in one element, the term $\dot{H}_{flowin} - \dot{H}_{flowout}$ can be approximated to be zero. Thus, a simplified heat balance comprises only the radiation and conduction parts of Equation (3-1.):

$$\dot{Q}_{radiation} = \dot{Q}_{conduction} \qquad (3\text{-}10.).$$

The influence of the simplifications on the heat balance was examined in Paper III (see "LIST OF PUBLICATIONS"). Specifically, Paper III analyzed step changes in the temperature of molten deposits flowing in the element T_{flowin} and the deposition rate $\dot{m}_{deposition}$. They reflect the two input components $\dot{H}_{flowin}$ and $\dot{H}_{deposition}$ in the comprehensive heat balance, respectively. Contradicting results were obtained for the two cases considering the molten deposits in the Kraft recovery furnace and the slag in the coal gasifier. For the Kraft recovery furnace case, the variations in the surface temperature of the molten deposits and the radiation heat flux between the comprehensive heat balance and the simplified balance are small. However, this difference is relatively large for the coal gasifier case. The author conjectured that this contradiction related to the temperature of critical viscosity, i.e., T_{flow} in Figure 2.9 and Figure 3.1. In general, a lower temperature of critical viscosity leads to lower temperatures in the running molten

deposit layer and on the surface of the layer. This leads to dominance in the heat balance of the radiation heat flux, at typical gas phase temperatures in a black liquor recovery boiler. Hence, neglecting the terms $\dot{H}_{deposition}$ and $\dot{H}_{flowin} - \dot{H}_{flowout}$ is reasonable. On the contrary, in the coal gasifier case, the results showed that the heat fluxes carried by the inflowing slag and the impacting ash particles also played a significant role in the heat balance.

3.2.3 Calculation Algorithm

From the force balance and the heat balance, the thickness of the running molten deposit layer and the surface temperature of the layer exposed to the inner furnace are calculated iteratively. The calculation algorithm is shown in Figure 3.2. Several important input parameters are also listed in the figure.

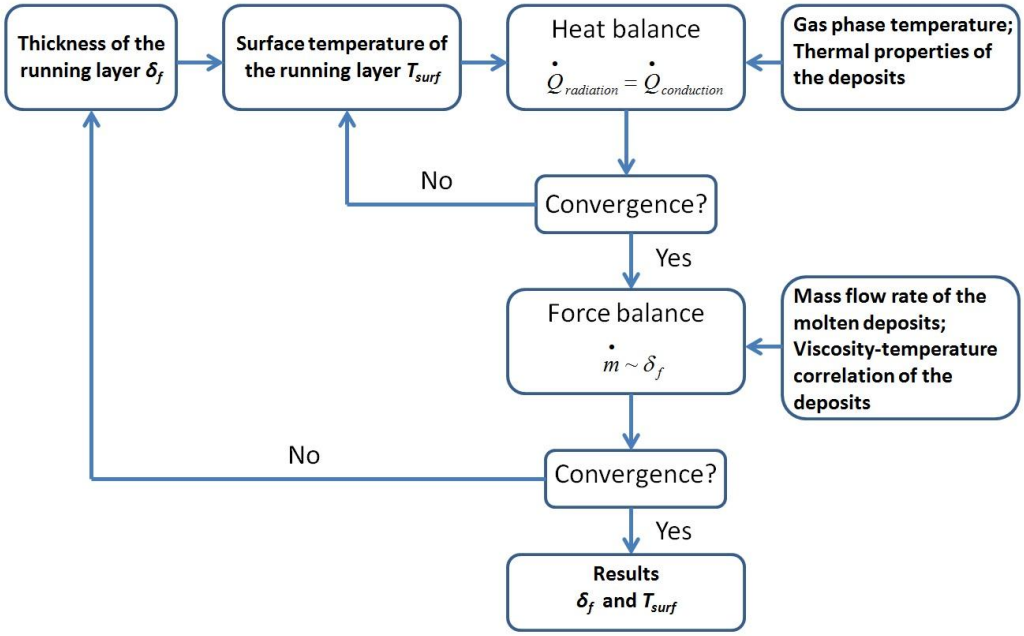

Figure 3.2: Iterative algorithm for the calculation of the thickness of the running molten deposit layer and the surface temperature of the layer exposed to the inner furnace.

3.3 TEST CASE AND RESULTS

In the framework of CFD, the slagging wall model was applied on the superheater tube bends (Paper II) and on the lower furnace walls (Paper I) of the Kraft recovery furnace. The set-up and the calculation results for the two cases are presented in the following sections.

3.3.1 Test Case One: Superheater Tube Bends

In this case, the slagging wall model is implemented into a CFD model for superheater tube sections. Specifically, it is applied to two tube bends on one of the first groups of

tube banks exposed to the flue gas. The model shows, for both tubes, that a thicker molten deposit layer leads to a higher surface temperature. This results in a lower heat flux through the super-heater wall at those locations. However, variations in the steel surface temperature from position to position are not as large as the variations in the heat flux.

Case Description

In kraft recovery boiler furnaces, the first group of super-heater tube banks exposed to flue gas is prone to heavy impaction deposition. The CFD model focuses on two tube bends that are located at the bottom of one of the first groups of super-heater tube banks, as shown in Figure 3.3 (a).

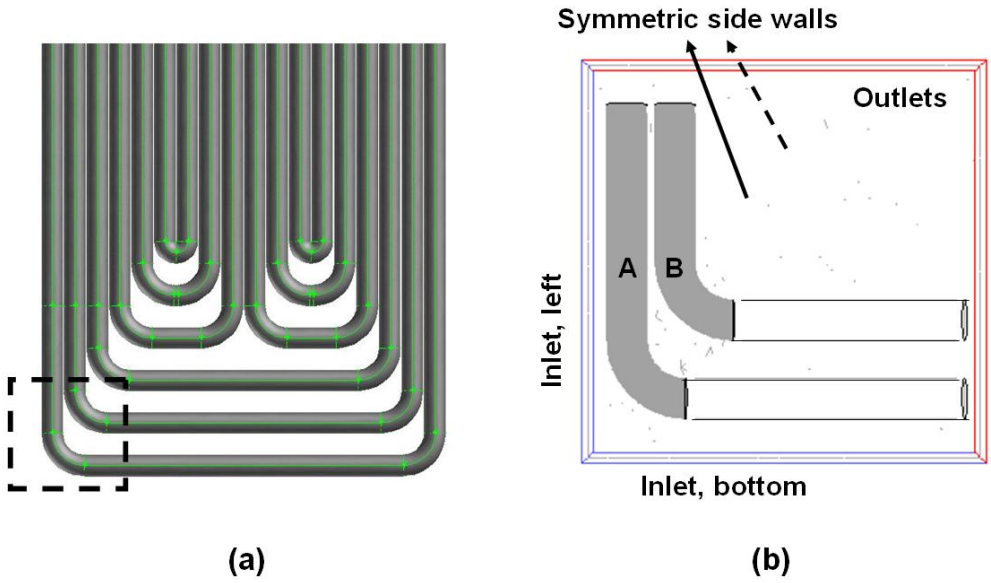

Figure 3.3: Geometry of the computational domain: (a), two tube bends at the lower section of a super-heater tube panel; (b), tube bends A and B in the computational domain with the other boundaries (Paper II).

The computational domain is illustrated in Figure 3.3 (b). It is a simple rectangular geometry including the two tube bends. Symmetric boundary conditions are used on the two side walls. The conditions are chosen to be similar to a furnace condition. At the left and the bottom inlets, the gas flow is at 7 m/s, 1200 K. The flow follows a diagonal direction from the left bottom corner to the right top corner of the rectangular domain. The left and the bottom inlets use external black body temperatures at 1173 K and 1073 K respectively. Molten particles at 1200 K are injected from the two inlets. The size of the particles follows a Rosin-Rammler distribution with the specific mean diameter at 0.3 mm and the spreading parameter at 2.75. The calculation of the mass flow rate of molten deposits includes no input to the tube from above. Instead, a large particle load, at 4 kg/Nm^3, is used to ensure a deposition on the tube bends. The CFD model is

implemented in the commercial software FLUENT 6.3.26^{TM} (FLUENT, 2013), and tracks the particle trajectories with a discrete phase model. An impaction deposition model is included, in which it is assumed that all impacting particles are deposited. The impaction deposition model is applied on tube A and tube B, as shown in Figure 3.3 (b). The mass flow rates of running molten deposits on tube A and tube B are calculated based on the deposit flows.

The slag wall model uses the physical properties of a typical black liquor recovery boiler smelt from Tran et al. (2004), although the reduction degree of the smelt is higher. The properties are shown in Table 3.1. The viscosity-temperature correlation is also based on their data for a recovery boiler smelt:

$$\mu = 1.994e-5 * \exp(5.69e3/T) \qquad (3\text{-}11.).$$

The thermal properties of super-heater tube materials used in this case are also included in Table 3.1. The steam temperature T_{cm} used in the calculation of the steel temperature is 673 K.

Table 3.1: Physical Properties of Deposits in a Kraft Recovery Boiler Furnace (Paper II).

Density ρ (kg/m^3)	1923
Thermal conductivity of deposit, solid k_s (W/m-K)	0.88
Thermal conductivity of deposit, liquid k_f (W/m-K)	0.45
Temperature at the interface of solid and liquid layer T_{flow} (K)	1023
Thermal conductivity of steel, k_{metal} (W/m-K)	16.27
Thickness of super-heater tube wall, δ_{metal} (mm)	2.5

Results and Discussion

The CFD calculation shows that the particles follow the gas flow. For tube A, a large amount of the particles land on the windward front, as shown in Figure 3.4 (a). Considerably fewer particles are deposited on tube B. The deposits on tube B appear on the sides where the turbulence brings some particles. Figure 3.4 (b) shows the mass flow rate of molten deposits. The molten deposits flow down along the tubes, and in general the mass flow rate increases downward.

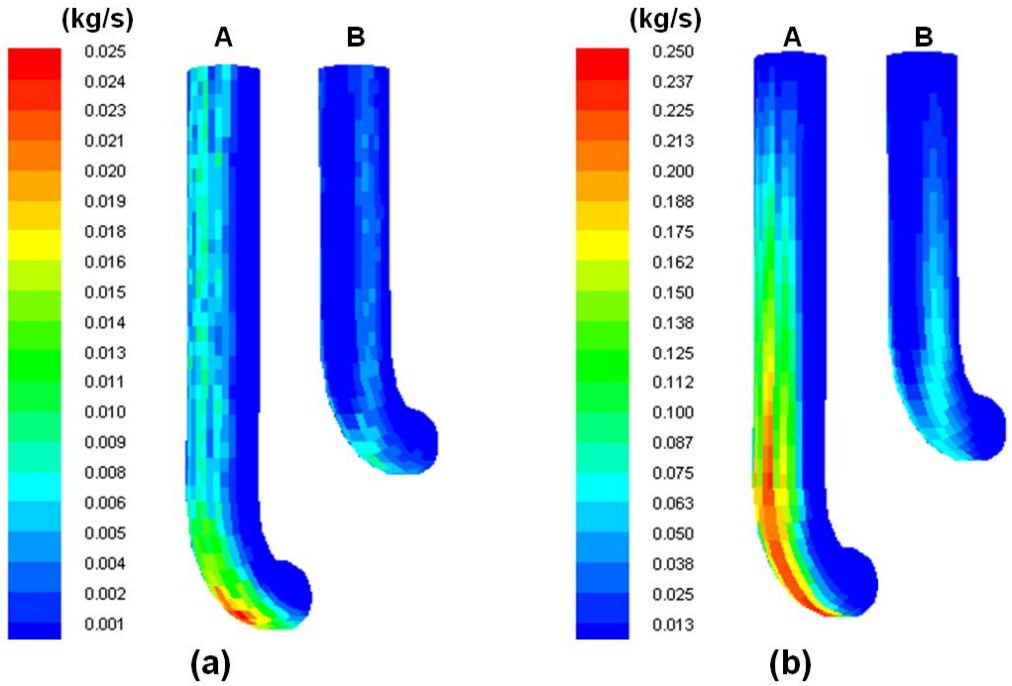

Figure 3.4: (a) Mass flow rate of particles landing on the tube surfaces; particles are assumed to be all sticky and fully molten; (b) Mass flow rate of molten deposits flowing down along the tube surfaces (Paper II).

As shown in Figure 3.5 (a), the largest thickness is at the lowest part of tube A where the molten deposit flow accumulates and flows down. The temperature at the surface of the molten deposit layer is shown in Figure 3.5 (b). Locations with larger thicknesses of the molten deposit layer have higher surface temperatures.

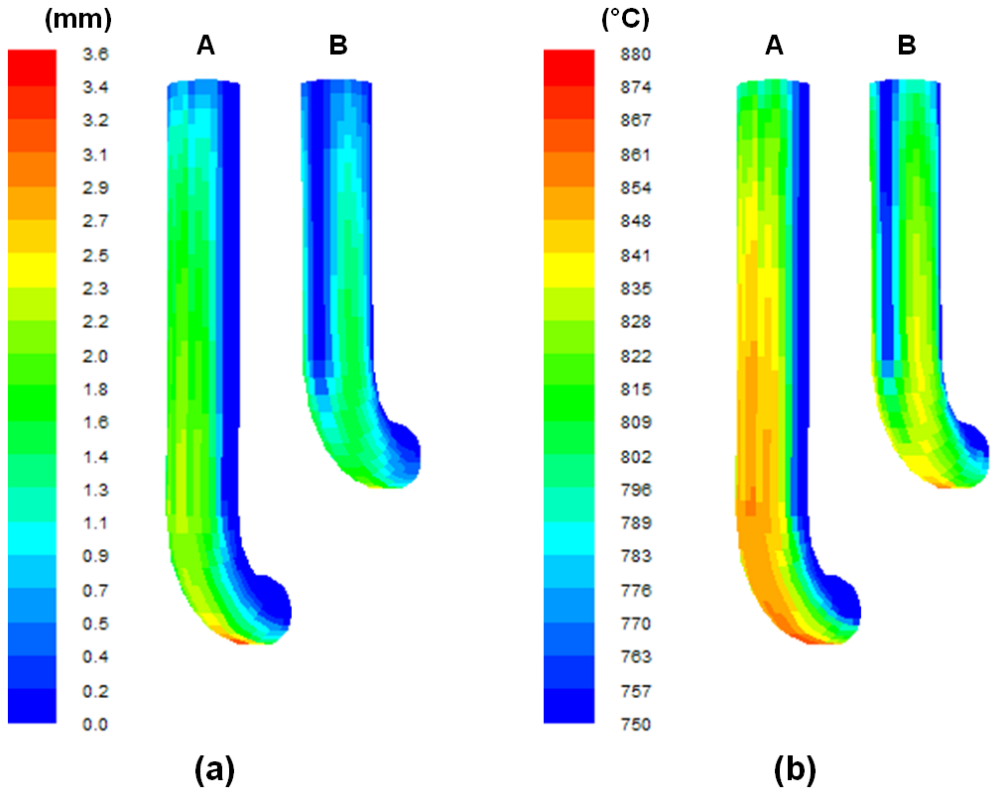

Figure 3.5: Properties of the molten deposits layer: (a) Thickness of the molten deposit layer; (b) Temperature at the surface of molten deposit layer exposed to the inner furnace (Paper II).

Figure 3.6 (a) shows the conductive heat flux through the molten deposit layer and demonstrates that the deposit layer hinders heat transfer. Higher surface temperature at the deposit surface reduces the temperature difference between the gas phase and the molten deposit layer. Consequently it leads to smaller radiative heat flux, and the conductive heat flux through the super-heater wall becomes smaller. The steel surface temperature is lower at locations where the deposit layer is thicker, as shown in Figure 3.6 (b). However, the difference in steel surface temperature is not as significant as in the heat flux.

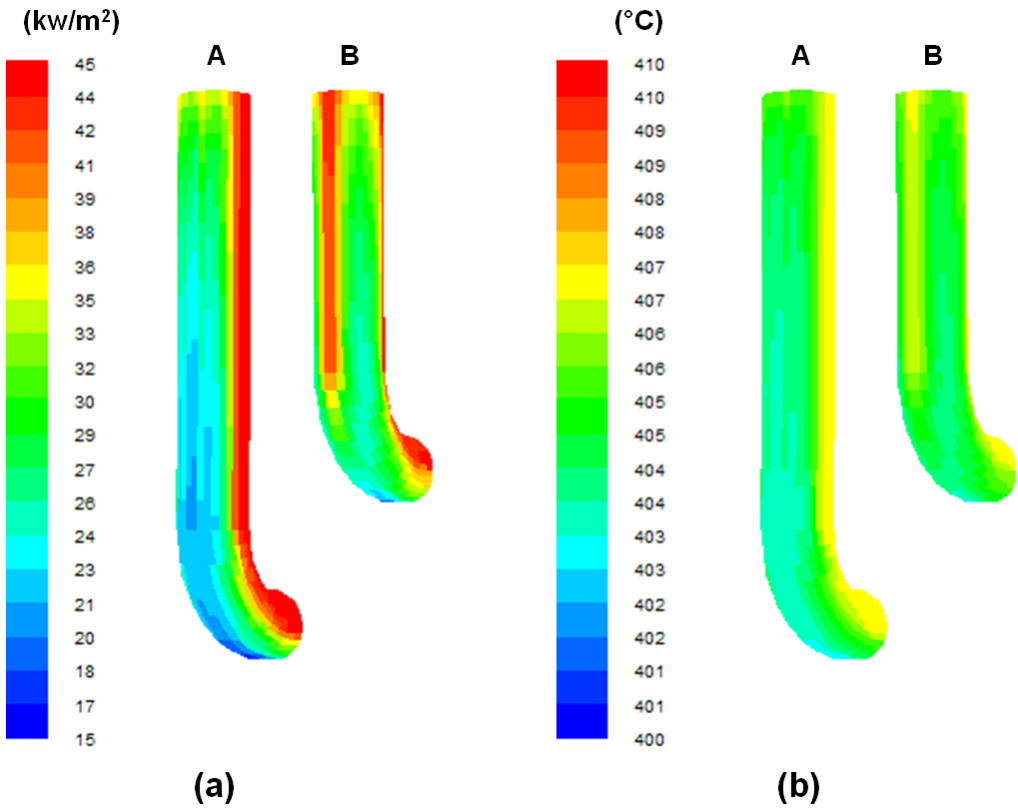

Figure 3.6: (a) Conductive heat flux through the molten deposit layer. As assumed, it is the same as the heat flux through the solid layer and the tube wall. (b) Temperature at the steel tube surface in contact with the solid deposit layer (Paper II).

Figure 3.7 shows the thickness of the solid deposit layer. The solid layer is thicker at locations where the steel temperature is lower, and it also corresponds with the places where the molten layer is thicker and the heat flux is smaller.

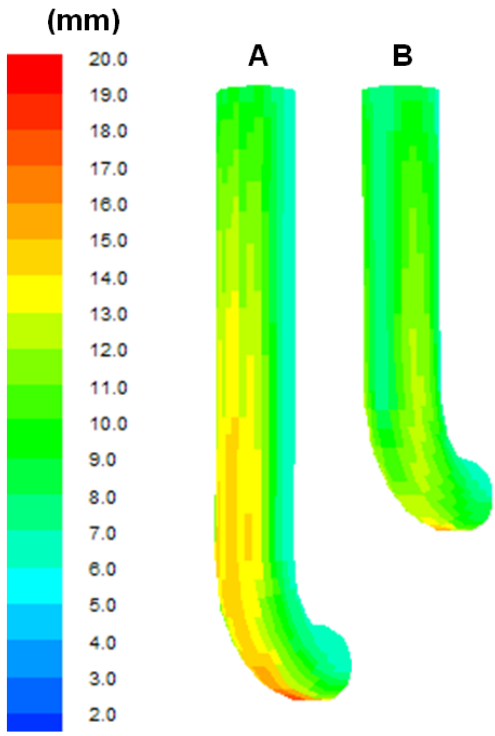

Figure 3.7: Thickness of the solid deposit layer in contact with the tube surface (Paper II).

3.3.2 Test Case Two: Wall Surface Temperature

This test case investigated wall surface temperature and incident radiative heat flux to the wall in the lower furnace of a Kraft recovery boiler. Three CFD simulations were performed with different set-ups for the wall surface temperature as the heat transfer boundary condition: A) the char bed burning model is applied on the wall, and the wall surface temperature is calculated; B) the T_{70} of the deposits is used as the wall surface temperature; C) the wall surface temperature is calculated with the slagging wall model. The three approaches emphasize different features of deposits in Kraft recovery furnaces. The simulation results were analyzed and evaluated with the experimental data from a measurement campaign.

Case Description

An extensive measurement campaign was carried out in the large black liquor recovery boiler simulated in this work. The black liquor burning capacity of the boiler was 4450 tds/day. During the campaign, the boiler ran at 70% of the normal capacity, and the dry solids content of the black liquor was approximately 82%. The aim of the measurement campaign was to produce validation data for evaluation of CFD-based recovery furnace models. Temperature measurements; heat flux measurements; gas composition measurements; spray characterizations; char bed observations; and carry-over measurements were carried out during the campaign. The gas composition measurements and the char bed observations can be found in the works of Vainio et al. (2010) and Engblom et al. (2010b), respectively. Some results of the temperature measurements and

the heat flux measurements are reported by Brink et al. (2010). Infrared (IR) video sequences of different parts of the furnace were captured with a portable single-band IR camera (IR-furnace Camera PYROINC 320). The camera operates at the radiation band of 3.9 μm where radiation by CO_2 and H_2O is almost negligible; it can detect a temperature range between 400 °C – 1500 °C. The camera was hand-held and took video sequences from the third and fourth floors. On the third floor, the camera was held on the same level with the liquor guns. On the fourth floor, the position of the camera was roughly in the middle between the liquor guns and the tertiary air ports. The video sequences were recorded at 50 frames per second, and they were mostly taken for the areas below or on the same level as the camera. Wall surface temperature can be obtained by evaluating the average of 400-1000 single frames from the video sequences.

CFD simulations of the large recovery boiler, in which the measurements were carried out, were performed with the Åbo Akademi Recovery Furnace Model. In order to evaluate the wall surface temperature as the wall boundary condition, three cases are investigated in this work: A) the char bed burning model provides the wall surface temperature; B) the "radical deformation temperature" T_{70} is used as the surface temperature; C) the slagging wall model is used to calculate the surface temperature. The Case A simulation was carried out first and was used as the base for the other two cases. All three cases have the same boundary conditions except for the wall surface temperature. The gas phase sources calculated by the droplet model and char bed model in Case A were kept constant in all three cases. The wall boundary condition models used in Case A and Case B are first described below, followed by a description of the implementation of the slagging wall model (Case C).

In Case A, the char bed burning model is used to calculate the wall surface temperature. The char bed burning model is from Frederick and Hupa (1991), and it has been modified and implemented into the Åbo Akademi Recovery Furnace Model by Bergroth et al. (2004&2010). The char bed burning model is fully coupled with the gas phase and a model for black liquor droplet conversion (Järvinen et al., 2007). It solves equations describing the mass and energy balance on the surface of the char bed. The model includes carbon conversion via direct oxidation, gasification reactions, and sulfate reduction. The char bed burning model predicts local rates of carbon conversion and carbon accumulation, as well as the local bed surface temperature. In the recovery furnace simulations, it is applied on the walls to model the wall burning process. In Case A, in order to calculate the wall surface temperature, an additional condition is added to the char bed burning model: on locations where the carbon is totally converted, the char bed burning model uses the "radical deformation temperature" of the deposits as the wall surface temperature.

The "radical deformation temperature" T_{70} is determined by the composition of the deposits, which is in turn affected by the composition of the black liquor; the location of the deposits; and the surrounding gas phase. T_{70} in Case B is estimated based on melting curves from thermodynamic modeling of black liquor combustion. The composition of black liquor dry solid in Table 3.2 is from the measurement campaign, and is used as the input to the thermodynamic modeling. The liquor has a rather high sulfur/sodium ratio of

0.44. The moisture content of the liquor is 18.7%. The oxygen content is the subtracted residue of all other components. The sulfur-containing compounds, mainly Na_2S and Na_2SO_4, can affect the melting behavior of the deposits. Combustion of black liquor with different air-fuel ratios was modeled. The thermodynamic calculations were carried out with the thermodynamic software package FactSage (Bale et al., 2009) version 6.3.1, which is based on minimization of Gibbs free energy to calculate the global chemical equilibrium. The thermodynamic properties of the multicomponent alkali salt liquid phase, solid solutions, stoichiometric phases, and the gas phase were taken from the FactPS/Fact53 database and the FTPulp database. Lindberg et al. (2007a) (2007b) presented the detailed thermodynamic properties of the relevant alkali salt mixtures. Figure 3.8 shows the reduction degree of the sulfur-containing compounds and the corresponding T_{70} of the ash after combustion of black liquor, with the air-fuel ratios ranging from 0 to 0.99. In the lower furnace of the black liquor recovery boiler, the deposits are generally in a reducing condition. In this work, the "radical deformation temperature" T_{70}, i.e., the temperature with 70% melt fraction, is estimated to be 750 °C.

Table 3.2: Composition of Black Liquor Dry Solid from a Kraft Recovery Boiler (Paper I).

	C	H	Na	K	S	Cl	O*
%(Wt, ds)	32.2	3.3	21.4	2.4	6.4	0.4	34.5

* Oxygen content by difference.

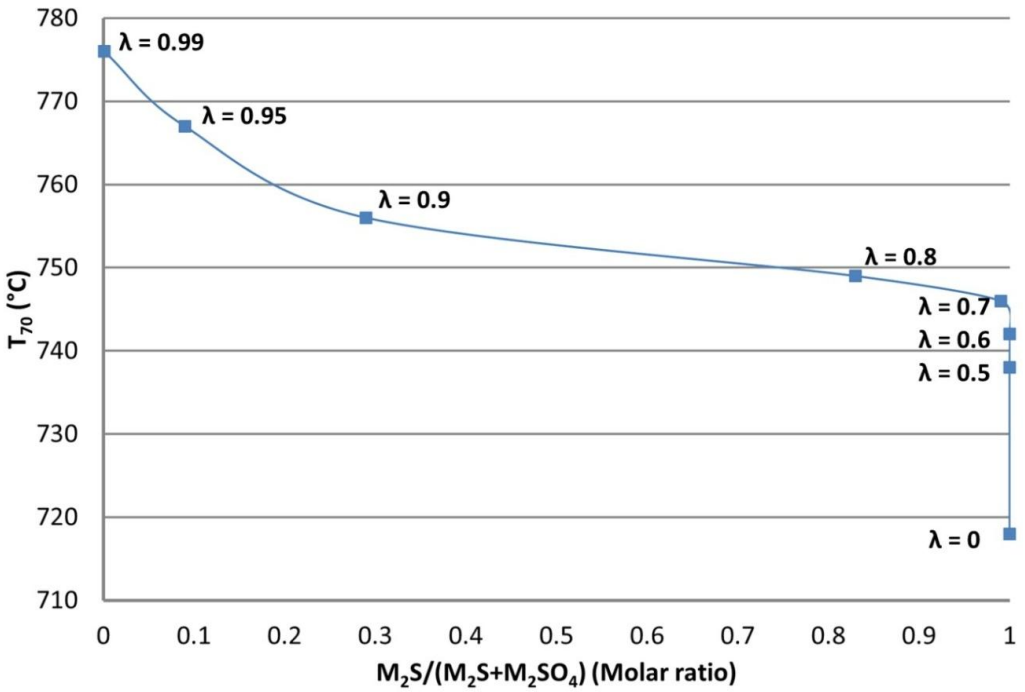

Figure 3.8: T_{70} of ash after combustion of black liquor versus the reduction degree of the sulfur-containing compounds in the ash (M: Na and K). λ denotes the air-fuel ratio under which combustion of black liquor was modeled (Paper I).

In Case C, the slagging wall model is implemented into the furnace model. The mass flow of the molten deposits element $\dot{m}$ is an input to the slagging wall model. With the assumption that all of the landing ash is fully molten, the mass flow is the sum of the ash landing on the element and the deposits flowing down from the element above. The landing ash includes the mass flow of inorganic salts: sulfides; sulfates; carbonates; and chlorides, which are obtained from the black liquor droplet conversion model. In Figure 3.9, the left picture shows the computational grid of a furnace wall, which features the cell zones of different densities and the openings representing the air inlets and the liquor gun ports. It is difficult to track the mass flow of molten deposits around the openings, thus a grid manipulation is applied to facilitate the calculation of the mass flow of molten deposits. As depicted in the right picture in Figure 3.9, the wall is divided into bigger cell sections, each of which consists of the computational cells it covers and is assigned with the information obtained from those cells. The left picture of Figure 3.10 shows the flux of ash landing on the wall for each cell, i.e., the deposition rate $m''_{deposition,cell}$, corresponding to the original grid in Figure 3.9. The deposition rate for one section in the simplified grid, $m''_{deposition,section}$, is the sum of the deposition flow of all the cells the section covers divided by the area of the section,

$$m''_{deposition,section} = \frac{\sum(m''_{deposition,cell,i} * A_{cell,i})}{A_{section}} \quad (3.12.),$$

where *i* is the numerical ID of cells in the section. The downward, accumulated mass flow rate of molten deposits on one section $m''_{section}$ can then be calculated with the sum of deposition flow of that section and those above in the same column divided by the area of the section,

$$m''_{section} = \frac{\sum(m''_{deposition,section,j} * A_{section,j})}{A_{section}} \quad (3.13.),$$

where *j* is the numerical ID of the current section and those above in the same column of the wall. The right picture in Figure 3.10 shows the section-based mass flow rate of molten deposits $m''_{section}$. Finally, the mass flow of deposits on one cell $\dot{m}_{cell}$ including both the ash landing on the cell and the deposits flowing down from the cells above can be approximately calculated as

$$\dot{m}_{cell} = m''_{section} * A_{cell} \quad (3.14.),$$

and the thicknesses of the deposits and the surface temperatures of the deposits are again calculated on a cell basis.

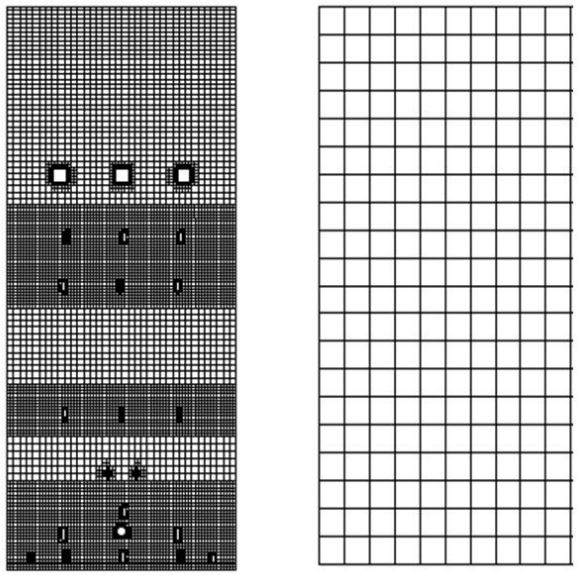

Figure 3.9: Left, computational grid of a furnace wall in the CFD model (original); Right, coarse grid of the same wall for the slagging wall model (simplified) (Paper I).

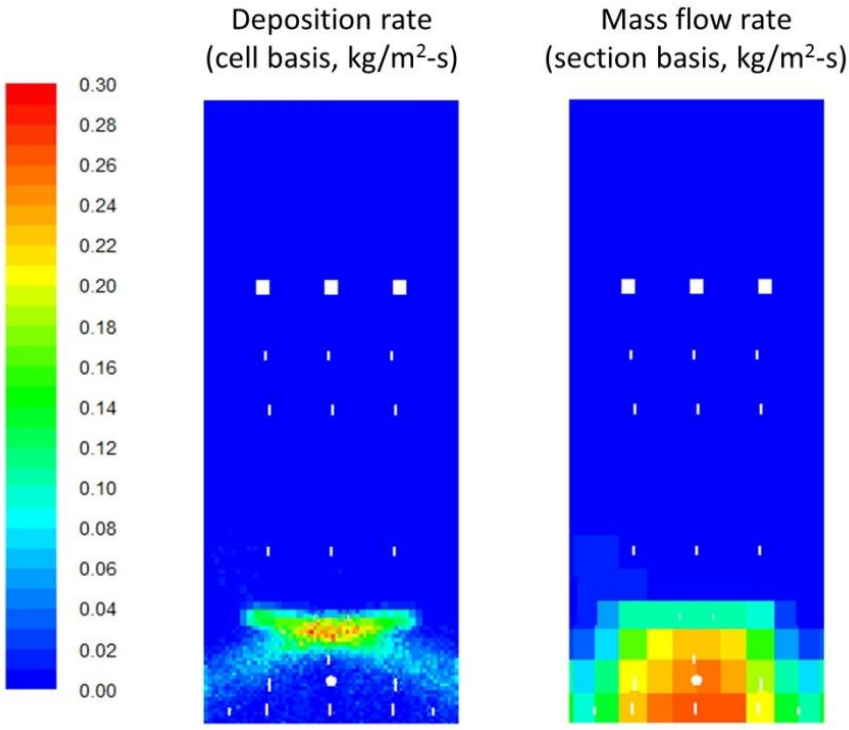

Fig. 3.10: Comparison between the cell-based deposition rate $m''_{deposition,cell}$ (left) and the section-based downward mass flow rate of the molten deposits $m''_{section}$ (right).

In the slagging wall model, the viscosity-position correlation $\mu(x)$ is obtained from the viscosity-temperature correlation by assuming a linear temperature profile across the molten deposit layer. Here, the viscosity-temperature correlation is given in Arrhenius form:

$$\mu = 3.47 \cdot 10^{-35} e\left(\frac{7.7 \cdot 10^4}{T}\right) \quad (3.15.).$$

The above correlation is based on the low-temperature part of the experimental viscosity-temperature correlation for recovery boiler smelt, from the work of Tran et al. (2004). In addition, the radiative heat transfer rate from the gas phase to the wall is available from the furnace model. The steam temperature in the water wall tubes is assumed to be location-independent at 450 °C.

Results and Discussion

IR video sequences are available from the measurements in the Kraft recovery boiler. Observations of the video sequences provide visual information about deposit formation and temperature distribution in the lower furnace. A video frame obtained with the IR camera is shown in Figure 3.11. It shows the liquor spray from the right wall hitting the back wall. In the blue circle where the major part of the spray is landing, the temperature is relatively low. Between the blue and the red circles, the temperature is high compared with the other areas on the back wall. The landing of black liquor droplets on the wall leads to heavy deposit build-up. The droplets burn on the wall in a fashion similar to that observed in the char bed, and is responsible for the local high temperatures. A pattern similar to that shown in Figure 3.11 is also observed on the front wall. The landing of spray on the wall is referred to as wall-spraying feature in the following text. Due to this wall-spraying feature, more droplets land on the front and back walls than on the left and right walls. The video also shows more deposits falling off of the front and back walls than off of the left and right walls, and also shows small “hills” forming at the foot of these walls. Larger numbers of droplets burning on the wall also leads to more areas with higher wall surface temperatures on the front and back walls. Locations with higher wall surface temperatures are identified from the video sequence and are indicated in Figure 3.12 as red areas. The blue areas indicate low-temperature regions where a large number of black liquor droplets are landing. The figure also includes the measured wall surface temperature for several locations. More information about the measurements can be found in the work of Brink et al. (2010).

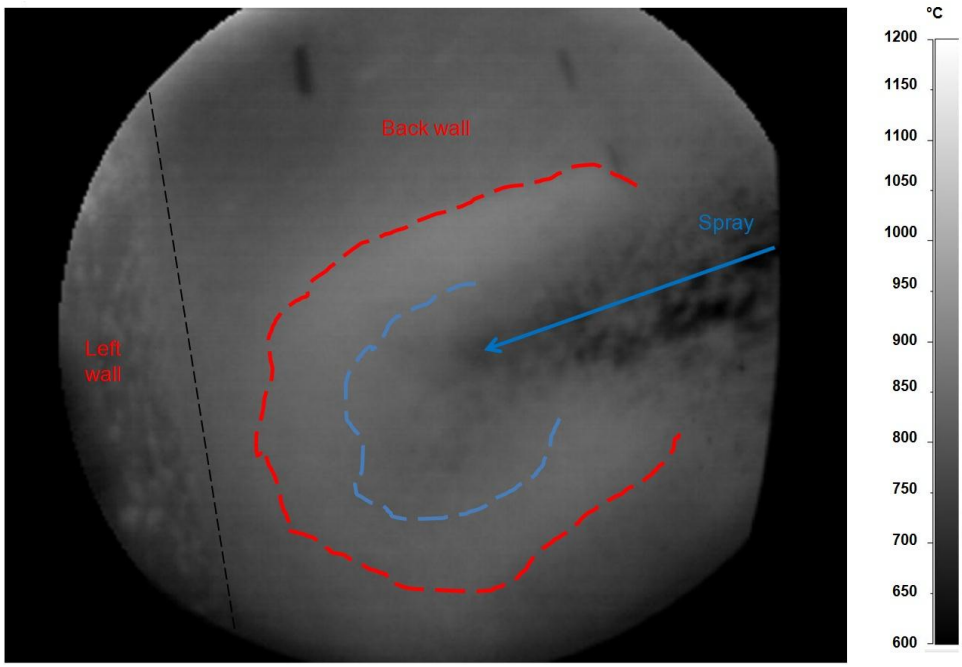

Figure 3.11: A video frame captured by the IR video camera, showing black liquor spray from the right wall hitting the back wall and leading to temperature variations on the wall (Paper I).

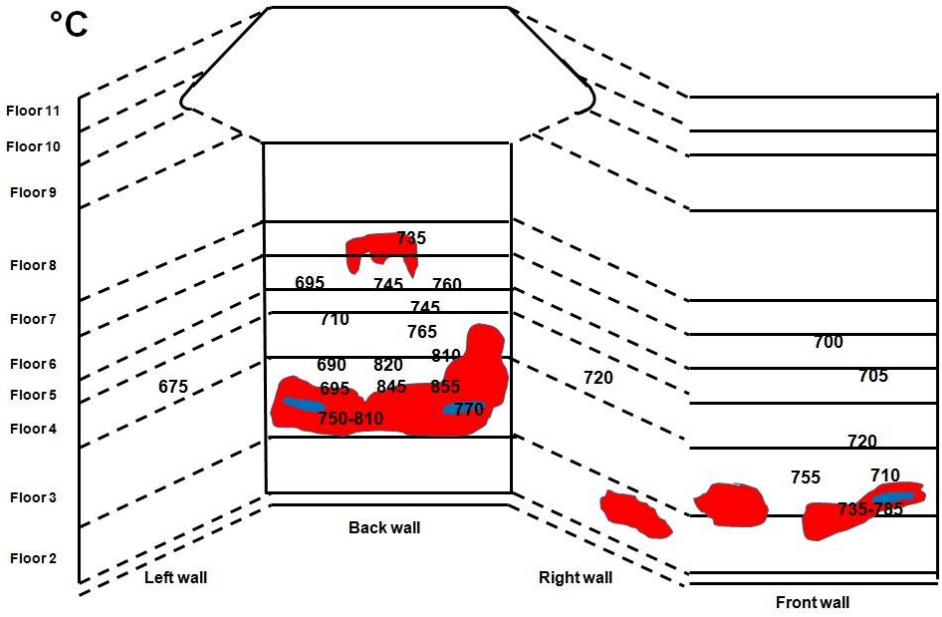

Figure 3.12: Hot areas identified from the video sequences are marked by red areas. The blue areas are the locations where a large number of black liquor droplets are landing.

Wall surface temperatures are obtained by evaluating the average of 400-1000 single frames (Brink et al., 2010) (Paper I).

From the simulations, the wall surface temperature of the lower furnace in Case B is equal to the "radical deformation temperature," which is 750°C. In Case A, the wall surface temperature is calculated with the char bed burning model. For cases in which the carbon is totally converted, the "radical deformation temperature" of the deposits is assigned to the wall. Figure 3.13 shows the wall surface temperature distribution on the lower furnace walls for Case A. For most parts of the walls, the in-furnace surface temperature is equal to the "radical deformation temperature" of 750°C. The divergences of the surface temperature can be seen on the furnace walls below the red line. The high-temperature areas, where the surface temperature reaches 930°C, are explained by the wall-spraying feature of the boiler. On each of the four side walls, the hot areas correspond to the locations where the black liquor droplets are landing. However, in the middle of the hot areas are colder areas where a large number of droplets at lower temperatures are landing. The hot areas on the back and front walls in Figure 3.13 roughly correspond to the observations shown in Figure 3.12. In Figure 3.13, the pattern of the hot areas on the left and right walls indicates that the landing droplets are from the injections on the opposite wall. However, the distributions of hot areas on the left and right walls are not observed in the IR video sequences; this may be because the black liquor spray cannot easily reach the opposite wall in the real recovery furnace.

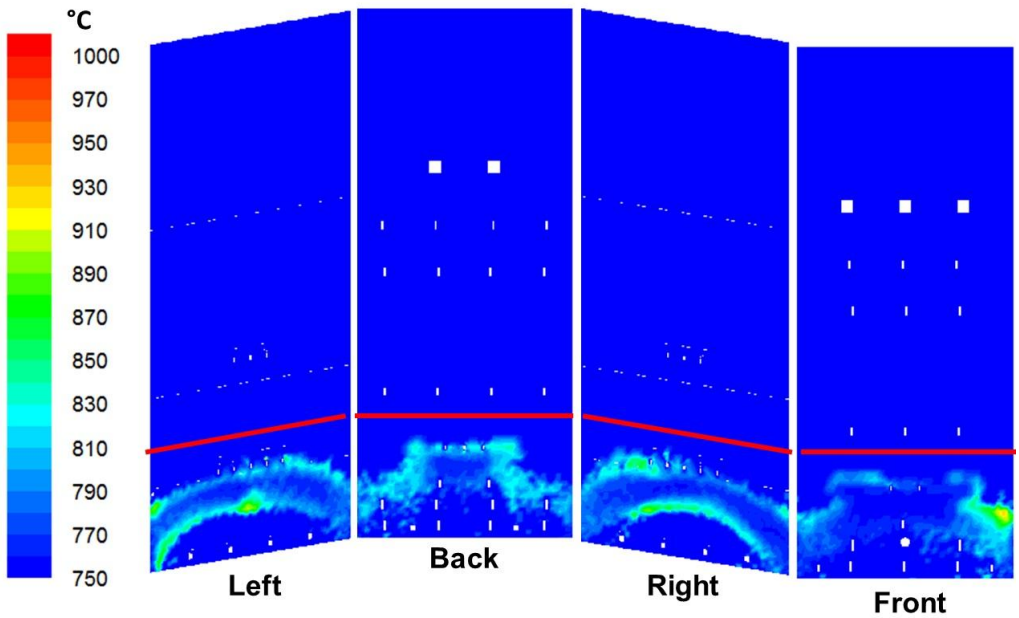

Fig. 3.13: Wall surface temperature from Case A: the wall surface temperature is calculated with the char bed burning model, complemented by the governing condition that the "radical deformation temperature" of the deposits is used if the carbon is totally converted (Paper I).

As shown in Figure 3.14, the wall surface temperature calculated with the slagging wall model in Case C varies by only an approximate 50°C. The highest temperature can be found at the lowest part of the walls, where the mass flow of molten deposits reaches its highest value. In general, the amount of molten deposits is rather small, so that the additional heat transfer resistance of the molten deposit layer does not cause a significant elevation of the surface temperature compared with the interface temperature between the solid and the molten layer, i.e., the "radical deformation temperature." With the slagging wall model, the hot areas caused by the wall-spraying feature cannot be identified.

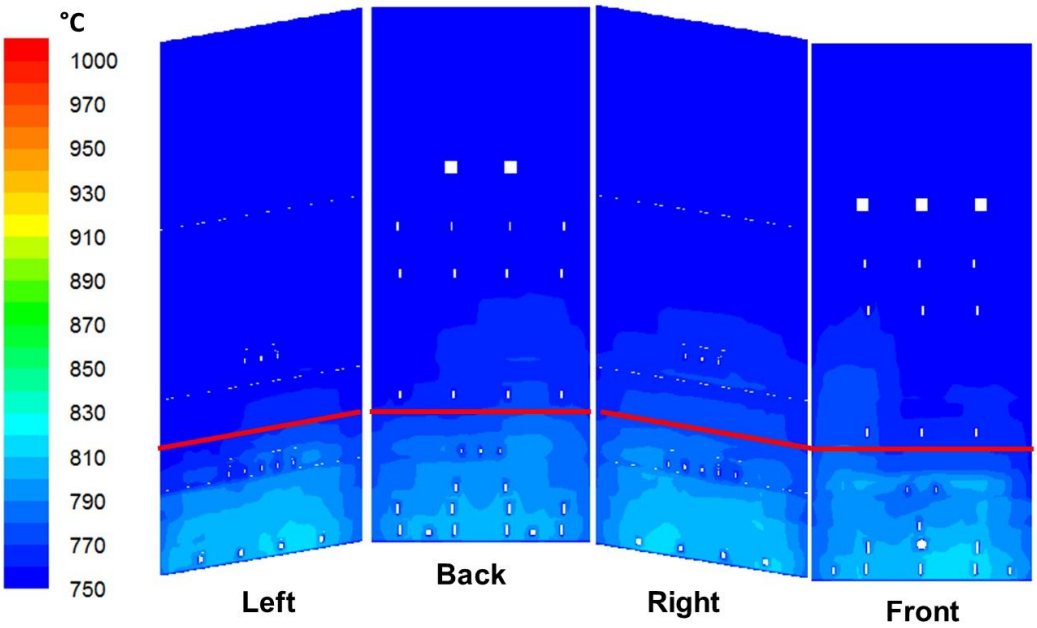

Figure 3.14: Wall surface temperature from Case C: the wall surface temperature is calculated with the slagging wall model (Paper I).

Generally, the predicted values of the incident radiative heat fluxes from the three cases are very well in-line with the measurement values from the measurements (Brink et al., 2010). In the lower furnace of a recovery boiler, the incident radiative heat flux to the wall is determined by the radiation from the particle-laden gas phase. As the only parameter that differs among the three cases, the wall surface temperature calculated in Case A and Case C are basically the same as that calculated in Case B for the major parts of the furnace walls. This results in little difference in the conditions of the gas phase, and thus in the similar incident radiative heat flux profiles. Figure 3.15 shows the incident radiative heat flux to the front wall in all three cases; the differences are insignificant. The total surface heat flux to the wall is affected by the wall surface temperature, and the small variations in the wall surface temperature give rise to slightly different profiles of the total surface heat flux. Figure 3.16 shows the total surface heat flux to the front wall for the three cases.

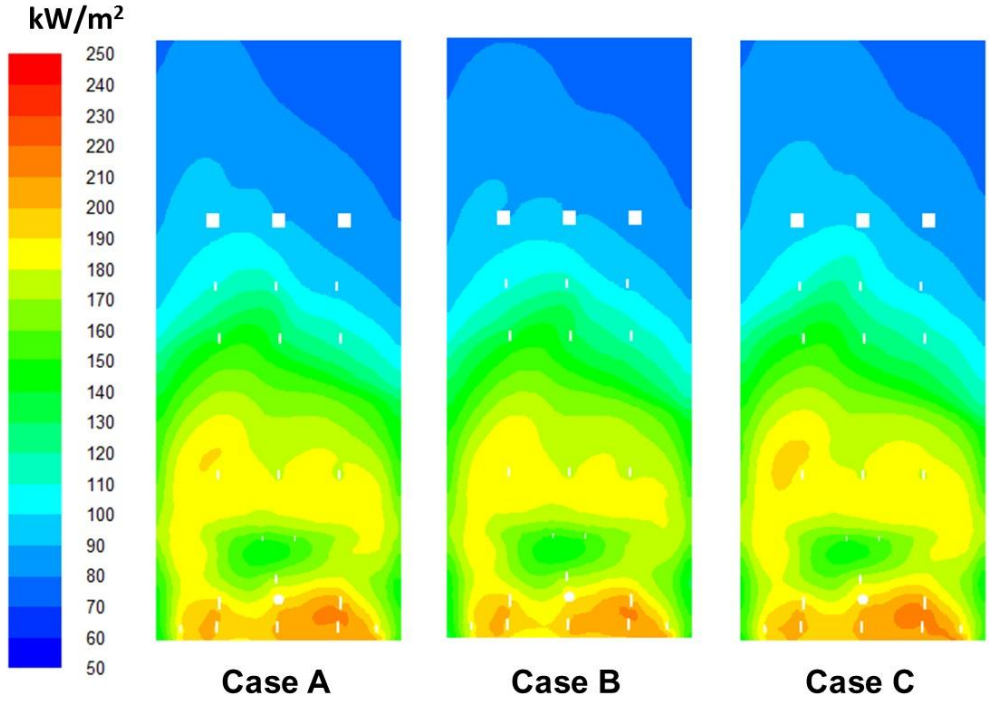

Figure 3.15: Incident radiative heat flux to the front wall for the three cases (Paper I).

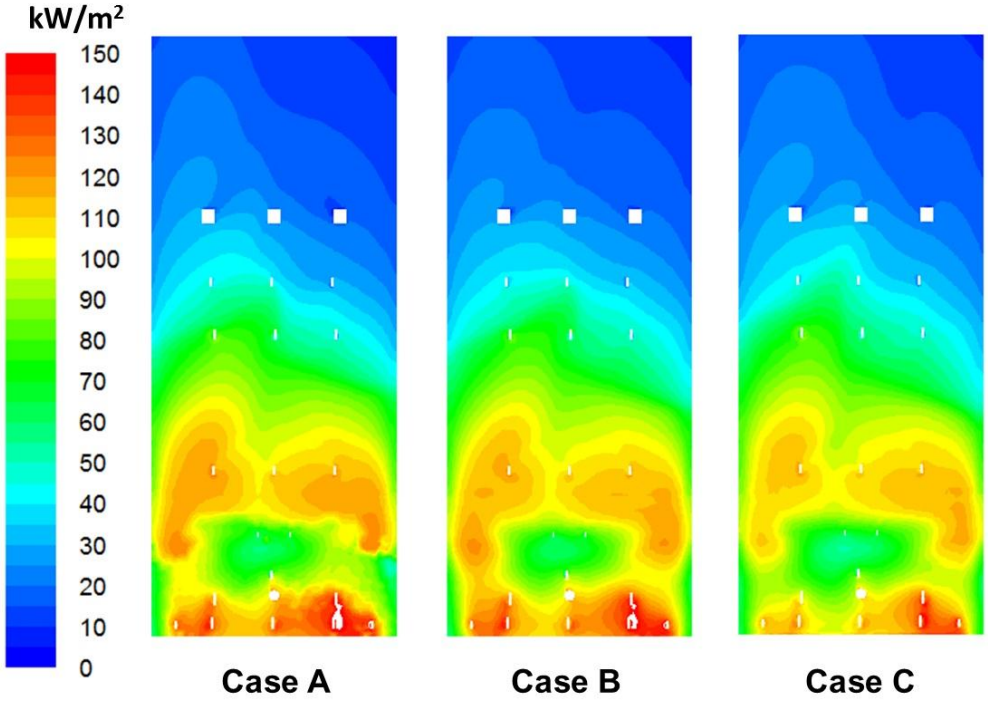

Figure 3.16: Total surface heat flux to the front wall for the three cases (Paper I).

4. FURNACE TWO: HEAT RECOVERY BOILER IN THE FLASH SMELTING PROCESS

This section presents the work related to chemical conversion and to the thermophoresis-induced deposit formation of dusts in the heat recovery boiler of the flash smelting process. The purpose of this part of the work was to investigate the deposit formation and its influence on the heat transfer in the heat recovery boiler. A particle conversion model was reported in Paper V (see "LIST OF PUBLICATIONS"), and the deposit formation simulation was presented in Paper IV.

4.1 BEHAVIOR OF DUST IN THE HEAT RECOVERY BOILER

In the Outokumpu flash smelting process (Kojo et al., 2000), significant quantities of dust particles are generated in the smelting furnace and directed into the heat recovery boiler. In the case of copper smelting, oxidic dust particles arrive in the heat recovery boiler together with SO_2-rich off-gas. Sulfation of dust particles commences when their temperature decreases in the radiation part of the boiler and the sulfates become thermodynamically stable. The dust particles can form deposits on the heat transfer surfaces of the boiler. The deposits can lead to decreased heat transfer efficiency for the boiler, and can even lead to blockage of the gas flow paths or other severe problems. In practice, the deposits are removed with spring hammers and recycled to the smelter.

Ranki-Kilpinen (2004) suggests that reaction heat from the sulfation conversion can heat the dust particles and cause softening of the particles, and the sulfated particles may stick to the heat transfer surfaces of the boiler. Skrifvars et al. (1991) studied superheater fouling due to limestone injection in coal-fired boilers; they found that particles reacting with the gas phase sinter to form denser deposits. Therefore, it is desirable to have the dust particles spend sufficient residence time in the gas phase in the correct temperature range to allow the small particles to reach complete conversion. In the case of larger particles, a thick sulfate layer should be formed before the particles come into contact with the heat transfer surfaces of the heat recovery boiler. Hence, the extent of conversion of the dust particles arriving at the heat transfer surfaces is an important indicator for the likelihood of deposition problems.

4.2 MODEL DESCRIPTION

In order to simulate deposit formation in the heat recovery boiler, a particle conversion model representing sulfation conversion of the flying dust particle and a deposit growth model describing the deposit formation were developed and implemented in FLUENT™ as user defined functions (FLUENT, 2013).

4.2.1 Particle Conversion Model

The particle conversion model builds on experimental results obtained by Hocking and Alcock (1966). The model assumes a sulfation process limited by solid state diffusion of Cu^{2+} ions. It further assumes that the initial mechanism can be described with the following overall reaction (Hocking & Alcock, 1966):

$$Cu_2O\ (s) + \frac{1}{2}SO_3\ (g) + \frac{1}{2}O_2\ (g) \rightarrow CuO\ (s) + \frac{1}{2}(CuO \cdot CuSO_4)\ (s),$$

$$\Delta H = -1653.38 \text{ kJ/kg } Cu_2O, \text{ at } 1000K \qquad (4\text{-}1.).$$

In the model, the CuO product layer forms inside the original particle, whereas the $CuO{\bullet}CuSO_4$ product layer forms on top of the original particle. This leads to a shrinking core model of a growing particle with dual reaction layers. To apply this model, the availability of SO_3 needs to be checked. There is more than 30% SO_2 in the copper flash smelter off-gas (Yang, 1996). In the off-gas line, 1-3% of SO_2 reacts to SO_3 (Sarkar, 1982). The gaseous reaction of SO_2 to SO_3 is not considered in the model.

4.2.2 Deposit Formation Model

The deposit growth model comprises two main subroutines: one is the deposition criterion, which determines whether the particles stick on the heat transfer surfaces after their landing; the other is for updates of deposit thickness and wall temperature.

Deposition Criterion

In general, the force balance on the particles landing on the heat transfer surfaces is used as the deposition criterion. It determines whether the particles are to stick on the wall or to rebound to the gas phase. The forces considered in the balance are gravity, friction force and thermophoretic force. In the heat recovery boiler, a significant temperature gradient exists across the viscous boundary sub-layer near the heat transfer surfaces that are exposed to the hot off-gas. Here, the thermophoretic force is important in the force balance. The correlation of thermophoretic force (Equation 2.3) from Kær et al. (2006) was used in the model.

In the evaluation of the force balance as the deposition criterion, the impaction or adhesion process of one dust particle landing on the heat transfer surface is not considered. The particle is treated as a static object on which only gravity, thermophoretic force, and friction force between the particle and the surface are taken into account. The position of the particle on a surface can affect the force balance. The heat recovery boiler has both vertical surfaces, such as the boiler walls and walls of heat exchangers, and horizontal surfaces such as the boiler ceiling and also sloping surfaces at the lower part of the boiler (Yang et al., 1999). Figure 4.1 illustrates the possible means by which one particle makes contact with different surfaces (walls) and how the forces act.

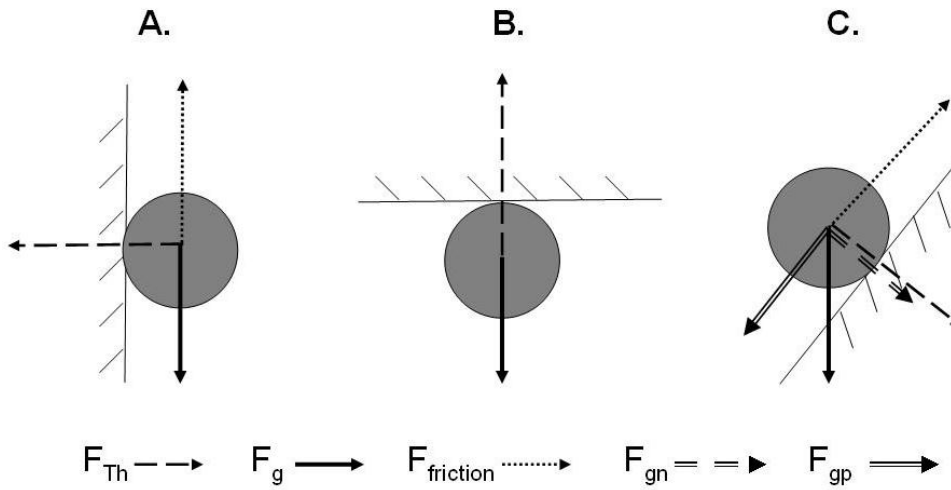

Figure 4.1: Possible means by which particles make contact with the heat transfer surfaces and how the forces act. F_{th}, thermophoretic force; F_g, gravity; $F_{friction}$, friction force; F_{gn}, normal component of gravity; F_{gp}, parallel component of gravity (Paper IV) .

In case A, friction force exists because the particle tends to slip down, and thermophoretic force exists normal to the surface. The particle will stay if the friction force is larger than its gravity:

$$F_{friction} > F_g$$
$$F_{friction} = F_{Th} * f_f \qquad (4\text{-}2.)$$

where $F_{friction}$ is the friction force; F_g is the gravity; F_{th} is the thermophoretic force and f_f is the friction coefficient between the particle and the surface. In case B, the particle will stick on the surface (roof) if the thermophoretic force is larger than the gravity.

$$F_{Th} > F_g \qquad (4\text{-}3.)$$

In case C, the friction force is the outcome of the combination of thermophoretic force and the gravity component normal to the surface. The particle does not slip down if the friction force is larger than the gravity component parallel to the surface:

$$F_{friction} > F_{gp}$$
$$F_{friction} = (F_{Th} + F_{gn}) * f_f \qquad (4\text{-}4.)$$

where F_{gp} and F_{gn} are the gravity components parallel and normal to the surface, respectively. The equation (4-4.) also pertains in case A where

$F_{gp} = F_g, F_{gn} = 0.$

Deposit Growth

The algorithm shown in Figure 4.2 is used in the simulation of the deposition process. First, a steady-state CFD calculation is performed to solve for composition, velocity and temperature of the gas flow. With the discrete phase model, the composition, velocity and temperature of particles are also solved. Based on the converged solution, the local deposit build-up rate is calculated from the mass flow of the sticking particles. The prediction is then advanced in a time step. Deposit thickness is calculated with the deposit build-up rate, and it is used to update wall boundary conditions for the next steady-state calculation.

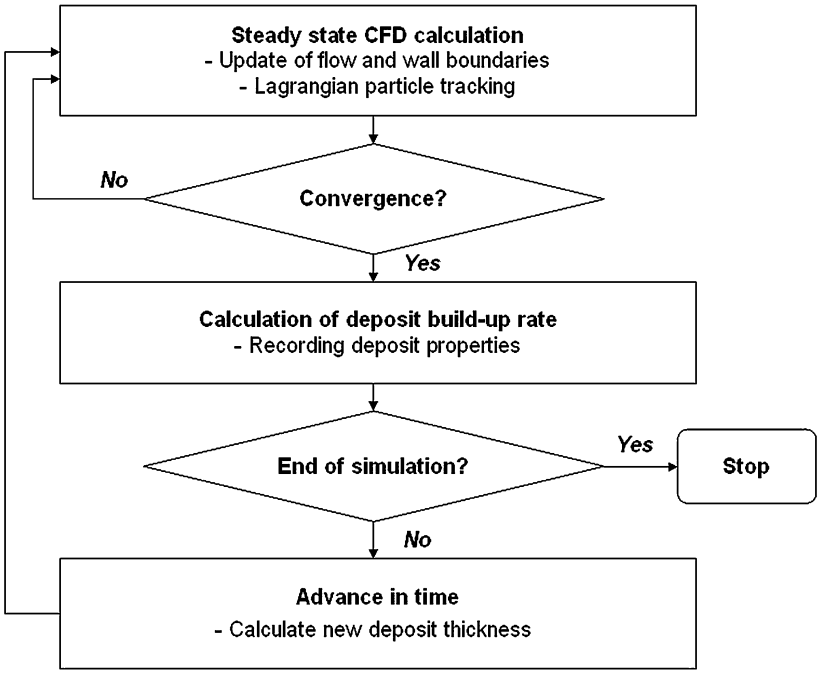

Figure 4.2: Algorithm in the simulation of the deposit formation process (Paper IV).

When the particles land on the heat transfer surfaces, the deposition criterion described in the above section is applied to determine whether the particles will deposit. Particles fulfilling the deposition criterion will stay on the surfaces, and they are eliminated from the stochastic particle tracking. The particles that do not fulfill the deposition criterion rebound to the gas phase, and the particle tracking continues. A rebound mechanism from FLUENT^{TM} is used, and the particles rebounding to the gas phase have a damped velocity (FLUENT, 2013). The increase in thickness of the deposits during one time step is calculated from the mass flow of sticking particles:

$$x_{dep} = \frac{\dot{m}_{dep}}{\rho A(1-\Phi_{dep})}\Delta t \qquad (4\text{-}5.)$$

where x_{dep} is the deposit thickness increased in one time step, $\dot{m}_{dep}$ is the mass flow of sticking particles, ρ is the deposit density, A is the area, Φ_{dep} is the deposit porosity and Δt is the time step size.

As mentioned above, the extent of conversion of the depositing dust particles can affect the sintering tendency; thus, the extent of conversion of the deposits is used to investigate the distribution of unreacted particles and the sintering problem. Here, the sulfation reaction taking place in the deposits is not considered. The extent of conversion of the deposit is calculated as a mass averaged value:

$$r_{ave} = \frac{r_{ave}^{0} M_{dep}^{0} + r M_{dep}^{'}}{M_{dep}^{0} + M_{dep}^{'}} \qquad (4\text{-}6.)$$

where r_{ave} is the mass average extent of conversion; r_{ave}^{0} is the mass average extent of conversion from the previous time step; r is the extent of conversion of the deposit added in the current time step; and M_{dep}^{0} and $M_{dep}^{\prime}$ are the masses of deposit from the previous time step and of deposit added in the current time step, respectively.

An increasing thickness of deposits leads to changes in the heat transfer property of the walls. Consequently, the surface temperature at the wall exposing to the off-gas will be influenced by the presence of the deposits. Based on a steady-state approximation, the wall surface temperature can be calculated from the total heat flux to the wall:

$$T_{wall} = \frac{q_{conv} + q_{rad}}{A}\left(\frac{X_{dep}}{k_{dep}} + \frac{X_{steel}}{k_{steel}} + \frac{1}{h_{water}}\right) + T_{water} \qquad (4\text{-}7.)$$

where T_{wall} is the surface temperature at the wall exposing to the off-gas; T_{water} is the temperature at the water side of boiler wall; q_{conv} and q_{rad} are the convective and radiative heat flux; X_{dep} and X_{steel} are the thickness of the deposit layer and the steel boiler wall; k_{dep} and k_{steel} are the thermal conductivity of the deposit layer and the steel; and h_{water} is the heat transfer coefficient from the steel to the cooling water. X_{dep} is the sum of x_{dep} for the elapsed time steps.

4.3 TEST CASE AND RESULTS

Simulations of the radiation part of a full-scale heat recovery boiler were performed. The lack of experimental data renders quantitative validation difficult. Nevertheless, the applicability of the models can be demonstrated by the simulation, e.g., by the calculated deposit growth on clean heat transfer surfaces and its influence on heat transfer.

4.3.1 Computational Grid and Boundary Conditions

The computational grid of the simulated heat recovery boiler is shown in Figure 4.3, where the configuration of the boiler is also illustrated. The shaft inlet is the main inlet of the computational domain. In practice, the particle-laden off-gas travels through the uptake shaft and then arrives in the heat recovery boiler. The upper part of the boiler

contains four groups of heat exchangers, while the lower part includes two ash hoppers. The outlet of the radiation part is connected to the convection part for further cooling of the off-gas. A more detailed description of the configuration of the heat recovery boiler can be found in the work of Yang et al. (1999). The tube banks of heat exchangers are modeled as four groups of slabs, as shown in Figure 4.4.

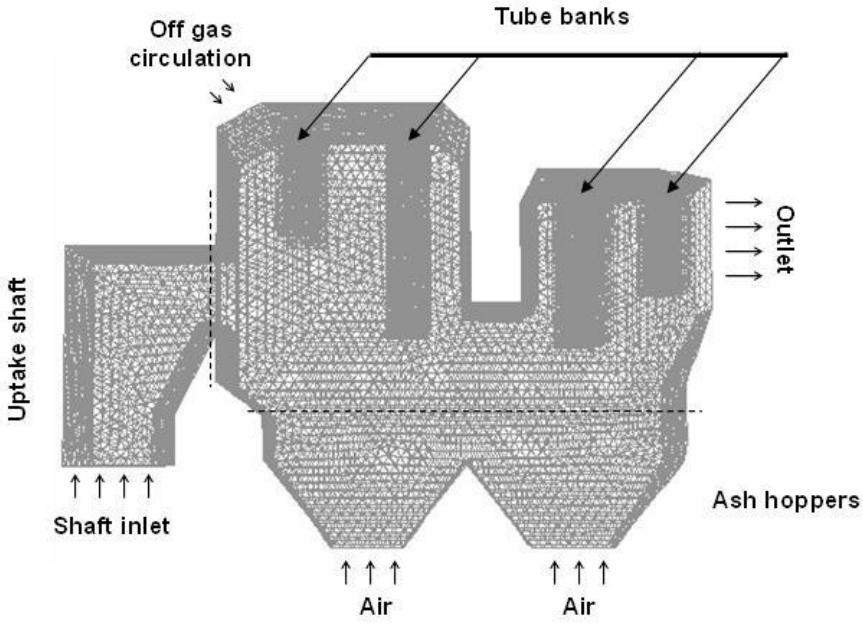

Figure 4.3: Computational grid of the radiation part of one heat recovery boiler (Paper IV).

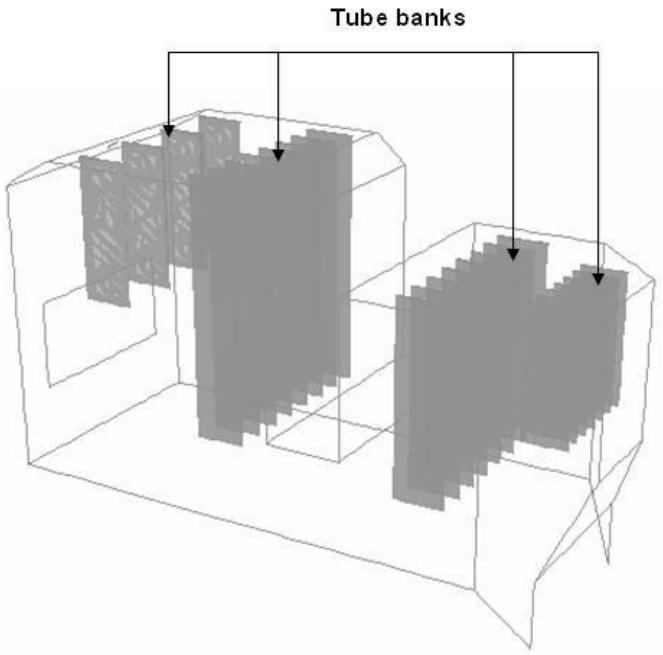

Figure 4.4: Slab models of the tube banks (Paper IV).

In the simulations, the main inflow and the particles enter from the shaft inlet. The main inflow of off-gas generated from the smelter contains primarily N_2, O_2, SO_2 and water vapor. The temperature of the main inflow and the particles is set to 1500K. Small gas inflows are positioned at the bottom of the ash hoppers as leakage, and from the off-gas circulation location. They are all set to air inputs at 300K. The deposit growth model is active on the boiler walls and on the walls of heat exchangers, where the wall temperature is calculated for the update of wall boundary conditions. In the uptake shaft, the adiabatic wall boundary condition is used. Consequently, the particles do not experience thermophoretic force in this section.

4.3.2 Flow Field and Particle Trajectories

The flow pattern in the heat recovery boiler can be complex due to bends in the boiler geometry and to blockage of the flow path by tube banks. Figure 4.5 shows the velocity vectors at the middle plane of the boiler, displaying swirls in the uptake shaft and the tube bank zones. The flow velocity in the ash hoppers is fairly low, a condition favored for the sedimentation of dust particles.

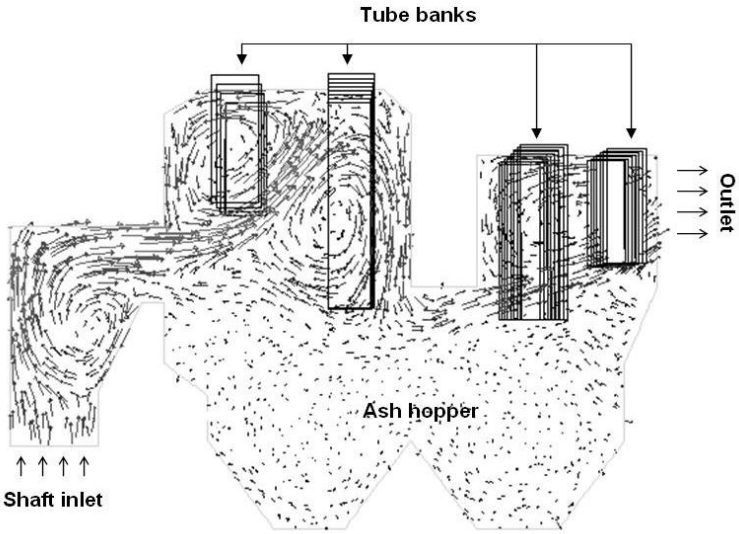

Figure 4.5: Velocity field at the middle plane of the boiler (Paper IV).

In the simulations, more than 12,000 particles are injected at the shaft inlet. Rosin-Rammler size distribution is used to present the diversity of particle size. The specific mean diameter used in the Rosin-Rammler distribution function is 50 μm, and the spread parameter controlling uniformity is 1. The initial velocity of the particles is 3 m/s, which is the same as that of the main inflow. Figure 4.6 shows the trajectories of 50 particles injected from one corner of the shaft inlet; the particles are largely following the flow. Particles are trapped in the swirls, especially in the uptake shaft. The trapped particles significantly increase the computational demand because tracking of such particles can take a very long time. Moreover, the particles trapped in tube bank zones are highly likely to hit on the wall due to impaction. The particles that arrive at the bottom of the ash hoppers and the outlets are leaving the computational domain. Along with the particles sticking on the wall, their trajectories are terminated.

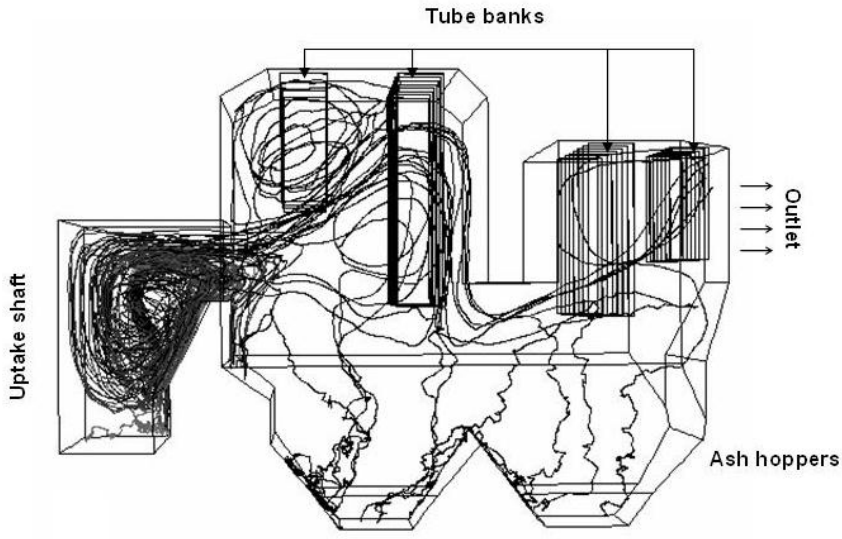

Figure 4.6: Trajectories of 50 particles (Paper IV).

4.3.3 Deposit Properties

In practice, the deposits on the heat transfer surfaces are removed with spring hammers and recycled to the smelter. Simulating deposit growth over an extended period is therefore not of primary interest; rather, locating the most problematic positions takes precedence. To investigate the initial deposit build-up, a one-hour period was studied and the simulation was carried out with discrete time steps of 10 minutes. Figure 4.7 shows plots of deposit thicknesses on the three main parts of the boiler at the 30th minute and at the 60th minute of simulation time. Although the simulations cannot be validated due to the lack of experimental data, the positions with high likelihoods of deposition problems can be identified. The deposit build-up is not significant, except for in one small section of the ash hopper wall in the circle and on the leading edge of the second group of tube banks.

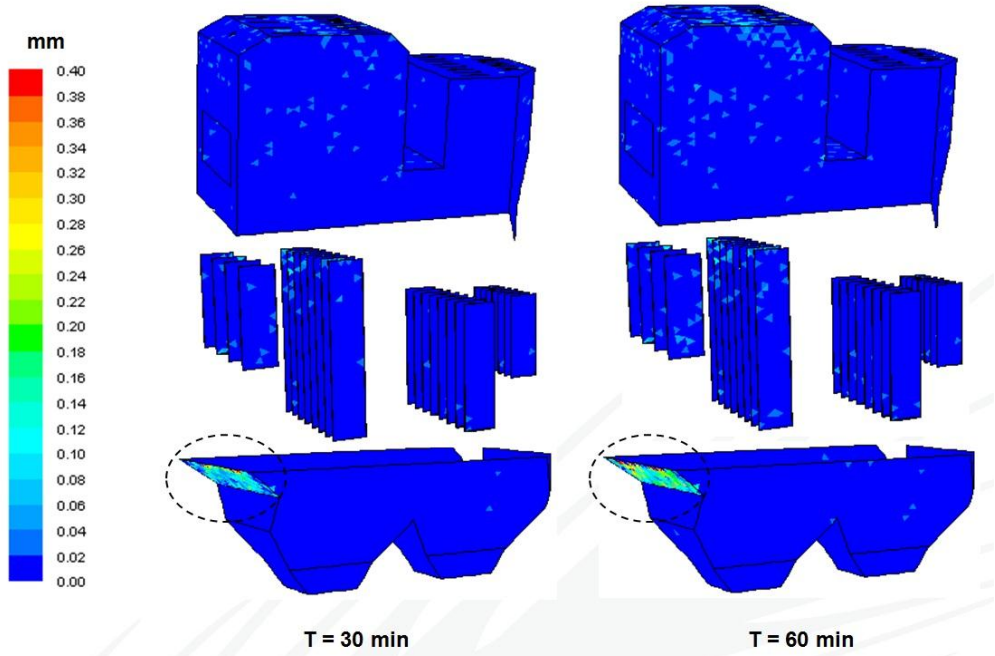

Figure 4.7: Deposit thickness at the 30th minute and the 60th minute of simulation time (Paper IV).

As mentioned above, it is desirable to have the dust particles spend sufficient residence time in the gas phase at a correct temperature range. Doing so will allow the small particles to reach complete conversion; for the larger particles, a thick sulfate layer can form before the particles come into contact with the heat transfer surfaces. Figure 4.8 shows the extent of conversion of the deposits, i.e., r_{ave} in Equation 4-6. The figure shows the instant value at the 60th minute for the mass averaged extent of conversion of the landing particles and of the deposits already on the wall. It should be noted that the extent of conversion is displayed in Figure 4.8 for even trace amounts of deposit; thus it does not conflict with Figure 4.7 with regard to the distribution of deposit. As mentioned earlier, the sulfation reaction of deposits on the wall is not considered. Nonetheless, Figure 4.8 indicates that some of the landing particles are not fully converted; the ongoing sulfation conversion can lead to a higher sintering tendency.

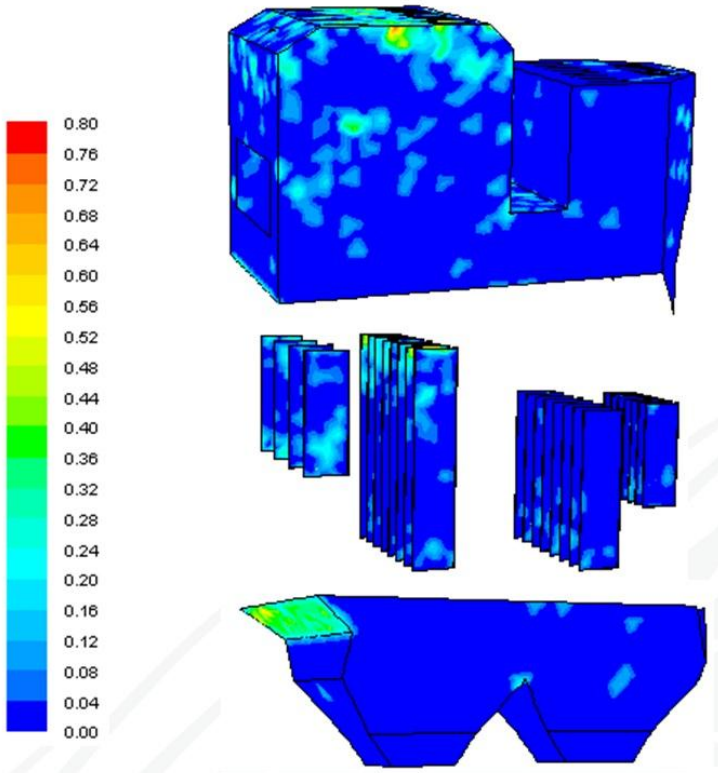

Figure 4.8: Mass average extent of conversion of deposits on the walls at the 60th minute of the simulation time (Paper IV).

The temperature of heat transfer surfaces can increase due to the deposit build-up. The heat transfer rate decreases because the temperature difference between the gas phase and the walls decreases, and because the deposits have poor thermal conductivity compared with steel. Figure 4.9 depicts significant differences for the heat flux distributions from the gas phase to the cooling water from the starting point to the 60th minute of simulation time. However, the increasing deposit build-up on the wall may not be the only factor that decreases the heat flux; other changes caused by the dust particles and the deposits, such as a different gas phase temperature distribution, can also contribute to the change of heat transfer properties of the boiler.

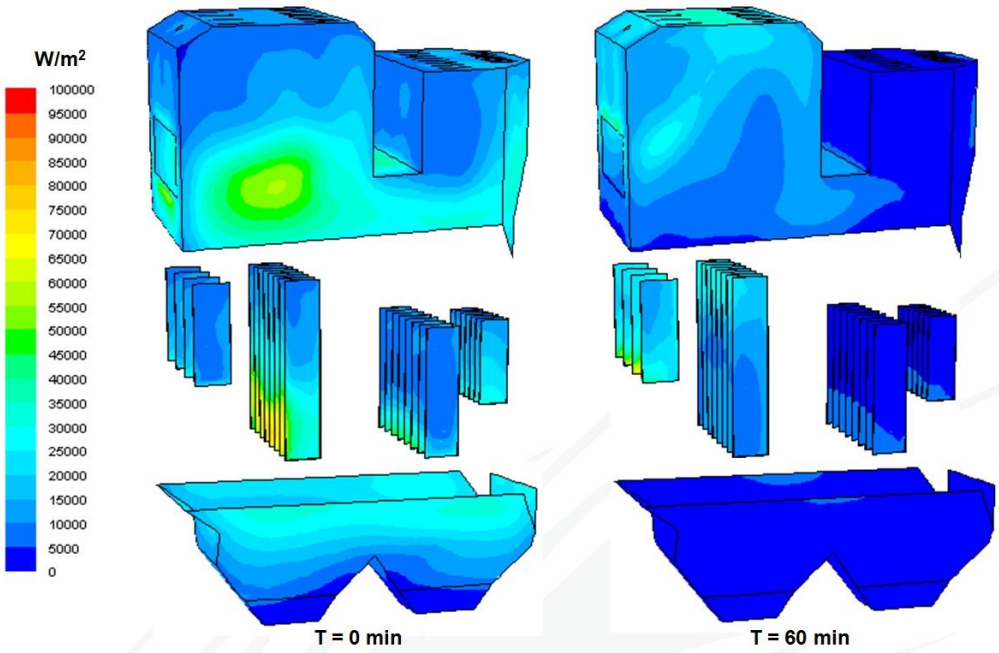

Figure 4.9: Total surface heat flux, showing no deposit on the wall at the starting point of the simulation (on the left) and at the 60th minute of simulation time (on the right) (Paper IV).

5. CONCLUSIONS AND FUTURE WORK

Fireside deposit formation is a complex process. The modeling of the deposit formation requires a variety of sub-models describing the behaviors of ash, gas phase, deposits, and their interactions. Fireside deposit formation is also case-specific, i.e., different combinations of sub-models are needed to model deposit formation in different furnaces. This work focuses on two sub-processes of deposit formation typical in two types of furnaces. One process is the slagging wall, found in Kraft recovery furnaces, with molten deposits running on the wall or on the superheater tubes. The other is deposit formation due to thermophoresis of fine particles on the heat transfer surfaces in the heat recovery boiler of the flash smelting process. Sub-models have been developed for these two processes, and they are implemented into CFD models of the two furnaces.

The slagging wall model takes into account the two-layer structure of the deposits. It allows calculation of the thickness and of the surface temperature of the molten deposit layer. The slagging wall model is used to calculate the surface temperature of a specific section of a super-heater tube panel with the boundary condition obtained from a Kraft recovery furnace model. In addition, the slagging wall model is used to calculate the heat transfer. The slagging wall model is implemented into the CFD-based Kraft recovery furnace model. The implementation of the slagging wall model includes a grid simplification scheme. The wall surface temperature calculated with the model is used as a heat transfer boundary condition. Simulation of a Kraft recovery furnace is performed and is compared with two other models and with measurements. In the other two models, a uniform wall surface temperature and a wall surface temperature calculated with a char bed burning model are used as the heat transfer boundary conditions, respectively. In this particular furnace, the wall surface temperatures predicted with the three models are similar, and they are all in the correct range of the measurements. A choice among the three different approaches for heat transfer boundary conditions would not affect the overall evaluation of the boiler performance. However, the difference in wall surface temperature can become significant. The slagging wall model is proven to be computationally efficient.

A deposit growth model is developed to describe the deposit formation due to thermophoresis of fine particles to the heat transfer surfaces. The model is used in the simulation of a heat recovery boiler in the flash smelting process. In order to determine whether the dust particles stay on the wall, a criterion based on the analysis of forces acting on the particle is applied. A time-dependent simulation of deposit formation in the heat recovery boiler is carried out and the influence of deposits on heat transfer is investigated. The locations prone to deposit formation are identified in the heat recovery boiler.

The modeling of the two processes enhances the overall understanding of the deposit formation and the behavior of the deposits in these two types of industrial furnaces. The sub-models developed in this work can be applied in other similar deposit formation processes. In this work, the focus on these two specific processes means that other aspects of deposit formation, e.g., inertial impaction of ash particles and the corresponding sticking criterion are simplified or overlooked. Additionally, the

simplifications and assumptions applied in the two sub-models, e.g., the heat balance around a molten deposit element and the sticking criterion based on the force analysis should be re-examined if the sub-models are adopted for modeling of other processes. Like in many applications of modeling, the validation of the sub-models under complex conditions in industrial furnaces is very difficult. Therefore, the author recommends experimental work under simpler conditions to validate the sub-models as the immediate next step of this work. In the end, the sub-models developed in this work form a part of the basis for a comprehensive deposit formation model. Choosing a combination of sound sub-models is necessary for a reliable prediction of deposit formation in a specific type of furnace.

6. REFERENCES

ANSYS Fluent Flow Modeling Simulation Software. (2013). Retrieved February 24, 2013, from ANSYS - Simulation Driven Product Development: http://www.ansys.com/Products/Simulation+Technology/Fluid+Dynamics/Fluid+Dynamics+Products/ANSYS+Fluent

Adams, T. N. (1997). General characteristics of Kraft black liquor recovery boilers. In T. N. Adams, W. J. Frederick, T. M. Grace, M. Hupa, K. Iisa, A. K. Jones, et al., & T. N. Adams (Ed.), *Kraft recovery boilers* (pp. 3-37). Atlanta, GA, USA: Tappi Press.

Akbar, A., Schnell, U., & Scheffknecht, G. (2010). Modelling of potassium release and the effect of potassium chloride on deposition mechanisms for coal and biomass fired boilers. *Combustion Theory and Modelling, 14*(3), 315-329.

Åmand, L.-E., Leckner, B., Eskilsson, D., & Tullin, C. (2006). Deposits on heat transfer tubes during co-combustion of biofuels and sewage sludge. *Fuel, 85*(10-11), 1313-1322.

Backman, R., & Nordin, A. (1998). High temperature equilibrium calculations of ash forming elements in biomass combustion/gasification systems - state of the art, possibilities and applications. *Internation Biomass Ash Workshop*. Graz, Austria.

Backman, R., Hupa, M., & Uppstu, E. (1987). Fouling and corrosion mechanisms in the recovery boiler superheater area. *Tappi Journal, 70*(6), 123-127.

Bale, C. W., Bélisle, E., Chartrand, P., Decterov, S. A., Eriksson, G., Hack, K., et al. (2009). FactSage thermochemical software and databases - recent developments. *CALPHAD: Comput. Coupling Phase Diagrams Thermochem., 33*, 295-311.

Barta, L. E., Beér, J. M., & Sarofim, A. F. (1994). Coal fouling tendency model. In J. Williamson, & F. Wigely, *The impact of ash deposition on coal fired plants* (pp. 177-188). Washington, DC, USA: Taylor and Francis.

Baukal, C. E., Gershtein, V. Y., & Li, X. (2001). *Computational Fluid Dynamics in Industrial Combustion.* Boca Raton, London, New York, Washington D.C.: CRC Press.

Baxter, L. L. (1993). Ash deposition during biomass and coal combustion: a mechanistic approach. *Biomass and Bioenergy, 4*, 85-102.

Baxter, L. L. (1998). Influence of ash deposit chemistry and structure on physical and transport properties. *Fuel Processing Technology, 56*(1-2), 81-88.

Baxter, L. L., & DeSollar, R. W. (1993). A mechanistic description of ash deposition during pulverized coal combustion: predictions compared with observations. *Fuel, 72*, 1411-1418.

Beér, J. M., Sarofim, A. F., & Barta, L. E. (1992). From properties of coal mineral matter to deposition tendencies of fly ash - a modeling route. *Journal of the Institute of Energy, 65*, 55-62.

Benson, S. A., Hurley, J. P., Zygarlicke, C. J., Steadman, E. N., & Erickson, T. A. (1993b). Predicting ash behavior in utility boilers. *Energy & Fuels, 7*, 746-754.

Benson, S. A., Jones, M. L., & Bryers, R. W. (1993a). Practical measures to minimize ash deposition. *Engineering Foundation Conference on the Impact of Ash Deposition in Coal-Fired Plants*, (pp. 657-678). Solihull, England.

Bergroth, N., Engblom, M., Mueller, C., & Hupa, M. (2010). CFD-based modeling of kraft char beds - part I: char bed burning model. *Tappi Journal, 9*(2), 6-13.

Bergroth, N., Mueller, C., & Hupa, M. (2004). CFD-based modeling of recovery boiler char beds. *International Chemical Recovery Conference; 11th International Symposium on Corrosion in the Pulp and Paper Industry* (pp. 670-685). Charleston: Tappi press.

Bird, R. B., Stewart, W. E., & Lightfoot, E. N. (2007). *Transport Phenomena.* New York: John Wiley & Sons.

Blasiak, W., Tao, L., Vaclavinek, J., & Lidegran, P. (1997). Modeling of kraft recovery boilers. *Journal of Energy Conversion and Management, 38*(10-13), 995-1005.

Boysan, F., Weber, R., Swithenbank, J., & Lawn, C. J. (1986). Modeling coal-fired cyclone combustors. *Combustion and Flame, 63*, 73-86.

Brink, A., Kilpinen, P., & Hupa, M. (2001). A simplified kinetic rate expression for describing the oxidation of volatile fuel-N in biomass combustion. *Energy&Fuels, 15*(5), 1094-1099.

Brink, A., Lauren, T., Hupa, M., Koschack, R., & Mueller, C. (2010). In-furnace temperature and heat flux mapping in a Kraft recovery boiler. *Tappi Journal, 9*(9), 7-11.

Bryers, R. W. (1977). *Ash deposits and corrosion due to impurities in combustion gases.* (R. W. Bryers, Ed.) New Hampshire: Taylor&Francis Group.

Bryers, R. W. (1996). Fireside slagging, fouling, and high-temperature corrosion of heat-transfer surface due to impurities in steam-raising fuels. *Progress in Energy and Combustion Science, 22*, 29-120.

Carling, R. W., Mar, R. W., & Nagelberg, A. S. (1983). On the application of complex equilibrium calculations to the study of mineral matter during coal combustion. *Preprints of Papers - American Chemical Society, Division Fuel Chemistry, 28*, 223-233.

Dees, C., Simonen, J., & Tran, H. (1992). Experience of recovery boiler superheater corrosion at Willamette Hawesville. *Proceedings of the 7th International Symponium on Corrosion in the Pulp and Paper Industry.* Orlando.

Eddings, E. G., Davis, K. A., Heap, M. P., Valentine, J. R., & Sarofim, A. F. (2001). Mineral matter transformation during pulverized coal combustion. *Developments in Chemical Engineering and Mineral Processing, 9*(3/4), 313-327.

Engblom, M. (2010). *Modeling and field observations of char bed processes in black liquor recovery boilers.* Department of Chemical Engineering. Turku: Painosalama Oy.

Engblom, M., Bergroth, N., Mueller, C., Jones, A., Brink, A., & Hupa, M. (2010a). CFD-based modeling of krfat char beds - part 2: a study on the effects of droplet size and bed shape on bed processes. *Tappi Journal, 9*(2), 15-20.

Engblom, M., Mueller, C., Brink, A., Hupa, M., & Jones, A. (2008). Toward predicting the char bed shape in kraft recovery boiler. *Tappi Journal, 7*(10), 12-16.

Engblom, M., Rönnqvist, A., Brink, A., Mueller, C., Jones, A., & Hupa, M. (2010b). Recovery boiler char bed dynamics - measurements and modeling. *International Chemical Recovery Conference. 1*, pp. 119-133. Williamsburg: Tappi press.

Epple, B., Krohmer, B., Hoppe, A., Mueller, H., & Leithner, R. (2005). CRFD studies for boilers fired with high ash containing and slagging lignites. *Clean Air*, 137-155.

Esaki, S., Dees, C., Kawaji, M., & Tran, H. (1993). A heat transfer model for predicting superheater tube temperatures in Kraft recovery boilers. *Heat Transfer in Fire and Combustion Systems, HTD-Vol. 250*, 235-242.

Fan, J., Zha, X., Sun, P., & Cen, K. (2001). Simulation of ash deposition in a pulverized coal-fired boiler. *Fuel, 80*, 645-654.

Ferreira, D., Cardoso, M., & Park, S. (2010). Gas flow analysis in a Kraft recovery boiler. *Fuel Processing Technology, 91*, 789-798.

Forstner, M., Hofmeister, G., Jöller, M., Dahl, J., Braun, M., & Kleditzsch, S. (2006). CFD simulation of ash deposit formation in fixed bed biomass furnaces and boilers. *Progress in Computational Fluid Dynamics, 6*(4/5), 248-261.

Frandsen, F. J. (2009). Ash research from Palm Coast, Florida to Banff Canada: entry of biomass in mordern power boilers. *Energy & Fuels, 23*, 3347-3378.

Frederick, W. J. (1997). Black liquor droplet burning process. In T. Adams, W. Frederick, T. Grace, M. Hupa, K. Iisa, A. Jones, et al., *Kraft Recovery Boilers.* Atlanta, Georgia, USA: Tappi press.

Frederick, W. J., & Hupa, M. (1991). *Steady-state Kraft char bed model.* Report 91(9), Combustion and Material Chemistry Group, Åbo Akademi University, Turku.

Friedlander, S., & Johnstone, H. (1957). Deposition of suspended particles from turbulent gas streams. *Industrial Engineering Chemistry, 49*, 1151-1156.

Grabke, H. J., Reese, E., & Spiegel, M. (1995). The effects of chlorides, hydrogen chloride, and sulfur dioxide in the oxidation of steels below deposits. *Corrosion Science, 37*(7), 1023-1043.

Grace, T., & Frederick, W. (1997). Char bed process. In T. N. Adams, W. J. Frederick, T. M. Grace, M. Hupa, K. Iisa, A. K. Jones, et al., *Kraft Recovery Boilers.* Atlanta, GA, USA: TAPPI press.

Gupta, R. P., & Backman, R. (2004). Ash deposition in Kraft recovery boilers. *Proceedings of the 29th International Technical Conference on Coal Utilization & Fuel Systems. Volume 1*, pp. 539-550. Newcastle: Coal Technology Association.

He, C., & Ahmadi, G. (1998). Particle deposition with thermophoresis in laminar and turbulent duct flows. *Aerosol Science and Technology, 29*(6), 525-546.

Hecken, M., Reichelt, L., & Renz, U. (1999). Numerical simulation of slagging films in the pressurized coal combustion facility Aachen. *Proceedings of the 4th International Symposium on Coal Combustion.* Peking.

Hocking, M. G., & Alcock, C. B. (1966). The kinetics and mechanism of formation of sulfates on cuprous oxide. *Transactions of the Metallurgical Society of AIME, 236*, 635-642.

Huang, L., Norman, J., Pourkashanian, M., & Williams, A. (1996). Prediction of ash deposition on super heater tubes from pulverized coal combustion. *Fuel, 75*(3), 271-279.

Isaak, P., Tran, H. N., Darham, D., & Reeve, D. W. (1986). Stickiness of fireside deposits in kraft recovery units. *Journal of Pulp and Paper Science, 12*(3), J84-J88.

Israel, R., & Rosner, D. (1983). Use of a generalized Stokes Number to determine the aerodynamic capture efficiency of Non-Stokesian particles from a compressible gas flow. *Aerosols Science and Technology, 2*, 45-51.

Järvinen, M., Fogelholm, C.-J., Mueller, C., & Hupa, M. (2007). A new comprehensive black liquor droplet combustion model for CFD applications. *Proceedings of the International Chemical Recovery Conference* (pp. 81-86). Tappi Press.

Jenkins, B. M., Baxter, L. L., Miles Jr, T. R., & Miles, T. R. (1998). Combustion properties of biomass. *Fuel Processing Technology, 54*, 17-46.

Jones, A. (1989). *A model of the kraft recovey furnace.* PhD thesis, The Institue of Paper Chemistry, Appleton, Wisconsin, USA.

Jones, W. P., & Lindstedt, R. P. (1988). Global reaction schemes for hydrocarbon combustion. *Combustion and Flame, 73*, 233-249.

Kær, S. K. (2001). *Numerical investigation of deposit formation in straw-fired boilers - Using CFD as the framework for slagging and fouling predictions.* Aalborg University, Denmark, Institute of Energy Technology.

Kær, S. K., Rosendahl, L. A., & Baxter, L. L. (2006). Towards a CFD-based mechanistic deposit formation model for straw-fired boilers. *Fuel, 85*(5-6), 833-848.

Karvinen, R., Siiskonen, P., & Hyöty, P. (1989). Role of combustion simulation during the operation and in the design of a modern recovery boiler. *International Forum on Mathematical Modeling of Processes in Energy Systems.* Sarajevo.

Kawaji, M., Shen, X. H., Tran, H., Esaki, S., & Dees, C. (1995, October). Prediction of heat transfer in the Kraft recovery boiler superheater region. *Tappi Journal, 78*(10), 214-221.

Kojo, I. V., Jokilaakso, A., & Hanniala, P. (2000). Flash smelting and converting furnaces: a 50 year retrospect. *JOM, 52*(2), 57-61.

Lee, F. C., & Lockwood, F. C. (1999). Modeling ash deposition in pulverized coal-fired applications. *Progress in Energy and Combustion Science, 25*, 117-132.

Li, B., Brink, A., & Hupa, M. (2009). Simplified model for determining local heat flux boundary conditions for slagging wall. *Energy & Fuels, 23*, 3418-3422.

Lindberg, D., Backman, R., & Chartrand, P. (2007a). Thermodynamic evaluation and optimization of the (Na_2CO_3+Na_2SO_4+Na_2S+K_2CO_3+K_2SO_4+K_2S) system. *J.Chem.Thermodyn., 39*, 942-960.

Lindberg, D., Backman, R., & Chartrand, P. (2007b). Thermodynamic evaluation and optimization of the (NaCl+Na_2SO_4+Na_2CO_3+KCl+K_2SO_4+K_2CO_3) system. *J.Chem.Thermodyn., 39*, 1001-1021.

Liu, B. Y., & Agarwal, J. K. (1974). Experimental observation of aerosol deposition in turbulent flow. *Aerosol Science, 5*, 145-155.

Markova, T., Boyanov, B., Pironkiv, S., & Shopov, N. (2000). Investigation of dusts from waste-heat boiler and electrostatic precipitators after flash smelting furnace for copper concentrates. *Jounral of Mining and Metallurgy, 36*(3-4), 195-208.

Miettinen, E. (2008). *Thermal conductivity and characteristics of copper flash smelting flue dust accretions.* Helsinki: Helsinki University of Technology.

Miles, T. R., Miles Jr, T. R., Baxter, L. L., Bryers, R. W., Jenkins, B. M., & Oden, L. L. (1995). *Alkali deposits found in biomass power plants: a preliminary investigation of their extent and nature.* National Renewable Energy Laboratory, Golden, CO.

Mueller, C., Brink, A., & Hupa, M. (2005b). Numerical simulation of the combustion behavior of different biomasses in a bubbling fluidized bed boiler. *Proceedings of the 18th International Conference on Fluidized Bed Combustion.* Toronto.

Mueller, C., Eklund, K., Forssén, M., & Hupa, M. (2002). Simplified black liquor droplet combustion model based on single droplet experiments. *Proceedings of Finnish-Swedish Flame Days.* Helsinki University of Technology.

Mueller, C., Eklund, K., Forssén, M., & Hupa, M. (2004). Influence of liquor-to-liquor differences on recovery furnace processes - a CFD study. *International Chemical Recovery Conference; 11th International Symposium on Corrosion in the Pulp and Paper Industry*, (pp. 720-738). Charleston.

Mueller, C., Selenius, M., Theis, M., Skrifvars, B.-J., Backman, R., Hupa, M., et al. (2005a). Deposition behaviour of molten alkali-rich fly ashes - development of a submodel for CFD applications. *Proceedings of the Combustion Institute, 30*, 2991-2998.

Mueller, C., Skrifvars, B.-J., Backman, R., & Hupa, M. (2003). Ash depostion prediction in biomass fired fluidised bed boilers - combination of CFD and advanced fuel analysis. *Progress in Computational Fluid Dynamics, 3*(2-4).

Owen, P. (1969). Pneumatic transport. *Journal of Fluid Dynamics, 39*, 407-432.

Plumley, A. L., Lewis, E. C., & Tallent, R. G. (1966). External corrosion of water wall-tubes in Kraft recovery boilers. *Tappi Journal, 49*, 72-81.

Raask, E. (1985). Deposition mechanisms, rate measurements, and the mode of formation of boiler deposits. In R. E, *Mineral impurities in coal combustion: behavior, problems, and remedial measures* (pp. 189-216). Hemisphere Publishing Corporation.

Ranki-Kilpinen, T. (2004). *Sulphation of cuprous and cupric oxide dusts and heterogeneous copper matte particles in simulated flash smelting heat recovery boiler conditions.* Academic dissertation, Aalto University, Helsinki.

Reeve, D. W., Tran, H., & Barham, D. (1981). Superheater fireside deposits and corrosion in kraft recovery boilers. *Tappi, 64*(5), 109-113.

Richards, G. H., Slater, P. N., & Harb, J. N. (1993). Simulation of ash deposit growth in a pulverized coal-fired pilot scale reactor. *Energy & Fuels*, 774-781.

Robinson, A. L., Junker, H., & Baxter, L. L. (2002). Pilot-scale investigation of the influence of coal-biomass cofiring on ash deposition. *Energy and Fuels, 16*, 343-355.

Rosemount Analytical. (2012, August 3). *Combustion flue gas analysis reduces NOx and slag*. Retrieved November 27, 2012, from Analytic Expert: http://www.analyticexpert.com/2012/08/combustion-flue-gas-analysis-reduces-nox-and-slag/

Sarkar, S. (1982). Effect of SO_3 on corrosion of process equipment in copper smelters. *JOM, 34, 43-47*.

Sarofim, A. F., & Helble, J. J. (1994). Mechanisms of ash and deposit formation. In J. Williamson, & F. Wigley, *The Impact of Ash Deposition on Coal-Fired Power Plants, Proceedings of the United Engieering Foundation International Conference.*

Saviharju, K., Pakarinen, L., Kyttälä, J., Jukola, P., Viherkanto, K., & Näkki, I. (2006). Modeling and feeback measurements give new understanding about recovery boiler behavior. *7th International Colloquium on Black Liquor Combustion and Gasification.* Jyväskylä, Finland.

Schnell, U., Richter, S., & Hein, K. R. (2001). Numerical simulation of slagging and fouling in a pulverized coal-fired utility boiler. *United Engineering Foundation Conference on Heat Exchanger Fouling.* Davos, Switzerland.

Schwendiman, L. C., & Postma, A. K. (1962). Turbulent deposition in sampling lines. *United States Atomic Energy Commission, TID-7627*, 127-136.

Seggiani, M. (1998). Modeling and simulation of time varying slag flow in a Prenflo entrained-flow gasifier. *Fuel, 77*(14), 1611-1621.

Sehmel, G. (1968). A particle size distribution function for data recorded in size ranges. *The Annals of occupational hygiene, 11*(2), 87-98.

Senior, C., & Srinivasachar, S. (1995). Viscosity of ash particles in combustion systems for prediction of particle sticking. *Energy & Fuels, 9*, 277-283.

Silvennoinen, J., & Hedman, M. (2013). Co-firing of agricultural fuels in full-scale fluidized bed boiler. *Fuel Processing Technology, 105*, 11-19.

Skrifvars, B.-J., Hupa, M., & Hyöty, P. (1991). Superheater fouling due to limstone injection in coal-fired boilers. *Journal of the Institute of Energy, 64*, 196-201.

Sommersacher, P., Brunner, T., & Obernberger, I. (2012). Fuel indexes: A novel method for the evaluation of relevant combustion properties of new biomass fuels. *Energy & Fuels, 26*, 380-390.

Sugawara, A., & Yoshizawa, Y. (1961). An investigation on the thermal conductivity of porous materials and its application to porous rock. *Australian Journal of Physics, 14*(4), 469-480.

Sumnicht, D. (1989). *A computer model of a kraft char bed.* PhD thesis, The Institute of Paper Chemistry, Appleton, Wisconsin, USA.

Sutinen, J. (2006). *Numerical modelling of recovery boiler furnace.* PhD thesis, Tampere Univeristy of Technology, Tampere, Finland.

Talbot, L., Cheng, R. K., Schefer, R. W., & Willis, D. R. (1980). Thermophoresis of particles in heated boundary layer. *Journal of Fluid Mechanics, 101*, 737-758.

Tallent, R. G., & Plumley, A. L. (1969, October). Recent research on external corrosion of waterwall tubes in Kraft recovery furnaces. *Tappi Journal, 52*(10), 1955-1959.

Theis, M. (2006). *Interaction of biomass fly ashes with different fouling tendencies.* Turku, Finland: Laboratory of Inorganic Chemistry, Process Chemistry Centre, Åbo Akademi University.

Theis, M., Skrifvars, B.-J., Hupa, M., & Tran, H. (2006). Fouling tendency of ash resulting from burning mixtures of biofuels. Part 1: Deposition rates. *Fuel, 85*, 1125-1130.

Thornton, C., & Ning, Z. (1998). A theoretical model for the stick/bounce behaviour of adhesive, elastic-plastic spheres. *Powder Technology, 99*, 154-162.

Thornton, C., & Yin, K. K. (1991). Impact of elastic spheres with and without adhesion. *Powder Technology, 65*, 153-166.

Tomeczek, J., & Waclawiak, K. (2009, August). Two dimensional modeling of deposit formation on platen superheaters in pulverized coal boilers. *Fuel, 88*(8), 1466-1471.

Tran, H. (1997). Upper furnace deposition and plugging. In T. Adams, W. Frederick, T. Grace, M. Hupa, K. Iisa, A. Jones, et al., *Kraft Recovery Boilers.* Atlanta, Georgia, USA: Tappi Press.

Tran, H., Reeve, D., & Barham, D. (1983). Formation of kraft recovery boiler superheater fireside deposits. *Pulp & Paper Canada, 84*(1), 36-41.

Tran, H., Sunil, A., & Jones, A. K. (2004). The fluidity of recovery boiler smelt. *International Chemical Recovery Conference; 11th International Symposium on Corrosion in the Pulp and Paper Industry*, (pp. 660-669). Charleston.

Urbain, G., Cambier, F., Deletter, M., & Anseau, M. R. (1981). Viscosity of silicates melts. *Transactions and Journal of the British Ceramic Society, 80*, 139-141.

Vainio, E., Brink, A., DeMartini, N., Hupa, M., Vesala, H., Tormonen, K., et al. (2010). In-furnace measurement of sulfur and nitrogen species in a recovery boiler. *Journal of Pulp and Paper Science, 36*(3-4), 135-142.

Vergas, S., Frandsen, F. J., & Dam-Johansen, K. (2001). Rheological properties of high-temperature melts of coal ashes and other silicates. *Progress in Energy and Combustion Science, 27*, 237-429.

Wall, T. F., Bhattacharya, S. P., Zhang, D. K., Gupta, R. P., & He, X. (1993). The properties and thermal effects of ash deposits in coal-fired furnaces. *Progress in Energy and Combustion Science, 19*(6), 487-504.

Wall, T. F., Lowe, A., Wibberley, L. J., & Steward, I. M. (1979). Mineral matter in coal and the thermal performance of large boilers. *Progress in Energy and Combustion Science, 5*(1), 1-29.

Walsh, A. (1989). *A computer model for in-flight black liquor combustion in a kraft recovery furnace.* PhD thesis, The Institue of Paper Chemistry, Appleton, Wisconsin, USA.

Walsh, P. M., Sayre, A. N., Loehden, D. O., Monroe, L. S., Beer, J. M., & Sarofim, A. F. (1990). Deposition of bituminous coal ash on an isolated heat exchanger tube: effects of coal properties on deposit growth. *Progress in Energy and Combustion Science, 16*(4), 327-345.

Wang, H., & Harb, J. N. (1997). Modeling of ash deposition in large-scale combustion facilities burning pulverized coal. *Progress in Energy and Combustion Science, 23*, 267-282.

Wang, X. H., Zhao, D. Q., He, L. B., Jiang, L. Q., He, Q., & Chen, Y. (2007). Modeling of a coal-fired slagging combustor: development of a slag submodel. *Combustion and Flame, 149*, 249-260.

Weber, R., Mancini, M., Schaffel-Mancini, N., & Kupka, T. (2013a). On predicting the ash behaviour using Computational Fluid Dynamics. *Fuel Processing Technology, 105*, 112-128.

Weber, R., Schaffel-Mancini, N., Mancini, M., & Kupka, T. (2013b). Fly ash deposition modelling: Requirements for accurate predictions of particle impaction on tubes using RANS-based computational fluid dynamics. *Fuel, 108*, 586-596.

Wells, A. C., & Chamberlain, A. C. (1967). Transport of small particles to vertical surfaces. *British Journal of Applied Physics, 18*(12), 1793-1799.

Wessel, R. A., & Righi, J. (1988). Generalized correlation for inertial impaction of particles on a circular cylinder. *Aerosol Science and Technology, 9*, 29-60.

Wessel, R., Parker, K., & Verrill, C. (1997). Three-dimensional kraft recovery furnace model: implementation and results of improved black liquor combustion models. *Tappi Journal, 80*(10), 207-220.

Wood, N. B. (1981). The prevention of acid smuts. The mass transfer of particles and acid vapour to cooled surfaces. *Journal of the Institute of Energy, 54*(419), 76-93.

Yang, Y. (1996). *Computer simulation of gas flow and heat transfer in waste-heat recovery boilers of the Outokumpu copper flash smelting process.* Helsinki: Acta Polytechnica Scandinavia.

Yang, Y., Jokilaakso, A., Taskinen, P., & Kytö, M. (1999). Using computational fluid dynamics to modify a wate-heat boiler design. *JOM, 51*(5), 36-39, 47.

Young, J., & Leeming, A. (1997). A theory of particle deposition in turbulent pipe flow. *Journal of Fluid Mechanics, 340*, 129-159.

Yuan, J., Xiao, Z., Salcudean, M., Singh, P., & Gorog, P. (2007). Numerical study on mid-furnace corrosion in a kraft recovery boiler. *Proceedings of the International Chemical Recovery Conference.* Tappi Press.

Zbogar, A., Frandsen, F. J., Jensen, P. A., & Glarborg, P. (2005). Heat transfer in ash deposits: A modelling tool-box. *Progress in Energy and Combustion Science, 31*(5-6), 371-421.

Zbogar, A., Frandsen, F. J., Jensen, P. A., & Glarborg, P. (2009). Shedding of ash deposits. *Progress in Energy and Combustion Science, 35*, 31-56.

Zhou, H. S., Jensen, P. A., & Frandsen, F. J. (2007). Dynamic mechanistic model of superheater deposit growth and shedding in a biomass fired grate boiler. *Fuel, 86*(10-11), 1519-1533.

RECENT REPORTS FROM THE COMBUSTION AND MATERIALS CHEMISTRY GROUP OF THE ÅBO AKADEMI PROCESS CHEMISTRY CENTRE:

08-01	Erik Vedel	Predicting the Properties of Bioactive Glasses
08-02	Tarja Talonen	Chemical Equilibria of Heavy Metals in Waste Incineration -Comparison of Thermodynamic Databases-
08-03	Micaela Westén-Karlsson	Assessment of a Laboratory Method for Studying High Temperature Corrosion Caused by Alkali Salts
08-04	Zhang Di	*In vitro* Characterization of Bioactive Glass
08-05	Maria Zevenhoven, Mikko Hupa	The Environmental Impact and Cost Efficiency of Combustible Waste Utilization - The Potential and Difficulties of On-going Technology Developments
08-06	Johan Werkelin	Ash-forming Elements and their Chemical Forms in Woody Biomass Fuels
08-07	Hanna Arstila	Crystallization Characteristics of Bioactive Glasses
10-01	Markus Engblom	Modeling and Field Observations of Char Bed Processes in Black Liquor Recovery Boilers
11-01	Leena Varila et al.	Fyrtio År Oorganisk Kemi vid Åbo Akademi
11-02	Johan Lindholm	On Experimental Techniques for Testing Flame Retardants in Polymers
11-03	Minna Piispanen	Characterization of Functional Coatings on Ceramic Surfaces
11-04	Sonja Enestam	Corrosivity of Hot Flue Gases in the Fluidized Bed Combustion of Recovered Waste Wood

RECENT REPORTS FROM THE COMBUSTION AND MATERIALS CHEMISTRY GROUP OF THE ÅBO AKADEMI PROCESS CHEMISTRY CENTRE:

12-01	Xiaoju Wang	Enzyme Electrode Configurations: for Application in Biofuel Cells
12-02	Patrycja Piotrowska	Combustion Properties of Biomass Residues Rich in Phosphorus
12-03	Dorota Bankiewicz	Corrosion Behavior of Boiler Tube Materials during Combustion of Fuels Containing Zn and Pb
12-04	Mikael Bergelin, Jan-Erik Eriksson, Xiaoju Wang, Max Johansson,et al.	Printed Enzymatic Power Source with Embedded Capacitor on Next Generation Devices, Tekes-PEPSecond
12-05	Susanne Fagerlund	Understanding the in vitro dissolution rate of glasses with respect to future clinical applications
13-01	Oskar Karlström	Oxidation rates of carbon and nitrogen in char residues from solid fuels
13-02	Juho Lehmusto	The Role of Potassium in the Corrosion of Superheater Materials in Boilers Firing Biomass

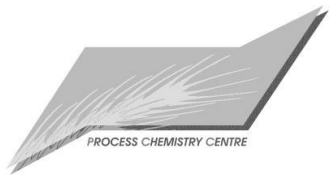

ISSN 1459-8205
ISBN 978-952-12-2953-4 (paper version)
ISBN 978-952-12-2964-0 (pdf version)
Åbo, Finland, 2013